1-23-2019 10:30 AM

Bouncing Dynamics of a Class of MEM/NEM Switching Systems

Mohamed Bognash, *The University of Western Ontario*

Supervisor: Dr. S. F. Asokanthan, *The University of Western Ontario*

A thesis submitted in partial fulfillment of the requirements for the Doctor of Philosophy degree in Mechanical and Materials Engineering

ABSTRACT

The aim of the present research is to understand the bouncing dynamic behavior of NEM/MEM switches in order to improve the switch performance and reliability. It is well known that the bouncing can dramatically degrade the switch performance and life; hence, in the present study, bouncing dynamics of a cantilever-based NME/MEM switch has been studied in detail. To this end, a model of a MEM switch that incorporates electrostatic force, squeeze film air damping force as well as asperity-based contact force has been proposed for an electrostatically actuated switch. An actuation force due to piezoelectric effects is further included in an alternative micro-switch model of combined actuation for the purposes of bounce mitigation. For a NEM switch, an asperity-based contact model along with repulsive van der Waals force are incorporated in a nano-switch to capture the contact dynamics. Intermolecular forces, surface effects, and gas rarefication effects are also included in the NEM switch model. Further, an intermolecular force, specifically the Casimir force, is also used to actuate this class of switches in addition to the classical electrostatic actuation. Euler-Bernoulli beam theory and an approximate approach based on Galerkin's method have been employed for predicting transient dynamic responses. In the present study, performance parameters such as initial contact time, permanent contact time, major bounce height, and the number of bounces have been quantified in the presence of interactive system nonlinearities.

For a MEM switch, improvement of bouncing behavior has been investigated using harmonic dither in the actuation voltage of an electrostatically actuated switch or using harmonic dither in the secondary piezoelectric actuator voltage. Improvements have been achieved in both types of switches at specific frequency ranges. Uncertainty quantification of parameters that affect the bouncing is also performed since MEM switches are prone to uncertainties during the fabrication. Measure of performance in terms of second order statistics is predicted, particularly for the beam as well as beam tip parameters and the influence of uncertainty in parameters on the system performance has been quantified.

For a NEM switch, the performance parameters are also used to investigate the influence of surface effects and rarefication effects on the performance of an electrostatically actuated switch. Influence of some pull-in parameters on the switch bouncing behavior have also been investigated in the presence of surface effects at different vacuum conditions for purely Casimir actuated NEM switch. Recommended operating conditions or actuation parameters are suggested for the purposes of avoiding excessive bouncing for both types of NEM switches.

The present investigation on the bouncing dynamic behavior of a class of MEM/NEM switches is envisaged to yield greater insight into the design, reliability and performance predictions for this class of switches.

KEYWORDS: MEMS, NEMS, transient response, bounce mitigation, harmonic dither, harmonic perturbations, secondary actuator, piezoelectric, electrostatic, uncertainty quantification, Casimir force, van der Waals force, surface effects, contact bouncing, asperity contact model, switch.

CO-AUTHORSHIP

This doctoral thesis has been carefully prepared according to the regulations for monograph format thesis stipulated by the school of graduate and postdoctoral studies at the University of Western Ontario. The work was carried out by the author under the supervision of Dr. S. F. Asokanthan. Results from this thesis have been published in journal and conference proceedings with Dr. S. F. Asokanthan as a co-author. Future publications resulting from this work will also be published with Dr. S. F. Asokanthan as a co-author.

ACKNOWLEDGEMENTS

I would like to express my gratitude to those who provided me with encouragement and assistance during this thesis work.

I am deeply indebted to my thesis supervisor Dr. S. F. Asokanthan for introducing me to this research area and for his continuous guidance, encouragement and expertise and valuable contribution to this thesis. It simply would not have been possible without him.

My thanks also go to my colleagues and friends for their help and friendliness. It is very fortunate for me to work in such a good company.

Finally, I would like to express my sincere gratitude to my wife Negia and my children Abdeljewad, Hala, Ahmed and Nouh, words cannot just describe how valuable your love, encouragement and patience have been to my completion of this work.

TABLE OF CONTENTS **Page**

LIST OF TABLES **Page**

LIST OF FIGURES **Page**

NOMENCLATURE

A	beam's cross-sectional area
a	beam width
a_p	piezoelectric layer width
A_n	nominal contact area
A_p	cross-sectional area of the piezoelectric layer
b	beam thickness
b_p	piezoelectric layer thickness
BH	major bounce height
C	speed of light
C_A	neutral axis of a section that includes the piezoelectric layer
C_f	variable damping coefficient
d	air gap
d_{31}	piezoelectric constant
d_T	beam tip contact gap
E	Young's modulus for the beam material
E_p	Young's modulus for the piezoelectric
E^s	surface elastic modulus
$(EI)_{eff}$	effective bending rigidity of the nano beam
f_C	contact force per unit length of the beam
f_{CA}	Casimir force per unit length of the beam
f_D	damping force per unit length of the beam
f_E	electrostatic force per unit length of the beam
f_S	distributed transverse load along the longitudinal direction of the beam due to surface effects
f_{VDW}	Van der Waals force per unit length of the beam
A_h	Hamaker constant
$H(x)$	Heaviside function
h	gap separation between the beam and substrate

$\bar{h}$	Planck's constant divided by 2π
I	moment of inertia of the beam's cross-section
$\boldsymbol{K}$	stiffness matrix
k	gain
K_B	Boltzmann's constant
k_{ij}	stiffness matrix elements
K_n	Knudsen number
L	beam length
L_1, L_2	starting and ending points of electrostatic electrode
L_3, L_4	starting and ending points of piezoelectric secondary actuator
L_T	beam tip length
$\boldsymbol{M}$	mass matrix
m_{ij}	mass matrix elements
m_m	mass of the molecules
M_p	distributed moment due to the piezoelectric actuator
M_H	asperity height mean value
BH	major bounce height
$\boldsymbol{N}$	vector of modal forces
NB	number of single significant bounces
n	number of modes
n_i	unit normal vector to the surface
P	pressure
P_a	ambient atmospheric pressure
P_0	applied load for contact
$\boldsymbol{q}$	vector of temporal coordinates
$q_r(t)$	temporal coordinates
R	radius of sphere asperity
t	time
t_i	initial contact time
t_b	bouncing time

t_p	permanent contact time
T	temperature
V	actuation voltage
V_p	piezoelectric actuation voltage
V_{th}	theoretical pull-in dynamic voltage
v_0	initial velocities
w	contact interference
x	spatial co-ordinate
x_0	initial displacements
$Y_r(x)$	mode shapes
z_c	cut-off value
y	beam lateral deflection
β	fringe effect correction coefficient
$\delta(x)$	Dirac delta function
ε	equilibrium distance at which f_{VDW} becomes zero
ε_p	piezoelectric induced strain
ε_{lp}	longitudinal strain due to the piezoelectric
ϵ_x	longitudinal strain for nano beam
ε_0	permittivity of air
η	area density of asperities
κ	beam curvature
ξ	asperity height
λ	mean free path of the molecule
μ	air viscosity
ρ	material mass density of the beam (mass per unit volume)
ρ_p	piezoelectric layer mass density
$\sigma_a,\ \sigma_b$	standard deviation in width, thickness
σ_E	standard deviation in Young's modulus
σ_{BH}	standard deviation in major bounce height H
σ_{AH}^2	variance of the asperity height

σ_{L_T}	standard deviation in beam tip length L_T
σ_R	standard deviation in radius of asperities
σ_{t_i}	standard deviation in initial contact time t_i
σ_V	standard deviation in actuation voltage V
σ_η	standard deviation in area density of asperities
σ_{ij}^{+} , σ_{ij}^{-}	stresses above and below the surface interface, respectively
τ	surface stress
τ^0	residual surface stress
v_1, v_2	Poisson's ratios of contact surfaces
$\phi(\xi)$	asperity height distribution

CHAPTER 1

INTRODUCTION AND LITERATURE REVIEW

1.1 Introduction

Microelectromechanical Systems (MEMS) is an important area of technology that combines different engineering disciplines such as material, mechanical, electrical, chemical, optics and fluids. This technology integrates interrelated device components into comprehensive systems at very small scales that complete functions such as sensing and actuation (Ostasevicius & Dauksevicius, 2010). The characteristic length of MEM devices is typically less than $1mm$ but more than $1\mu m$. With the new advancement in nanofabrication methods, a size reduction of microelectromechanical systems originates the nanoelectromechanical systems (NEMS) in which the characteristic length of NEM devices is less than $1\mu m$. Advantages of MEMS/NEMS technology such as low-cost, low power consumption, high functionality, and small size and light weight of the devices open enormous opportunities in the commercial markets and make them attractive for many engineering applications (Leondes, 2006, Voiculescu & Zaghloul, 2016).

MEMS and emerging NEMS are expected to have a major impact on our lives, comparable to that of semiconductor technology, information technology, or cellular and molecular biology. In the past decades, MEMS/NEMS technology has received much attention due to its successful commercial applications in many fields such as automotive, aerospace, electronics instrumentation, industrial process control, appliances, biotechnology, healthcare, office equipment, and telecommunications. Unlike conventional integrated circuits, micro/nano devices can have many functions including sensing, communication, and actuation (Bhushan, 2005) and this technology has been successfully applied to different areas since it manifested itself into applications, such as inertial sensors, micro-machined pressure sensors, surface-micro-machined mechanisms, micro-robotics, micro-scale vacuum pumps and flow control, radio frequency (RF) devices, etc.

Recent advances in MEMS/NEMS technology have led to development of a multitude of new devices that can be used in a variety of industrial as well as consumer product applications. The wide range of applications for MEMS/NEMS could be classified into four main categories: (1) sensors, gathering information from environments; (2) actuators, controlling the environment by positioning, regulating, pumping, and filtering in response to actuation sources; (3) switches, such as two-terminal and three-terminal relays; (4) resonators; such as oscillators and filters in communication systems and signal processing applications (Ma, 2011).

Among these applications, switches are fundamental building blocks in the design of MEMS/NEMS. These structures have advantages of low power consumption, low insertion loss, and high isolation. MEM/NEM switches work by using a force to mechanically deflect an active element into physical contact with an opposing element, thus changing the state of the device. When the applied force is removed or minimized to a specific value, the deflected element restores its original shape and the state of the device changes accordingly. The forces required for the mechanical movement can be obtained using electrostatic, magnetostatic, piezoelectric, or thermal designs or by utilizing of intermolecular force. Electrostatic actuation is often regarded as the main drive source for MEM/NEM switches due to its virtually zero power consumption, small electrode size, thin layers used, and relatively short switching time. In NEM devices, the intermolecular forces such as Casimir and van der Waals force have considerable magnitudes as the characteristic dimensions of these devices reduces to nanometers scale. The emerging of Casimir force alteration could open a new avenue to replace or enhance the electrostatic actuation in the future and this could reduce the energy consumption.

The most common structures for typical MEM/NEM electrostatic switches are based on cantilever beam and clamped-clamped beam. Among these, the cantilever-based micro or nano-mechanical switches are one of the most often used configurations in MEM/NEM switch applications, but its instability behavior and its transient response are not adequately understood. In the present research, the emphasis will be placed on NEM/MEM devices, in particular, the bouncing dynamic response. The dynamic behavior of cantilever type switch has been studied in detail. Typically, upon closing, the nano / micro-beam (switch)

bounces several times before making permanent contact with the adjoining structure. Bouncing due to switching can dramatically degrade the performance due to an increase in the transition time and the electrical breakdown. In the present study, the contact bouncing behavior of a typical cantilever type MEM switch is investigated incorporating electrostatic forces, squeeze film air damping forces and asperity-based contact forces in the system model. Reducing or eliminating bounces in MEM switch is investigated in the present study using harmonic dither in actuation voltages for electrostatically actuated switch or using harmonic perturbations voltage in a secondary PZT actuator of combined actuated switch. Bouncing behavior improvement has been achieved for the two types of switches at frequencies below the second and third natural frequencies of the free beam of the electrostatically actuated and the combined actuated switches, respectively, both at high or low actuation voltages. Uncertainty quantification of switch and switch tip parameters that affect the bouncing has also been performed in the present study. Influences of these parameters on switch performance parameters have been quantified in the presence of interactive system nonlinearities. The quantitative predictions reveal several varying patterns as well as similar trends for output measure second order statistics. In addition to the MEM switch dynamics, this study is also concerned with the dynamic behavior of a NEM based cantilever switch with consideration of intermolecular forces, surface effects, gas rarefication effects under pure Casimir actuation or under electrostatic actuation. Effects of some relevant parameters on the bouncing behavior have been investigated when this class of NEM switches are actuated by both types of forces. For an electrostatic nano switch, simulation results show that significant improvement in switching time is attained when the applied voltage is about 1.3 times the dynamic pull-in voltage; however, beyond this voltage, bouncing deteriorates the performance and limits the advantage of using higher voltages. For the Casimir actuated switch, the results show that using short beam lengths with smaller gaps provide better bouncing performance.

The following sections provide a brief review about the MEM/NEM devices and some of the relevant previous research work.

1.1.1 Introduction to MEM switches

MEM switch devices represent a class of appealing applications utilizing MEMS technology. Figure 1.1 illustrates a typical RF switch electrostatically actuated for a gold-on-gold contact MEMS inline series switch on silicon substrates and the current is considered to flow from the source to the drain when the contact takes place. This switch was developed at Northeastern University and Analog Devices Inc. (Zavracky *et al.* 1999). This typical micro-switch device can be considered to represent a cantilever configuration. The cantilever beam is fabricated using a thick layer of electroplated gold and is

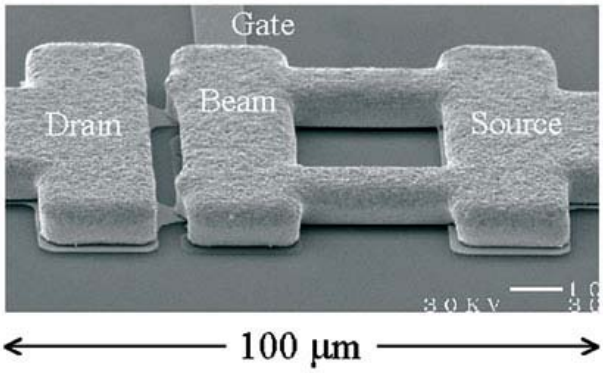

Fig. 1.1. Analog device inline MEMS series switch (Zavracky *et al.*, 1999).

suspended $0.6\sim1.2\ \mu m$ above the pull-down electrode. During the operation stage, voltage is applied between the actuation electrode and the beam. This voltage difference generates an electrostatic force that pulls down the cantilever towards the substrate. If the generated electrostatic force is large enough, the beam collapses and free end beam tip contacts the drain and closes the switch. It should be noted that when the applied voltage to such beam-based switches exceeds a critical value, the generated electrostatic force becomes greater than the corresponding restoring forces, resulting in the unstable collapsing of the beam to the ground position. This behavior is known as the pull-in instability.

Cantilever type surface micro-machined electrostatic switches are by far the most widely studied. Despite the improvements in design, analysis, and fabrication of micro-switches, the dynamic behavior has not been adequately understood, in particular the transient

response due to contact bouncing. Typically, during the switch closure stage, the beam bounces several times before making a permanent contact with the drain (McCarthy *et al.*, 2002). This phenomenon is likely to result in significant performance degradation. For instance, an increase in the transition time or a complete breakdown of the switch can occur as result of bouncing. Longer transition times interrupt the signal flow and limit the performance. Hence, in most applications, the maximum switching frequency is limited to approximately 50 kHz (Kogut & Komvopoulos, 2004). Therefore, bounce elimination or reduction is necessary to improve the performance of this class of devices. Moreover, batch fabrication processes used to produce MEM systems are prone to uncertainties in the system geometrical and contact parameters as well as material properties. Hence, it is necessary to get more insight into their variations and effects on the system dynamics and performance. An in-depth investigation into the dynamic behavior of this type of micro-switch is necessary to enhance the device performance and reliability.

1.1.2 Introduction to NEM switches

Figure 1.2 illustrates a titanium nitride based NEM switch with the smallest dimensions ever made by typical ‘‘top-down” complementary metal-oxide-semiconductor fabrication technology (Jang *et al.*, 2008). This NEM cantilever switch has a $30\ nm$-thick titanium nitride beam and a $20\ nm$-thick air-gap. It should be noted that the working principle of electrostatically actuated NEM switches is similar to the working principle of MEM switches. In recent years, many models of electrostatic MEM switches have been developed based on conventional theories available in mechanics. However, due to nano scale effects that characterize the NEM devices, new physics may emerge, and the theory typically applied to MEMS at microscale may not be applicable for NEMS. In particular, when the characteristic sizes of these devices shrink to nanometers, intermolecular forces, such as van der Waals force (Israelachvili, 1992) and the Casimir force (Lamoreaux, 2004, Mostepanenko & Trunov, 1997), may play an important role in predicting the dynamic behavior of NEM switches. Such forces are measurable when the separation between the surfaces is at nano level. Their magnitudes grow rapidly with extremely small distance as

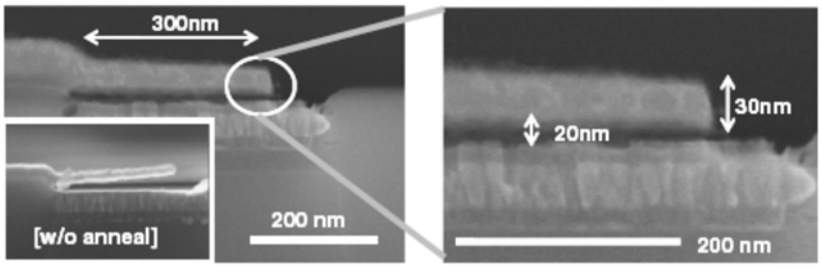

Fig. 1.2. NEM electrostatic switch with $30nm$-thick beam and $20nm$-thick air-gap (Jang *et al.*, 2008).

in NEMS applications; therefore, in MEMS applications these forces can be neglected. In addition to intermolecular forces, the material properties of nanostructures, in particular at the surface, differ from those of micro and macro scale structures due to the size dependent behavior. Hence, characterization of the dynamic behavior of NEM switches with the consideration of nanoscale features and effects has become increasingly important in this research area. Bouncing phenomenon in NEM switches is also reported in a study by Loh and Espinosa (2012) and it has similar performance degradation as for the MEM devices. To improve the performance and reliability of NEM switches, transient response due to contact bouncing needs to be investigated with the consideration of the related nano physics. Understanding of the effects of different aspects that shape the bouncing dynamics facilitate the road to improve the device performance and reliability.

1.2 Literature review

MEMS/NEMS is a multidisciplinary field, which has gained rapid growth during the past decades. The NEMS and MEMS technology have been attractive fields for many researchers and the literature is extensive in these fields. The relevant previous research performed on micro and nano switch dynamic analysis is reviewed in this section.

1.2.1 MEM switches

The simplest model for an electrostatically actuated MEM switch is the single degree of freedom model of equivalent mass-spring-damper with a gap that separates the mass from an actuation electrode. Although this model can capture some of the switch behavior, it is often unsuitable for predicting the full range of quantitative results for a MEM switch system. The consideration of a continuous system beam model has received significant attention in the literature. A detailed study of the transient dynamics of an electrostatically actuated micro-cantilever beam has been carried out by Krylov and Maimon (2004). Galerkin's method with orthogonal modes is employed to predict the system transient response. The device is modeled as a prismatic Euler-Bernoulli beam. Linear and nonlinear damping models have been taken into account to investigate the dynamic pull-in stability. Simulation results have been confirmed by experiments and this study suggested that a high level of damping leads to an increase in the voltage required to cause dynamic instability and a high level of damping might reduce bouncing. Galerkin's approach is also employed by Younis *et al.* (2003) to formulate a reduced-order model of electrostatically actuated microbeam-based MEMS. The model robustness is validated over the whole device operation range up to the instability limit of the device. In this study, static pull-in stability and dynamics of micro-beam are investigated. Caruntu and Knecht (2015) employed Galerkin's approach to formulate a reduced-order model of electrostatically actuated microbeam. The system is modeled as an Euler-Bernoulli cantilever beam. The method is employed to investigate the nonlinear parametric dynamics of a cantilever resonator under soft alternating current (AC) voltage of frequency near half the natural frequency as well as to investigate the pull-in phenomenon. It may be noted that bouncing behavior was not considered in these studies.

Contact bounce phenomenon has been considered in several previous studies. Recently, Ostasevicius *et al.* (2009) proposed a finite element model for a cantilever-type electrostatic actuated micro-switch considering the electrostatic actuation and squeeze-film damping effects as well as the impact interactions that take place during switching. In their conclusion, the authors emphasized that the bounce phenomenon is still not fully explained and required comprehensive treatment. Guo *et al.* (2007) used a 3-D nonlinear finite

element model for the structure, along with a finite difference scheme in time to simulate MEMS switch closing events. The contact is represented with a nonlinear spring to model the interaction between the contact tip and the drain. The authors pointed out that a sophisticated more realistic contact model needed to better predict the bouncing dynamics of the switch. A recent contribution has been made in a study by McCarthy *et al.* (2002) in which the contact bounce effects are included in the dynamic model of an electronically actuated micro-switch. In this study, a simple linear spring model for the contact tips, the electrostatic actuation force, and squeeze-film damping were included, and finite difference method was employed to predict the switch dynamic behavior. Later, a simplified one-degree-of-freedom model was also proposed by Granaldi and Decuzzi (2006) to predict the switching time and bouncing. In another study, Decuzzi *et al.* (2006) examined the bouncing dynamics of a cantilever micro-switch via finite difference method with the consideration of adhesive force at the tip. Recently, Tung *et al.* (2014) investigated the bouncing behavior of a device using reduced order model and considering the squeeze film damping. The contact is approximated by point contact models and assumed to be linear with hysteresis. Results show that using two modes in the simulation captures the real dynamics of the system as the bouncing has several short-spaced impacts during the actual impact. The influence of contact stiffness and actuation voltage on the final bouncing characteristics has been investigated in this study. It is worth noting that in these studies only a simple linear model is employed in representing the contact bouncing.

In micron scale, contact forces play important roles in forming the dynamical behavior of MEM switches. Greenwood and Williamson (1966) proposed an asperity-based model for surface contact. The model has been widely used, and in this model, the rough surface is represented by a collection of spherical asperities with identical end radii. Several researchers have improved Greenwood and Williamson's model to account for elastic, elastic-plastic contact of asperities and interaction of asperities. A fully plastic model of contact interaction is proposed in a study by Chang *et al.* (1987) in which the basic asperity model of Greenwood and Williamson has been extended to include condition for plastically deformed asperities at moderate loads. Elastoplastic transitional deformations are included by Zhao *et al.* (2000) to overcome some shortcomings of Chang's model. In this model, the transition region from elastic to plastic deformation is considered. Further refinements

to this model is performed in a study by Zhao and Chang (2001) in which a model of asperity interactions in elastic-plastic contact of rough surfaces are considered. Recently, Wang (2009) adopted the asperity contact model in a MEM switch to simulate the contact between the beam tip and the substrate. The model is based on the Greenwood and Williamson model with uniform distribution of asperity heights. Theoretical predictions of typical switch bounce nature have been verified experimentally using a micro scanning Laser doppler vibrometer.

As mentioned previously, the phenomena of bouncing in switches degrades the performance and shortens their life. It is natural to expect that elimination or reduction of bouncing could result in improvement in extension of their life. Hence, much effort has been devoted to optimizing the switch parameters to reduce the bouncing by adjusting the damping or using special structure configurations. Other techniques such as open loop control via special wave form, feedback control, and utilizing dual actuation are also used to mitigate the bouncing. For the purpose of bounce mitigation, Kim *et al.* (2011) designed and fabricated a switch with an electrode and dimple extended along the length of beam. The long electrode provides a higher holding force that suppresses the bouncing while the long dimple prevents the beam collapse. Tung *et al.* (2014) simulated a switch bouncing by considering reduced order modeling. The influence of contact stiffness and actuation voltage on the final bouncing characteristics are investigated. Open-loop configurations via carefully designed input pulse shape waveform allows for gentle pull-in which results in bounce reduction have been used in a study performed by Czaplewski *et al.* (2006) and Sumali *et al.* (2007); however, damping has not been considered in these studies. A disadvantage of this strategy is that the waveform is only applicable to a single device and does not account for parameter variation. Guo *et al.* (2007) used a simple voltage-pulse actuation scheme to eliminate the switch bouncing. In this study, the authors pointed out that despite the success achieved to mitigate the bouncing, the dynamics of the device become sensitive to wave shape parameters. According to the authors' conclusion, this method may not be as effective as expected if the switch parameters such as threshold voltage or fundamental frequencies deviate from the design parameters. Wong and Lai (2013) discussed the different merits of different dual pulse waveforms and their robustness with respect to changes in the switch parameters. Blecke *et al.* (2009) proposed a learning

control actuation waveform that can iteratively reduce bouncing by refining the timing of the input pulse to obtain a soft landing. In this technique, measurements must be made for each switch and complex active driver circuitry is required to generate the optimal waveforms. A double electrode switch is investigated by Rahim and Younis (2016) to control the bouncing. In Rahim and Younis' study, both electrodes are electrostatically operated. Pulse shape waveforms and constant actuation voltage are applied to the controlling and the primary electrodes, respectively. The waveforms parameters are tuned so that the bounce is minimized. This dual electrode configuration allows further modifications to the known pulse shape waveforms existed in literature. In addition to electrostatic actuation, piezoelectric action may be used in switch actuation / control and it may lead to different dynamic bouncing behavior. In this type of actuation, the expansion or contraction of a ferroelectric material as a result of voltage application are utilized to deflect the switch toward or away from the substrate. For instance, Zhang *et al.* (2005) modeled the MEM actuator with piezoelectric actuator (PZT) in order to apply adaptive control scheme that eliminates the unwanted vibrations of the micro-cantilever beam system. Liu and Liu (2014) investigated the effect of combined electrostatic and piezoelectric actuation on the pull-in behavior of actuator; however, the contact and bouncing has not been considered in this study. Using combination of two different types of actuations is scarce in literature in particular with consideration of bouncing; hence, the present work aims at to investigate the effects of using a secondary piezoelectric actuator in addition to the primary electrostatic actuator on the bouncing behavior of a MEM switch.

The above-mentioned studies are based on deterministic models that describe the system parameters. However, batch fabrication processes used to produce MEM systems are prone to uncertainties in the system geometrical and contact parameters as well as material properties. These manufacturing uncertainties may cause significant variations in performance characteristics. Understanding the influences of uncertainties accompanied by these processes allows better prediction and optimization of device output and improves the performance and the reliability. Many techniques are used to evaluate the output uncertainty due to the input uncertainty propagation in a system. Monte Carlo (MC) methods are one of the most used technique since they are easy to implement and understand (Kalos & Whitlock, 2008). However, these MC methods can be

computationally expensive since they need a large number of samples for accurate prediction. In MEM devices, generating a large number of samples is very time expensive. Snow and Bajaj (2010) employed the Monte Carlo approach to investigate uncertainty quantification in a MEM switch using different sampling techniques to reduce the cost of computation. Effects of parameter variations on certain performance characteristics have been investigated in this study. A faster stochastic framework for quantifying the effect of stochastic variations in various design parameters on the performance of MEM devices has been performed by Agarwal and Aluru (2009). It may be noted that the performance characteristics of immediate interest are limited to the static and dynamic pull-in voltages for the switch in the first study while the equilibrium tip displacement of the beam and time taken by the beam to strike against the drain corresponding to a step voltage are the outputs in the second study. Shanmugavalli *et al.* (2006) used interval analysis to find ranges of static pull-in voltage based on ranges of some of switch parameters as inputs. A simple one degree of freedom model is used for the analysis. However, the effect of uncertainty of the system parameters on bouncing behavior after the contact takes place has not been considered in these studies. To date, only limited studies are available in the literature on the topic of parameter uncertainties associated with switch dynamics, particularly with consideration given for bouncing. Hence, to improve the switch performance and reliability, contact bouncing with consideration of parameter uncertainty needs to be investigated.

Based on the research carried out in previous studies, it is proposed that a more accurate and realistic model incorporating realistic non-linear tip-contact forces is warranted for a cantilever beam type micro-switch, especially for an accurate prediction of the beam transient behavior. The literature review suggests that more research need to be carried out to eliminate or reduce the bouncing to improve the device performance. The literature review also suggests that an effective uncertainty quantification analysis to assess the influences of parameter variations on the device performance considering the bouncing dynamics is essential.

1.2.2 NEM switches

In general, dynamic behavior analysis of nanoscale devices is challenging due to the nonlinear coupling of the different physics and the influences that are accompanied by small size effects. When the size of a device is reduced from micro to nano scale, models based on the classical theories of mechanics that are valid at the micro scale may not provide accurate predictions for nano-structures. In particular, when the characteristic sizes of these devices shrink to nanometers, intermolecular forces such as van der Waals force and Casimir force, surface effects of nanostructured materials such as surface stress and surface elasticity and rarefication effects may play an important role in predicting the dynamic behavior of NEM switches. Due to the demand on the small size devices and low power consumptions, an alternative actuation technique such as pure Casimir force actuation may replace the traditional electrostatic actuation provided that the Casimir force magnitude can be altered. The performance and reliability of switches can be improved by understanding of bouncing behavior due the influence of these effects and the new actuation method. The research in this field is still a very active area of research and the bouncing associated with the switching has not been considered thus far in the literature.

Intermolecular forces such as van der Waals force (Israelachvili, 1992) and Casimir force (Lamoreaux, 2004, Esquivel-Sirvent *et al.*, 2009) have been considered in the modeling of nano structures. Although these intermolecular forces describe the same physical phenomena at different nano levels (Palasantzas, 2008), authors model the intermolecular forces in nano systems separately or simultaneously. In NEM switches, actuation is typically performed by applying a voltage difference between two electrodes (Rotkin, 2002, Dequesnes *et al.*, 2002, Liu, 2016). The effect of the van der Waals force on the pull-in voltage has been investigated for the electrostatically actuated nano devices in a study performed by Rotkin (2002). In this study, an analytical model for calculating pull-in parameters of electromechanical system is presented and a single degree of freedom model has been used to investigate the van der Waals effects on the pull-in behavior. Dequesnes *et al.* (2002) studied the pull-in voltage characteristics of several nanotube electromechanical switches considering the elastostatic, the electrostatic and the van der Waals energy domains. Van der Waals force has been taken into account in a simple

continuum model. The influence of van der Waals force in the design of nanoelectromechanical switches has been investigated. An analytical expression, based on a lumped model, is derived to compute the pull-in voltage of cantilever and fixed–fixed switches. Molecular dynamic simulation is employed to confirm the continuum model results. It is worth noting that damping, surface effects and Casimir force have not been considered in these studies.

Pull-in instability of the electrostatically actuated nanostructures with the consideration of Casimir force has been investigated by Lin and Zhao (2005). Approximate analytical expressions for a one degree of freedom model is used to describe the nonlinearity of system; however, surface effects have not been considered in this investigation. Liu (2016) investigated the nonlinear pull-in behavior of a cantilever-type nano-mechanical electrostatic actuator considering the influence of surface effects, the fringing field effect and the Casimir force effect. It should be mentioned that van der Waals force was not included in these models by justifying that typically, the gap for this force to be effective is not reached. However, for a switch the gaps between the contacting elements are small upon contact and van der Waals force should be considered.

Effects of both Casimir and van der Waals forces on the pull-in stability of nano-actuator are considered in a study performed by Soroush *et al.* (2010). Adomian decomposition is used to obtain an analytical solution of distributed parameter model; however, the study has ignored both the surface effects of nanostructured materials as well as the damping in the system. Static behavior and dynamic responses of a nano-beam subjected to the electrostatic force in present of intermolecular forces have been investigated in a study performed by Vakili-Tahami *et al.* (2009). In this study, Euler-Bernoulli beam theory is employed to model the switch and Galerkin's approach is used to discretize the system then solved numerically. However, only simple constant damping without the rarefaction effect is considered and surface effects have been ignored in this investigation.

Due to the inherently large surface area to volume ratio that is exhibited by typical nanoscale structures, the surface energy becomes a significant part of the total elastic energy and surface energy may play important role in the elastic deformation of these

nanostructures and their material properties. In macroscopic materials, the mechanical properties are considered independent from the size and the surface effects such as surface stress (or surface tension) and surface elasticity are neglected. In contrast to macro and micro materials, the dependence of mechanical properties on their size is considered in many nano-related researches (Miller & Shenoy, 2000, C. Q. Chen *et al.*, 2006, Jing *et al.*, 2006, Guo & Zhao, 2007, Rudd & Lee, 2008). Hence, much effort has been devoted to understanding the effect of the size of structures on the material properties. It may be noted that the influence of surface effects on the mechanical properties of nanostructures has been investigated in the literature via experiments, atomistic models and continuum models.

Using contact atomic force microscopy, C. Q. Chen *et al.* (2006) measured the Young's modulus of the silver nanowires for different diameters. The dependence of the Young's modulus on the size of the wires due to surface effects has been demonstrated experimentally. Results show that the Young's modulus increases as the size of the wires decreases. Moreover, in this study, a theoretical analysis of the elastic properties of the nanowires is carried out using the classical continuum model with consideration of the surface effects. Dependency of properties on the material size is also measured by Jing *et al.* (2006) for [0001] oriented ZnO nanowires. In their experiments, a dramatic increase of Young's modulus for smaller diameter (less than $120\ nm$) is measured while for larger diameters (up to $550\ nm$) the modulus approaches the bulk value. In addition to the above mentioned experimental investigations, atomistic models were also used to characterize the size dependency of materials for nano structures. Miller and Shenoy (2000) developed a theoretical model for the effective Young's modulus of nano wires (NWs) with surface effects and explain the dependency of Young's modulus on NWs size. Rudd and Lee (2008) studied the size dependence of Young's modulus of NWs based on first-principles density functional theory and compared the results with classical molecular dynamics. Park (2009) also studied the size-dependent resonant frequencies of silicon nanowire with finite deformation. In this study, the author concluded that the residual surface stress affects the resonance frequencies of nanowires.

The continuum modeling is also considered in many investigations related to surface effects of nanostructures based on the linear surface elastic theory developed by Gurtin and

Murdoch (1975) and the generalized Young–Laplace equations (T. Chen, 2006). This approach is used by Wang and Feng (2007) where the effects of both surface elasticity and surface stress on the natural frequencies of a micro-beam have been investigated. He and Lilley (2008) investigated the elastic behavior of static bending of NWs for different support configurations. Euler-Bernoulli beam theory is used with modified Young–Laplace equations to introduce the surface effects on nanowires. Ma *et al.* (2010) investigated the influence of surface effects on the pull-in instability of nano-electrostatically actuated switch using an Euler–Bernoulli beam model considering the Casimir force. He's homotopy perturbation method is used to approximate the analytical solutions for the static bending of NEM switches and validated by numerical solutions using the finite difference method. It is worth noting that this study focused only on static deflection and pull-in instability. Liu (2016) studied the effects of surface effects on the pull-in behavior of a cantilever-type nano-mechanical electrostatic actuator using continuum model via Euler–Bernoulli beam. The influence of surface effects, the fringing field effect and the Casimir force effect are taken into explicit account in this study. Hybrid computational scheme of differential transformation method and the finite difference approximation technique is employed to predict the behavior of the actuator. It should be noted that many of the above-mentioned studies have ignored the damping in the modeling which may lead to less accurate and realistic results for the dynamic investigations while ignoring the damping for static studies provide reasonable accuracy.

In the dynamics of MEM/NEM devices, squeeze-film damping has significant influence on the device behavior. Several models have been developed for these devices but when dimensions become very small, certain macro and micro scale models do not accurately predict nanoscale behavior. In nano-structures, where the characteristic length of the gaps is very small as well as the surrounding pressure is low, rarefied gas effects need to be considered in the damping. In the literature, the rarefaction condition can be identified by the Knudsen number and the continuum models can fail at a certain threshold without considered the rarefication effect. Guo and Alexeenko (2009) proposed a compact model of squeeze-film damping based on rarefied flow simulations. The model provides a simple expression for the damping coefficient valid for free-molecular regimes. The model is also valid for high the Knudsen number and accurately captures the damping between a

vibrating micro-cantilever and nearby wall. This model is based on the numerical solution to the Boltzmann kinetic equation. Effective viscosity that takes into account the Knudsen number is also used along with Reynolds-equation-based models in some studies (Nayfeh & Younis, 2004, Li *et al.*, 2007). In these studies, the effective viscosity of the fluid in the gap accounts for the rarefied gas effect through its dependence on the Knudsen number. Gallis and Torczynski (2004) developed a molecular-dynamics-based model by the direct simulation Monte Carlo method incorporating squeeze-film damping for a rigid beam. Their model takes advantage of both Reynolds equation and molecular dynamics. Sumali (2007) validated experimentally some of existed models, among them Gallis and Torczynski model, of squeeze-film damping in the free molecular regime for wide range of Knudsen number. Further improvements on Gallis and Torczynski model have been made by Parkos *et al.* (2013) and lead to a near-contact gas damping model. This model has also been validated experimentally and shown to be applicable for nano switches since the parameters are comparable.

As mentioned earlier, in this class of nano switches, actuation is typically performed by applying a voltage difference between two electrodes; however, the emergence of a Casimir force alteration could open a new avenue to replace the electrostatic actuation in the future especially with the high demand for smaller size devices and lower power consumption. Recently, continuous efforts have been devoted to the adjustment of the Casimir force in order to use this force for switching actuation. Altering of the magnitude of the Casimir force has been successfully demonstrated via many techniques such as manipulating the dielectric properties of a material with light (Chen *et al.*, 2007), imposing an external magnetic field (Esquivel-Sirvent *et al.*, 2009) and changing the carrier density of the semiconductor (Chen *et al.*, 2006). Torricelli *et al.* (2010) experimentally demonstrated an increase of Casimir force of 25% through controlling of dielectric properties of materials by laser heating a thin film made of Ag-In-Sb-Te (AIST), which reversibly changed from a crystalline state to an amorphous state. This alteration in the magnitude of Casimir force may be utilized to actuate a switch device and make the contact.

It is worth noting that the bouncing phenomenon is not exclusive to MEM switches since contact also exists in nano-switches. In NEM switches the bouncing is reported in a study

carried out by Loh and Espinosa (2012) and it is expected to have a similar performance degradation as for the MEM devices. Liao *et al.* (2010) fabricated electrostatically actuated suspended single-crystal diamond nanowires for high-performance nanoelectromechanical switches. The current-voltage characteristics of the switch have been experimentally measured. An abrupt behavior is observed in the ON-state as the applied voltage increases. This abrupt behavior may be attributed to bouncing of the nano switch. Yahiaoui *et al.* (2014) fabricated and tested a nano-gap radio frequency microelectromechanical system metal-contact switch. Bouncing of the switch in a vacuum condition was also reported in this study. To the best of the author's knowledge, the dynamics of nano switches with consideration of bouncing has not been addressed in the in literature so far. Therefore; in the present study, a comprehensive model of a NEM switch that incorporates a realistic contact force along with consideration of nanostructure forces and effects such intermolecular forces and surface effects as well as the damping is essential for an in-deep understanding of the switch bouncing dynamics.

Based on the findings from the above literature review, it can be concluded that a comprehensive model for the nano switch is essential for providing insight into the switch dynamics. The literature proposes that intermolecular forces, surface effects, and rarefied squeeze-film damping need to be included in the model. It also proposes that a more accurate and realistic model incorporating asperity tip-contact force, the intermolecular forces, surface effects need to be considered in order to accurately predict the dynamic behavior of the switch when it is actuated electrostatically. The use of Casimir force actuation may lead to smaller and less energy-consuming devices; therefore, investigating the bounce behavior under this new class of actuating forces is also beneficial in the development of this class of switches with the consideration of these forces and effects.

1.3 Research objectives

The primary goal of the present research is to understand the bouncing dynamic behavior of a class of NEM/MEM switching systems in order to achieve necessary performance improvements. In particular, the transient dynamic behavior (i.e. contact bounce) of a

cantilever type NEM/MEM switching system have been investigated in detail. The following aspects will be investigated to achieve this primary goal:

- Develop comprehensive models that accurately predict the switch bouncing dynamics using a more realistic asperity-based contact model as well as the relevant forces and effects for cantilever-based MEM switch structures. Perform transient contact bouncing analysis incorporating the squeeze film air damping forces, electrostatic forces, force due to piezoelectric effects, and the asperity-based contact forces. From the predicted responses, quantify pertinent parameters that govern the bounce behavior.

- Investigate bouncing dynamic behavior of the switch under harmonic perturbations in actuation voltage and examine the possible performance degradation as well benefits. Assess the improvement in the bouncing behavior when harmonic perturbations in the actuation voltage of electrostatically actuated switch are used. Investigate the possible usefulness of using combined primary electrostatic and secondary piezoelectric actuations to examine the influences of harmonic dither in the secondary actuator voltage on the bouncing behavior via numerical simulation.

- Quantify the effect of switch and switch tip parameter uncertainties on the bouncing behavior. Assess the influence of uncertainty in beam as well as beam tip parameters on the switch performance via measure of second order statistics of pertinent bounce performance parameters.

- Develop models that characterize the bouncing behavior of cantilever-based NEM switches incorporating van der Waals force, Casimir force, surface effects and damping rarefication effect as well as asperity-based contact force. Predict dynamic response of electrostatically actuated and quantify pertinent parameters that govern the bounce behavior. Investigate the possibility of using pure Casimir force for nano-switch actuation and quantify relevant bounce parameters.

1.4 Thesis outline

This dissertation is divided into seven chapters, and is organized in the following way:

Chapter 1 introduces an overview of MEMS/NEMS technology and then provides literature review of mathematical modelling for both MEM and NEM switches and the related aspects for modeling.

Chapter 2 introduces the governing equations that characterize the micro-switch flexural motion for the purposes of dynamic response predictions. The electrostatic actuation force, force due to a piezoelectric effect, the squeezed air film damping between the switch and the substrate, and the asperity-based contact boundary condition have also been incorporated. An approximate approach based on Galerkin's method is suggested to solve the discretized system numerically, since closed-form solutions are not achievable in this case.

Chapter 3 presents a transient dynamic analysis of a typical cantilever type MEM switch. Bouncing which is responsible for switch performance degradation is illustrated. Performance parameters that describe the bouncing behavior of the switch such as initial contact time, permanent contact time, major bounce height, and number of significant bounces have been introduced and quantified. In addition, effect of harmonic dither in actuation electrostatic voltage as well as harmonic perturbations in the secondary PZT actuator voltage on the bouncing behavior have been illustrated. Regions of improvement in the switch bounce behavior due to frequency and amplitude of the harmonic perturbations are also demonstrated.

Chapter 4 demonstrates the influences of uncertainty in switch and switch tip parameters on the switch performance. Second order statistical measures of the switch output response have been used to quantify the effects of uncertainty in the system parameters. These influences on significant switch performance parameters such as initial contact time and major bounce height have been quantified.

Chapter 5 provides the mathematical models that describe the dynamic behavior of cantilever NEM switches which are actuated electrostatically or via Casimir force. In both models, surface effects, intermolecular forces and damping are considered. Based on the surface elasticity model and the generalized Young-Laplace equation, both surface stress and surface elasticity are incorporated in governing equations, while intermolecular forces are taken into consideration using quantum field theory. Damping has also been incorporated in the model with consideration of the rarefication effect. The idea of switchable Casimir-force devices is proposed for the purpose of paving a new way to operate a switch by purely altering the magnitude of the Casimir force.

Chapter 6 presents the bouncing dynamic analysis of a typical electrostatically actuated cantilever type NEM switch. Performance parameters similar to the ones described of MEM switches are also introduced. The influence of surface effects on the pull-in parameters has been studied considering the bouncing behavior under different vacuum pressures. For pure Casimir actuated switch, the bouncing dynamic response has also been studied. The influence of switching parameters on the bouncing behavior have also been presented for different vacuum pressure values.

Chapter 7 gives a summary of the thesis and highlights the contributions of candidate's work. Recommendations for further research are also presented.

CHAPTER 2

MODELING OF A MEM SWITCH

2.1 Introduction

In this chapter, mathematical models of cantilever beam-based MEM switches are derived to describe the bouncing dynamics. A model that includes a comprehensive set of interacting forces as multimodal interactions is employed to study the bouncing dynamics of micro-switches. For the purposes of capturing accurate bouncing dynamics, a more realistic asperity-based contact force which represents the nonlinear contact mechanics between the beam tip and the substrate has been developed. This model also incorporates a squeeze-film damping force based on a modified Reynolds' equation. An electrostatic actuation force with consideration of the fringing effect has also been incorporated in the model. In addition to these forces, an induced moment due to the piezoelectric layer effect has also been formulated and further incorporated in the equation of motion of an alternative switch model with combined actuation. Euler-Bernoulli beam theory is utilized to formulate the equation of motion that governs the switch dynamics. For response predictions, natural frequencies and mode shapes of the cantilever beam are evaluated and then an approximate numerical approach based on Galerkin's method is employed, since closed-form solutions are not achievable in such nonlinear systems.

2.1 Equations of motion for a switch under electrostatic actuation

The MEM switch is generally modelled as a cantilever beam or a clamped-clamped beam. In the current work, a typical micro switch device which has a cantilever configuration of length L, beam tip gap d_T, beam initial gap d , beam thickness b , beam tip length L_T , and beam width a as shown in Figure 2.1 is employed. In this configuration, an electrostatic force is used to actuate this switch. When sufficient voltage V is applied via an electrode of length $L_2 - L_1$, an electrostatic force is generated, and the beam is pulled down to make contact between the free end tip and the drain. Due to scale effects, the air damping force

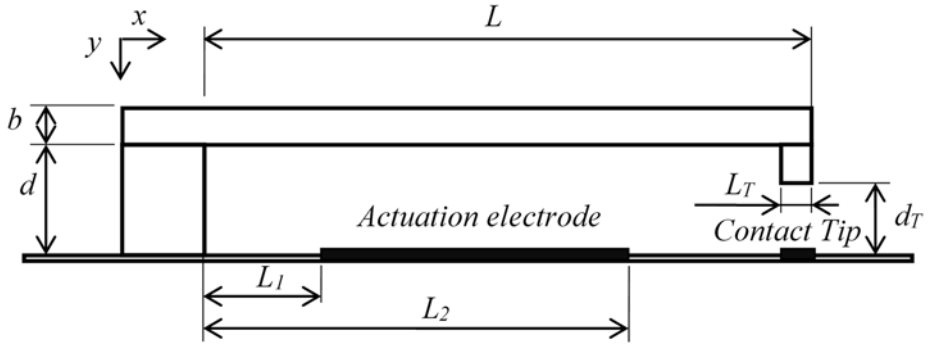

Fig. 2.1. Typical cantilever beam type micro-switch with electrostatic electrode.

cannot be ignored, and hence, a modified Reynolds' equation is employed to formulate the damping force. Further, the contact boundary condition is also included using an asperity-based contact model which is more realistic when compared with linear spring models. The material for the switch is assumed to be as isotropic and homogeneous.

Euler-Bernoulli beam theory is used to develop the equation of motion that governs the flexural dynamics of the switch. When the electrostatic force, air-damping force, and the contact force are incorporated in the modeling, the equation takes the form (Tung *et al.*, 2014):

$$\frac{\partial^2}{\partial x^2}\left(EI(x)\frac{\partial^2 y(x,t)}{\partial x^2}\right) + \rho A(x)\frac{\partial^2 y(x,t)}{\partial t^2} = f_E + f_D - f_C\,, \tag{2.1}$$

where $y(x,t)$ is the transverse displacement of the beam. E is the Young's modulus and ρ is beam material mass density per unit volume, while A , I, respectively, denote the area and moment of inertia associated with the beam's cross-section. f_E represents the actuation electrostatic force while f_D and f_C , respectively, denote the squeezed-film damping force and the contact force. It may be noted that all applied forces are expressed per unit length of the beam. The detailed expressions for these forces are discussed in the following sections

2.1.1 Electrostatic force

When a voltage V is applied between the two electrodes of the switch, an electrostatic force is generated, which is equivalent to applying a distributed transverse load to the movable electrode. Ideally the electrostatic field is uniform between the opposite electrodes; however, a uniform electrostatic field cannot drop to zero abruptly at the edges of the electrodes, and a "fringing field" always exists in a real situation. With the consideration of the fringing effect, the electrostatic force per unit length of the beam is denoted by f_E and it takes the following form (Bao, 2001):

$$f_E = \frac{\varepsilon_0 V^2 a}{2h^2}(1+\beta)[H(x-L_1) - H(x-L_2)]\,. \tag{2.2}$$

The parameter ε_0 denotes the permittivity of air, V represents the applied voltage between the electrode and the beam, $h = d - y$, and β represents the fringe effect correction coefficient. The function, $H(x)$, denotes the Heaviside step function, and the electrostatic force is considered to act on the beam segment between lengths L_1 and L_2. The fringe effect correction coefficient takes the following form (Bao, 2001):

$$\beta = \frac{h}{\pi a}\ln\frac{\pi a}{h} + \frac{h}{\pi a}\ln\left(1 + \frac{2b}{h} + 2\sqrt{\frac{b}{h} + \frac{b^2}{h^2}}\right). \tag{2.3}$$

2.1.2 Squeeze-film damping force

In general, at ambient or moderately low pressure, the major dissipation phenomenon is usually fluid damping: squeeze-film damping when the micromechanical structure moves perpendicular to the substrate, slide-film damping when it moves parallel to the substrate and viscous drag when it is far from the substrate. Switches generally fall in the first category. Due to large surface to volume ratio of a MEM switch, the squeeze film air damping has a significant effect on the switch dynamics. Therefore; the damping effects of air in micro-scale have been included in the form of the squeeze-film air damping. Xu and Jia (2008) utilized the modified Reynolds' equation to represent the squeeze-film air

damping force. A simplified form of the Navier–Stokes equation, the Reynolds equation, has been employed to derive the squeeze-film damping pressure due to the air film between the beam and the substrate. Reynolds equation assumes that the effects of inertia are small compared to those of viscosity and pressure forces in the fluid film. The motion of the beam is assumed to be in the transverse direction such that surfaces of the beam and substrate approaching normally. For this type of relative motion, the beam sliding velocity is equal to zero and the Reynolds equation can be reduced to

$$\frac{\partial}{\partial x}\left(\frac{\rho h^3}{12\mu}\frac{\partial P}{\partial x}\right)+\frac{\partial}{\partial z}\left(\frac{\rho h^3}{12\mu}\frac{\partial P}{\partial z}\right)=\frac{\partial(\rho h)}{\partial t}, \tag{2.4}$$

where μ denotes the air viscosity that takes a value of $1.86\times10^{-5}\ N.s/m^2$ at 30^oC and ρ is the density of air. The air gap between the beam and the substrate is denoted by h where $h=d-y$. When ρ and μ are constant throughout the fluid and assuming that h is independent of z, this equation can be further simplified by assuming that the pressure, $P(x,z)$, is a separable function in x and z directions and takes a parabolic shape in the z-direction. Further, the thin film pressure P consists of the ambient atmospheric pressure P_a and the dynamic pressure ΔP as given below:

$$P(x,z)=P_a+\Delta P=P_a+P(x)\left(1-\frac{4z^2}{a^2}\right). \tag{2.5}$$

Use of non-dimensional quantities $\bar{x}=x/L$, $\overline{h}=h/h_0$ and $\bar{a}=a/h_0$ where h_0 is the initial air gap between the beam and the substrate and substitution of Eq. (2.5) into Eq. (2.4), yield the following equation:

$$\begin{aligned}3\,\bar{h}^2\left(\frac{h_0}{L}\right)^2\frac{\partial\bar{h}}{\partial\bar{x}}\,\frac{\partial P(\bar{x})}{\partial\bar{x}}\left(\frac{1-4z^2}{a^2}\right)+\bar{h}^2\left(\frac{h_0}{L}\right)^2\frac{\partial\bar{h}}{\partial\bar{x}}\,\frac{\partial^2P(\bar{x})}{\partial\bar{x}^2}\left(\frac{1-4z^2}{a^2}\right)\\-\frac{8\bar{h}^3P(\bar{x})}{\bar{a}^2}=12\mu\,\frac{\partial\bar{h}}{\partial t},\end{aligned} \tag{2.6}$$

Since $h_0 \ll L$, Eq. (2.6) can be simplified by neglecting terms of order $\left(\frac{h_0}{L}\right)^2$ and the equation takes the following form:

$$P(x) = -12\mu \frac{\bar{a}^2}{8\bar{h}^3}\frac{\partial \bar{h}}{\partial t} = -12\mu \frac{a^2}{8h^3}\frac{\partial h}{\partial t}. \tag{2.7}$$

Thus, the squeeze film force per unit length is

$$f_D = \int_{-a/2}^{a/2} P(x)\left(1 - \frac{4z^2}{a^2}\right)dz = -\frac{\mu a^3}{h^3}\frac{\partial h}{\partial t}. \tag{2.8}$$

2.1.3 Contact force

The first statistical elastic contact model of rough surfaces was presented by Greenwood and Williamson (1966). In this model, the contact of two rough surfaces is equivalently treated as the contact between a smooth plane and a nominally flat surface with some roughness profile. Contact between individual asperities was assumed to deform elastically according to Hertz theory. The heights of the asperities vary randomly and are defined by a Gaussian height distribution function $\phi(\xi)$, where ξ denotes the asperity height. Asperities are spherical near their summits and all asperity summits have the same radius R; and are sufficiently separated to be mechanically independent. There is no bulk deformation and only the asperities deform during contact. Fig 2.2 shows the model of such contacting rough surfaces. Hence, the force upon contact can be formulated as follows:

$$\eta\, A_n \int_{y-d_T}^{\infty} P_0(w)\phi(\xi)d\xi\,, \tag{2.9}$$

where η is the area density of asperities, A_n represents the nominal contact area, $\phi(\xi)$ denotes the asperity height distribution function, while $w = \xi - (y - d_T)$. The applied load for a single asperity based on Hertzian contact theory is represented by $P_0(w)$ (Greenwood & Williamson, 1966):

$$P_0(w) = \frac{4}{3}E^* R^{\frac{1}{2}} w^{\frac{3}{2}}, \tag{2.10}$$

where

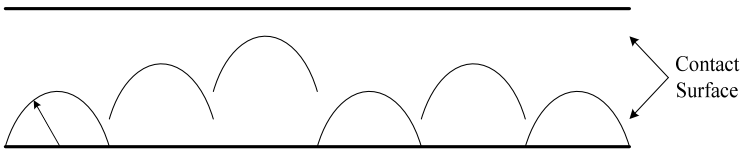

Fig. 2.2. Contacting rough surfaces (Wang, 2009).

$$\frac{1}{E^*} = \frac{1 - v_1^2}{E_1} + \frac{1 - v_2^2}{E_2} \ . \tag{2.11}$$

In Eq. (2.10), P_0 represents the applied load while R and w, respectively, denote the radius of the spherical asperity and the contact interference. The equivalent Young's modulus E^* is based on the Young's moduli E_1, E_2 and the Poisson's ratios v_1 , v_2 of the two contact surfaces. Since the asperity height distribution is Gaussian, therefore $\phi(\xi)$ can be formulated as:

$$\phi(\xi) = \frac{1}{\sqrt{2\,\pi\,\sigma_{AH}^2}}\ e^{-\frac{(\xi - M_H)^2}{2\,\sigma_{AH}^2}} \ , \tag{2.12}$$

where M_H denotes the mean value of the asperity height, while σ_{AH}^2 represents the variance of the asperity height.

Theoretically, the assumed height distribution implies that the height of the asperities can be infinity. This assumption is not practical for dynamic studies since impacting bodies (surfaces) must have a clear boundary before and after contact. In other words, no force acts on the surfaces before the contact is made. Wang (2009) modified this model to overcome this unrealistic dynamic situation and proposed two simplified models based on the Greenwood-Williams model. A model with uniformly distributed asperity height and identical radii and another model with a Gaussian asperity radius distribution and asperity height are equal to the asperity radius or equal to a fixed value whichever is less. Simulations of the above two models carried out by Wang (2009) revealed that both models provide more realistic situation since the contact force becomes zero for zero interference

and their outcomes are very similar and hence the first formulation is adapted in the present study for its simplicity. It may be noted that this contact-tip model is more appropriate for representing the contact dynamics when compared with simple linear spring models employed in previous studies (Wang, 2009). Hence, the dynamic response prediction using the present contact-tip model is expected to lead to more realistic predictions.

2.2 Equations of motion for a switch under combined electrostatic and piezoelectric actuation

In a switch with combined actuation, the model that represents the electrostatic force is similar to the one described in section 2.1 whereas the secondary piezoelectric actuator has a different concept for its action. The actuation mechanism in this case takes advantage of the inverse piezoelectric effect that a voltage, V_p, across certain surfaces of a ferroelectric material, e.g. PZT (Lead Zirconate Titanate, piezoelectric ceramic material), causes elastic deformation of materials. When this material expands or contracts in its plane against the constraint of the cantilever substrate due to bonding, the cantilever bends either upwards or downwards, depending on the polarisation of the piezoelectric film and the actuation voltage polarity. This deflection may be employed to close an initially open switch. The piezoelectric layer is sandwiched between two thin metal electrode layers, with thickness of the order of angstroms. In order to study the effect of a secondary actuator on the switch dynamic behavior, an additional piezoelectric actuator is assumed to be bonded perfectly to the beam top surface. Fig 2.3 shows the configuration with the piezoelectric actuator; however, the thin metal electrode layers are not shown in the figure. The actuation voltage is applied to the secondary actuator of length $L_4 - L_3$. The piezoelectric actuator is assumed to have a width, a_p , similar to the beam width and a thickness b_p. Other parameters of the switch are identical to the parameters of switch shown in Fig 2.1. Euler

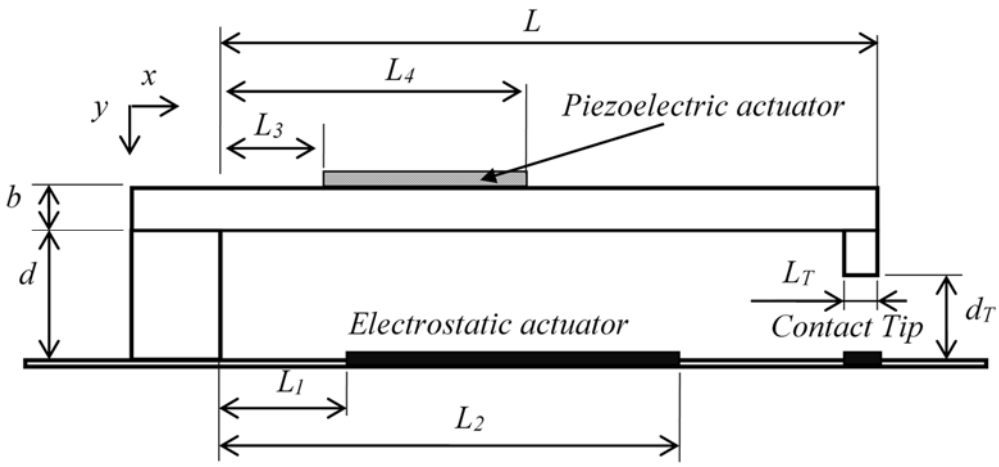

Fig. 2.3. Cantilever beam type micro-switch with electrostatic and piezoelectric actuators.

Bernoulli beam theory is used to develop the equation of motion that governs the flexural dynamics of the switch. In addition to the electrostatic force, air-damping force, and the contact force, a piezoelectric force is incorporated in the model. To this end, a distributed moment $M_p(x,t)$, between the PZT actuator and beam surfaces is induced when bonding between the beam and piezoelectric layer is ideal. This moment can be calculated by Kirchhoff's hypothesis (Zhang *et al.*, 2006). The piezoceramic actuator is assumed to be of a uniform geometry and the voltage applied along its length is assumed spatially uniform. The strain induced by the actuator when a control voltage $V_p(x,t)$ is applied is given by

$$\varepsilon_p = \frac{d_{31}}{b_p} V_p(x,t) \ , \tag{2.13}$$

where b_p represents piezoceramics thickness while d_{31} is a piezoceramic constant. In the cantilever configuration, the directions 1 and 3 correspond to the x and z axes, and the poling direction of the piezoelectric layer is parallel to the z-axis. This induced strain ε_p creates a longitudinal strain ε_{lp} due to the force equilibrium. The relationship between these strains can be given as:

$$\varepsilon_{lp} = \frac{E\ A}{EA+E_p\ A_p}\varepsilon_p\ , \tag{2.14}$$

where the subscript p refers to the piezoelectric parameters. An expression for bending moment $M_p(x,t)$, produced by the piezoceramic actuator, can be obtained from Eqs. (2.13) and (2.14) under consideration of the force equilibrium in the axial direction:

$$M_p(x,t) = E\ b\ a\ \varepsilon_{lp}\left(\frac{b}{2} - C_A\right) - \ E_p\ b_p\ a_p\ (\varepsilon_p - \varepsilon_{lp})\left(\frac{b_p}{2} + b - C_A\right)\ , \tag{2.15}$$

where C_A represents the location of the neutral axis of a section that includes the piezoelectric layer measured from the beam bottom layer and is given by:

$$C_A = \frac{E\ b^2\ a + \ E_p\ b_p^2\ a_p + 2E_p\ b\ b_p\ a_p}{2\left(E\ b\ a + E_p\ b_p\ a_p\right)}\ . \tag{2.16}$$

Substitution of Eqs. (2.13), (2.14), and (2.16) into Eq. (2.15) yields:

$$M_p(x,t) = \ C_0\ V_p(x,t)\ , \tag{2.17}$$

with C_0 representing a proportionality constant given by

$$C_0 = \frac{E\ E_p\ a\ a_p\ b(b_p + b)\ d_{31}}{2(E\ b\ a + \ E_p\ b_p\ a_p)}\ .$$

Considering the applied moment, the equation of motion that governs the flexural dynamics of the switch can be formulated using Euler-Bernoulli beam theory. The equation takes the form:

$$\frac{\partial^2}{\partial x^2}\left(EI(x)\frac{\partial^2 y(x,t)}{\partial x^2}\right) + \rho A(x)\frac{\partial^2 y(x,t)}{\partial t^2} = \ \frac{\partial^2 M_p(x,t)}{\partial x^2} + f_E + f_D - f_C\ . \tag{2.18}$$

Except for the moment induced force term on the right-hand side of Eq. (2.18), other terms are similar to the terms in Eq. (2.1). Thus, the micro-cantilever beam equation of motion can be rewritten as:

$$\frac{\partial^2}{\partial x^2}\left(EI(x)\frac{\partial^2 y(x,t)}{\partial x^2}\right)+\rho A(x)\frac{\partial^2 y(x,t)}{\partial t^2}= \\ C_0\, V_p(x,t)[\,\grave{\delta}(x-L_3)-\,\grave{\delta}(x-L_4)]+f_E+f_D-f_C\,, \tag{2.19}$$

where $\grave{\delta}(x)$ is the spatial derivative of the Dirac delta function with respect to x. It may be noted that the electrostatic and the squeeze-film damping forces are inversely proportional to different powers of the electrode separation and that the contact force has nonlinear characteristics due to the discontinuity definition as well as due to fractional proportionality of the interface of the asperities. Hence, MEM switches exhibit inherently nonlinear dynamic behavior which makes the prediction on the dynamics rather challenging.

2.3 Evaluation of cantilever beam natural frequencies and mode shapes

Based on the proposed models presented above, a partial differential equation that governs the beam dynamic behavior is established. Galerkin's approach is used to develop an approximate solution since closed-form solutions of the governing equations are not achievable. For this purpose, natural frequencies and mode shapes of the cantilever beam are evaluated first. By employing the Galerkin's method, the continuous system can be discretized to form a system of ordinary differential equations (ODE's) which is solved numerically. The solutions of these ODE's are then used to predict the response. To this end, the transverse displacement of the beam is written in the following form:

$$y(x,t)=\sum_{r=1}^{n} Y_r(x)\, q_r(t). \tag{2.20}$$

In Eq. (2.20), $Y_r(x)$ and $q_r(t)$, respectively, represent the normalized normal mode shapes and temporal coordinates that govern the beam motion. The cantilever beam is subjected to the following boundary conditions:

$$y(0,t)=0;\quad \frac{\partial y(0,t)}{\partial x}=0;\quad EI\frac{\partial^2 y(L,t)}{\partial x^2}=0;\quad EI\frac{\partial^3 y(L,t)}{\partial x^3}=0\,. \tag{2.21}$$

For the fixed end, both displacement and slope are zero; and for the free end, both shear force and bending moment are zero. The mode shapes are normalized as follows:

$$Y_r(x) = \frac{\bar{Y}_r(x)}{\sqrt{\int_0^L \rho A(x)\bar{Y}_r(x)\bar{Y}_r(x)dx}} \tag{2.22}$$

where $\bar{Y}_r(x)$ is the eigenfunctions which takes the form:

$$\bar{Y}_r(x) = C_r[\sin\beta_r x - \sinh\beta_r x - a_r(\cos\beta_r x - \cosh\beta_r x)] \tag{2.23}$$

where

$$a_r = \frac{\sin\beta_r L + \sinh\beta_r L}{\cos\beta_r L + \cosh\beta_r L}$$

The natural frequencies are expressed as $\omega_r = \beta_r^2\sqrt{\frac{EI}{\rho A}}$, where β_r is calculated through the frequency equation

$$\cos\beta_r L \,.\cosh\beta_r L = -1 \tag{2.24}$$

where $\beta_r L$ are the eigenvalues and L represents the length of the beam. Solution of Eq. (2.24) yields the eigenvalues. The first six eigenvalues for the cantilever beam are:

$$\beta_1 L = 1.875104;\ \beta_2 L = 4.694091;\ \beta_3 L = 7.854757;\ \beta_4 L = 10.995541;\ \beta_5 L = 14.137169;\ \ \beta_6 L = 17.278760;\ \ldots,$$

2.4 Discretized model for response predictions

By employing Galerkin's method, the continuous system can be discretized. For the purposes of response predictions, normalized modes associated with the natural frequencies and mode shapes as evaluated in previous section are employed. Substituting Eq. (2.20) into the beam equations of motion and multiplying by $Y_r(x)$ on both sides and

integrating over the length of the beam, the following ODE's representing the motion are obtained:

$$\boldsymbol{M\ddot{q}} + \boldsymbol{Kq} = \boldsymbol{N}, \tag{2.25}$$

The elements of the mass matrix, $\boldsymbol{M}$, and the stiffness matrix, $\boldsymbol{K}$, are given as follows:

$$m_{rs} = \int_0^L \rho A\, Y_r(x) Y_s(x) dx, \quad r, s = 1,2, \dots, n\,, \tag{2.26}$$

$$k_{rs} = \int_0^L EI\, \frac{d^2 Y_r(x)}{dx^2} \frac{d^2 Y_s(x)}{dx^2} dx, \quad r, s = 1,2, \dots, n. \tag{2.27}$$

and $\boldsymbol{N}$ represents the vector of modal forces given by the expression

$$N_r = \int_0^L Y_r(x) f dx\,, \quad r = 1,2, \dots, n, \tag{2.28}$$

where n represents the number of normal modes used in the simulation while f denotes the resultant external applied forces on the beam.

Discretization of the switch with a piezoelectric actuator is similar to the discretization of the electrostatically actuated switch. Eq. (2.25) has the similar form in the case of a piezoelectric actuated switch but with different elements for the corresponding matrices. In this case, the elements of the mass matrix, $\boldsymbol{M}$, the stiffness matrix, $\boldsymbol{K}$, and the modal forces vector, $\boldsymbol{N}$, are given as follows:

$$m_{rs} = \int_0^L \rho A\, Y_r(x) Y_s(x) dx + \int_{\mathrm{L_3}}^{\mathrm{L_4}} \rho_p A_p\, Y_r(x) Y_s(x) dx, \quad r, s = 1,2, \dots, n\,, \tag{2.29}$$

$$k_{rs} = \int_0^L EI\, \frac{d^2 Y_r(x)}{dx^2} \frac{d^2 Y_s(x)}{dx^2} dx + \int_{\mathrm{L_3}}^{\mathrm{L_4}} E_p I_p\, \frac{d^2 Y_r(x)}{dx^2} \frac{d^2 Y_s(x)}{dx^2} dx, \quad r, s = 1,2, \dots, n. \tag{2.30}$$

$$N_r = \int_0^L Y_r(x) f dx + C_0 \left(\frac{dY_r(L_4)}{dx} - \frac{dY_r(L_3)}{dx} \right), \quad r = 1,2, \dots, n, \tag{2.31}$$

The numerical calculation procedure for predicting the beam response is provided in the following section.

2.5 Response predictions

The equations of motion in the normal co-ordinates as given by Equations (2.25) represent a system of nonlinear equations since the force term includes forces that depend on the system output such as displacements and velocities. The system is subject to the initial displacement and velocity, $x(0) = x_0$ and $\dot{x}(0) = v_0$, respectively. If an assumption is made that during a sufficiently small time-step, only a finite small displacement is obtained, the forces N_r can be considered to take a constant value during this finite small-time step. Then the equations can be solved and the temporal coordinates in Eq. (2.25) can be used to calculate the system response during each time step. The detailed calculation procedures are provided in the flow chart illustrated via Figure 2.4. The ode45 solver of the MATLAB is used to solve the system of ordinary equations numerically. The ode45 is based on an explicit Runge-Kutta (4, 5) formula, the Dormand-Prince pair (The MathWorks, 2013).

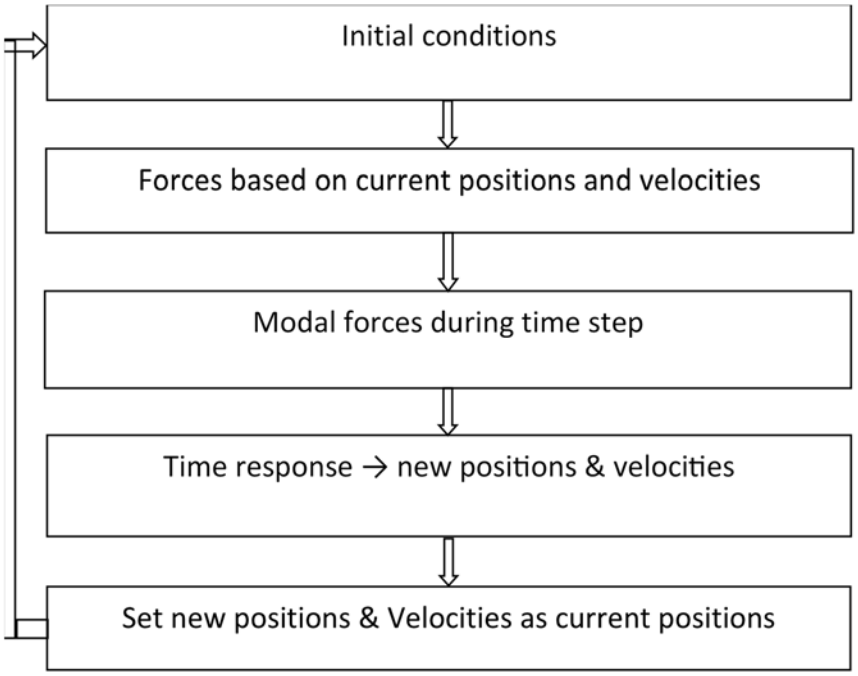

Fig. 2.4. Response prediction process.

2.6 Conclusions

In order to study the beam transient behavior, i.e. contact bouncing, a more realistic nonlinear asperity-based contact force has been incorporated into a comprehensive model for capturing the bouncing dynamics. Squeeze-film air damping force based on the modified Reynolds equation as well as the electrostatic actuation force are also included in the model. In addition to these forces, a secondary piezoelectric actuator model is incorporated into the equation of motion of the cantilever beam switch to investigate the effect of combined actuation on the switch bouncing behavior. Euler-Bernoulli beam theory has been used for the modeling of MEM based switch cantilever beam. Natural frequencies and mode shapes have been evaluated for the switch. Since exact closed form solution of such nonlinear system is not achievable, Galerkin's method is employed to discretize the partial deferential equation that governs the beam motion to get a system of ordinary equations which is solved numerically. Predicted responses from these models are expected to aid the design of micro-switches and improve their performance and reliability.

CHAPTER 3

BOUNCING DYNAMIC ANALYSIS AND MITIGATION FOR A MEM SWITCH

3.1 Introduction

The derived mathematical models of a cantilever-type switch along with the proposed numerical scheme are used to predict the switch response. Simulation of the switch transient response has been performed to quantify the bouncing behavior parameters for an electrostatically actuated switch. In addition, a combined electrostatic and piezoelectric actuation for this switch is also considered in the present study for the purposes of bounce mitigation. Performance parameters such as initial contact time, permanent contact time, major bounce height, and the number of significant bounces have been quantified for the switch response. The possibility of switch bounce improvement has been investigated using harmonic perturbations in the step voltage of an electrostatically actuated switch. In addition, bounce mitigation via secondary piezoelectric actuator has also been investigated using harmonic dither in the voltage of the secondary actuator. Improved response regions for some frequency-amplitude combinations of harmonic perturbations of actuating voltage have been achieved for both actuation methods.

3.2 Switch response under electrostatic actuation

Transient response simulation of a micro switch has been performed to quantify important switch design parameters based on the predicted response. For the purposes of comparison, the material and geometric properties of micro-switch used by Wang (2009) are employed in this work. The values of switch parameters and properties used in this study are described in section 2.2 and are listed in Table 3.1. It may be noted that for all predictions, five normal modes have been used, i.e. $n = 5$.

In order to highlight the system characteristics, the switch model has been used to calculate the pull-in voltage. During the operation of the switch, the inertial effects needs to be

accounted for, since the pull-in voltage is likely to be smaller than the static pull-in voltage. The corresponding voltage is called the dynamic pull-in voltage V_{th}. This instability behavior is known to play an important role in the design of this class of switches. This form of instability is due to the nonlinearities in the electrostatic force. The actuation voltage V_{th}, at this pull-in point has been found to be $80\ V$ for the present configuration. Actuating the switch at voltages below this voltage yields a damped free oscillation of the beam tip without any contact while operating the switch at voltages higher than the pull-in voltage produces a contact between the switch tip and the substrate; eventually the device switches on. During the switch closure stage, the beam contacts the substrate and bounces several times before making a permanent contact with the drain. It may be noted that this bouncing behavior is considered important and dictates the switch performance.

Table 3.1. MEM switch parameters and properties

Parameter	**Value**
Beam length, L	$130\ \mu m$
Beam width, a	$30\ \mu m$
Beam thickness, b	$1.25\ \mu m$
Beam tip contact gap, d_T	$1.5\ \mu m$
Air gap, d	$2.5\ \mu m$
Starting point of electrostatic electrode, L_1	$55\ \mu m$
Ending point of electrostatic electrode, L_2	$95\ \mu m$
Beam tip length, L_T	$10\ \mu m$
Young's modulus for the beam material, E	$78\ GPa$
Poisson's ratios of contact surfaces, v	0.44
Material mass density of the beam, ρ	$19300\ kg/m^3$
Radius of the sphere asperity, R	$100\ nm$
Area density of asperities, η	$150\ asperity/\mu m^2$

The responses of the tip end of the switch for different voltage levels obtained using this model are shown in Figure 3.1. It may be noted from Figure 3.1 that when the actuation voltage is equal to pull-in voltage, the beam touches the substrate without bouncing but it takes a longer time to make the initial contact. As the actuation voltage increases further beyond the pull-in voltage, the time to make the initial contact with the substrate decreases; however, more bounces with increased height appear in the response with the increase of voltage which leads eventually to a longer final permanent contact time. It is also observed from this figure that after the tip makes the first contact, several small bounces followed by a major significant contact bounce is noted and higher actuation voltages leads to earlier single significant bounce occurrence. The simulation results have been compared with previous experimental work performed by Wang (2009) in which the beam transverse motion is measured using a micro scanning Laser doppler vibrometer during typical switching operations employed in the simulation study. When the properties and dimensions are chosen similar to the ones used by Wang (2009), the numerical predictions have been found to match the nature of the experimental results when the area density of

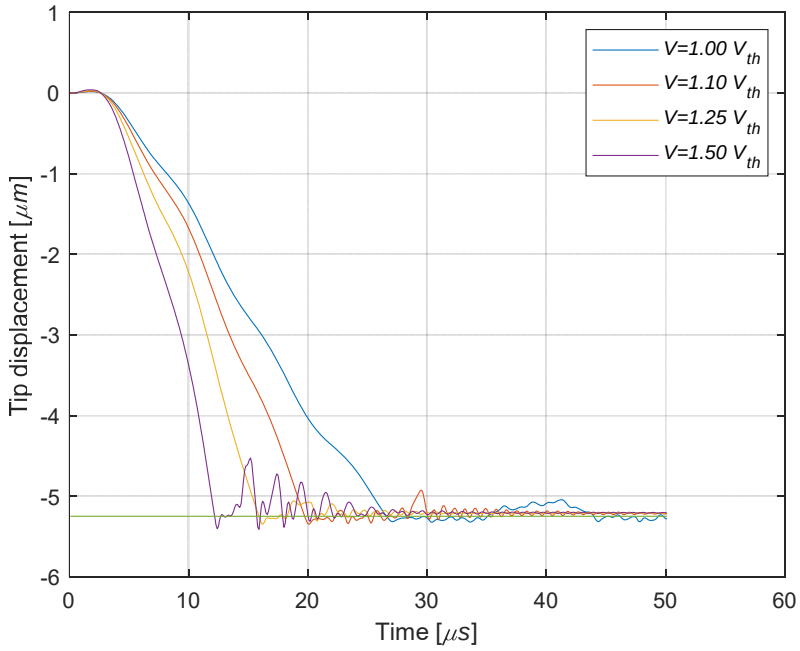

Fig. 3.1. Tip displacements for different actuation voltages.

asperities is 150 $asperity/\mu m^2$. For further verification of the employed model, predictions of the system natural frequencies are performed employing the dimensional parameters and the material properties. The predicted natural frequencies of the switch are listed in Table 3.2. It may be noted that the experimentally measured first two natural frequencies in the study by Wang (2009) are $146.6 \times 10^3\ rad/s$ and $874 \times 10^3\ rad/s$ and are reasonably close to those predicted in the present study. The equipment employed in Wang's experiment have limited band width and only allowed measurement up to the second natural frequency. Further, the other three natural frequencies which were theoretically predicted (2648.3×10^3, 5187.6×10^3 and $8578.8 \times 10^3\ rad/s$) are also in good agreement with those predicted in the present study. Moreover, the overall bounce nature captured by the model has been found to be similar to that found in the experimental study. In the experimental study, the predictions demonstrate that when the actuation voltage is close to V_{th}, the switch touches the substrate without bounce, and for higher voltages, occurrence of a few major bounces has been observed. This phenomenon has also been captured in the present simulation study. It may be noted that the simulation prediction is only based on the first 5 modes, while the experimental prediction, in theory, is based on multiple modes. As well, the imperfections due to fabrication process have not been considered in the simulation study. Owing to the above, it is natural to expect some discrepancies between the two studies and not expect the model to capture all bouncing characteristics. However, the similarities between the two studies provide adequate confidence in using the theoretical model as a basis for understanding switch dynamic characteristics.

Table 3.2. Predicted natural frequencies of the MEM switch

Mode	1	2	3	4	5
Natural frequency $[rad/s]$	150.9×10^3	945.8×10^3	2648.3×10^3	5189.6×10^3	8578.8×10^3

The simulated switch tip bounce response computed for the switch parameters given in Table 3.1 has been depicted in Figure 3.2. The figure shows some of the important parameters that characterize the switch performance as follows:

- Initial contact time, t_i, is the time taken for the first contact.
- Permanent contact time, t_p, is the time taken for the switch to maintain permanent contact.
- Bouncing time, t_b, is the time from the instant of making first contact to the instant when the single significant bounce ends.
- Major bounce height, BH.
- Number of significant bounces, N.

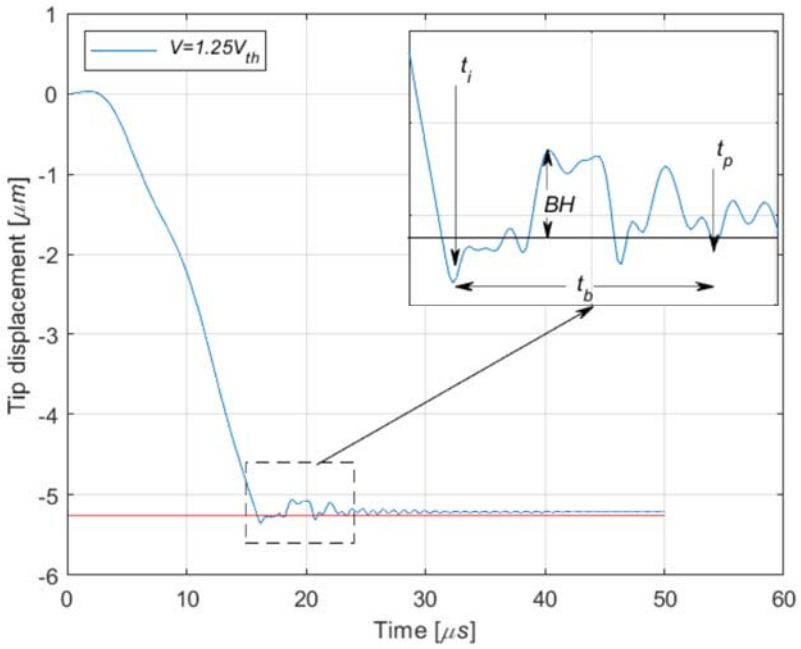

Fig. 3.2. Typical switch tip-end response for $V = 1.25\, V_{th}$.

The variation of the switch performance parameters at different actuation voltages are shown in Figure 3.3 and 3.4. An overall reduction in the switching time with increasing actuation voltages can be observed from Figure 3.3 which indicates that performance improvement can be achieved with higher actuation voltages. However, this improvement

is seen to be obtained at the expense of greater major bounce heights and a greater number of significant bounces as seen in Figure 3.4 which predicts that both the major bounce heights, BH and number of single significant bounces, NB increase with increasing actuation voltages, hence limiting the achievable actuation voltages. From Figures 3.3 and 3.4, it can be seen that a decrease of about 54% for switching time parameters t_i, t_p and t_b whereas there is an increase of 300%, 250% for BH and NB, respectively, when these performance parameters are calculated at $1.0V_{th}$ and $1.5\ V_{th}$, respectively. Further, for the present switch configuration based on the above bounce parameter behavior, it appears that an optimum voltage for operating the switch in the neighborhood of $1.25\ V_{th}$ where both major bounce height and the number of bounces are minimum while the reduction in the permanent contact time is considerable. Actuation of the switch at voltages below the optimal voltage and greater than the pull-in voltage leads to increase in number of bounces with relatively large heights which eventually leads to insufficient reduction in the permanent contact time. Actuation at a low voltage close to the pull-in voltage produces relatively few bounces with small heights, but with long switching time. This phenomenon

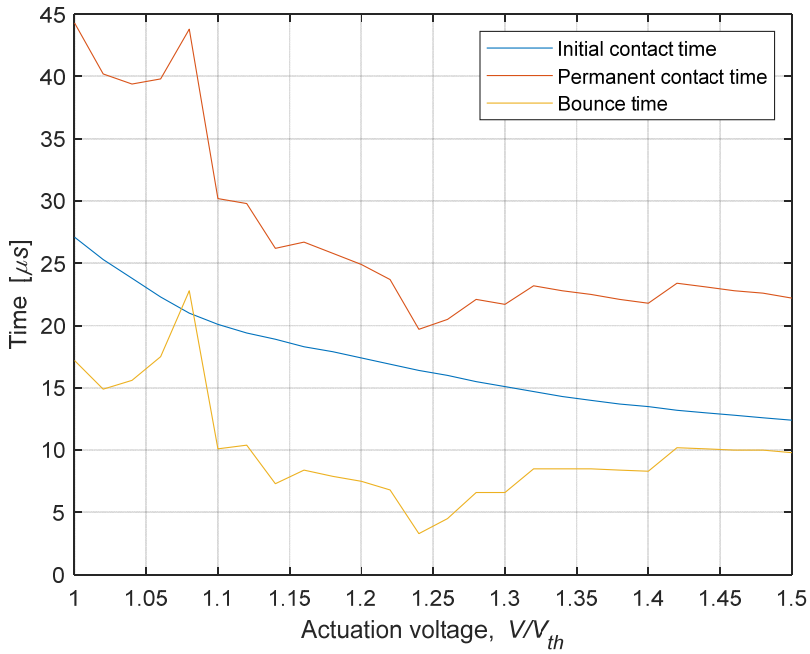

Fig. 3.3. Variation of initial contact time, permanent contact time, and the bounce time vs. actuation voltages.

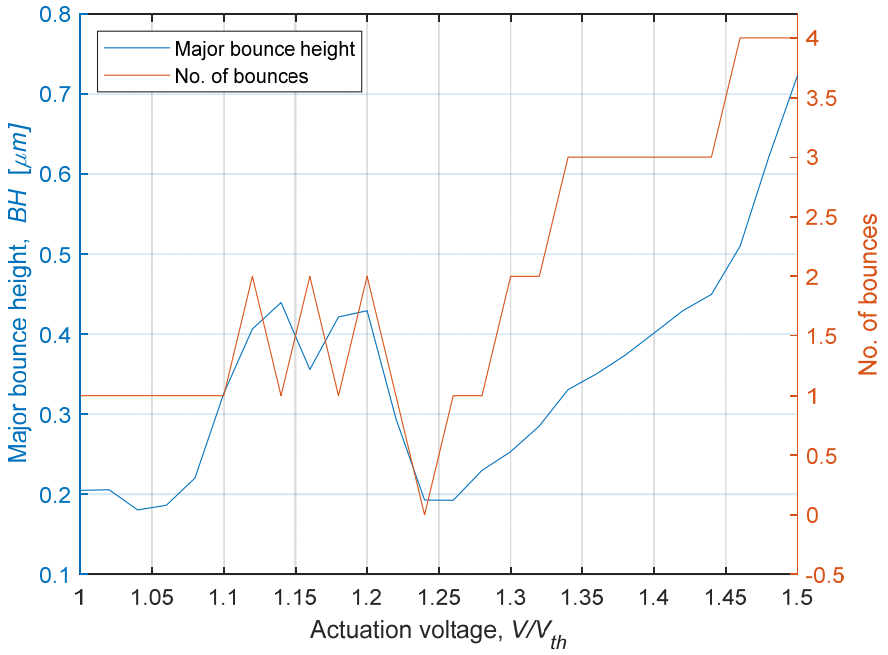

Fig. 3.4. Variation of major bounce height and number of bounces vs. actuation voltages.

may be attributed to the low attractive electrostatic force that pulls down the switch gently and allows the beam to rebound with small bounce heights for a long duration when the tip is close to the substrate. Actuation above the optimal voltage has high attractive force that pulls down the switch strongly with high velocity and initiates hard impact which leads to multiple bounces with large heights. It is worth noting that a threshold amplitude of $0.18\ \mu m$ for the bouncing oscillations is considered in calculation of these performance parameters. So, bounces or oscillations that are smaller than this threshold are designated as the permanent contact stage. A similar criterion has been considered in a study by Granaldi and Decuzzi (2006) and such small oscillations are noticed in previous study by McCarthy *et al.* (2002) where it was attributed to the compression of the tip and the drain during impact and the limitations of the contact tip model. In the next two sections, the possibility of improving the switch bounce performance using harmonic dither in the actuation step voltage of an electrostatically actuated switch and mitigation via secondary piezoelectric actuator using harmonic perturbations in the control voltage is investigated in detail.

3.3 Switch performance under harmonic dither in actuation voltage

It is well known that the bouncing in switches degrades the performance and shortens the switch life. The majority of the available techniques employed to eliminate or reduce the bouncing either use a measurement to perform feedback control in which complex active driver circuitry are essential or they use open loop control techniques which are applicable to a single device and do not account for parameter variations. The possibility of using small amplitude harmonic dither in the actuation voltage to improve the bouncing behavior is investigated in the present study. To this end, the influences of harmonic dither in the step actuation voltage on the bouncing characteristics have been investigated for different actuation voltages at different frequencies and amplitudes of the harmonic dither. Since bouncing appears at voltages higher than the pull-in voltage, three values of step actuation voltage are chosen, namely, $V = 1.1V_{th}$, $V = 1.25V_{th}$ and $V = 1.5V_{th}$, for the purposes of comparison. It may be noted that these voltages represent actuation at or below/above the optimal voltage predicted in section 3.2. Four values of harmonic amplitudes are employed to investigate the influence of the dither amplitude on the bouncing and these amplitudes take the values of 5% , 10%, 15%, and 20% of the step voltage magnitudes. Frequencies are swept from the step actuation waveform voltage (with zero frequency) up to a frequency that exceeds the fifth natural frequency of the MEM switch with linear incremental steps. These natural frequencies are also represented as vertical colored lines in some of the graphs that are associated with frequency variation for increased clarity in making comparison with dither frequency. The results show improvement in the bouncing at specific regions of frequencies and at dither amplitudes may be achieved without extensive prior knowledge of the switch parameters. This feature clearly is advantageous when compared to other mitigation techniques which require measurement of responses and/or knowledge of system parameters. Figures 3.5 through 3.10 show the effects of using harmonic dither in the step actuation voltage on the switch performance parameters.

For relatively low actuation voltages, $V = 1.1V_{th}$, the initial contact time t_i in most cases decreases or remains constant as the amplitude and frequency of harmonic dither increases. Other performance parameters such as the permanent contact time t_p, height of major bounce BH and the number of bounces NB vary with the increase of the amplitude and

frequency of the harmonic dither and this behavior can be seen in Figures 3.5 (a) and 3.5 (b). It may be seen from Figure 3.5 (b) that at this relatively low actuation voltage, relatively low amplitude of the harmonic dither and at a frequency just above the first natural frequency there is a region where the bounce height is moderate, and the region extends to the second natural frequency with increase of amplitude of the harmonic dither. In addition, the bounce height increases with increasing dither amplitudes. This phenomenon may be attributed to the weak attracting force at this low actuation voltage which allows larger bounces at these frequencies. Another region where the bounce heights are relatively small, but the number of bounces is relatively high can be observed in Figure 3.5 (b) at high frequencies closer to the third natural frequency as well as between the fourth and the fifth natural frequencies. In these regions, the number of these small bounces increases with the increase in the amplitude of harmonic dither, and at very high dither amplitude their heights go up as well. As mentioned earlier, an increase of the number of bounces or the height of bounces contributes to longer final permanent contact time therefore at high frequencies the permanent contact time increases in these frequency regions due to the number multiple small bounces or larger bounces as can be observed from Figure 3.5(a).

The reduction in the initial contact time at this level of actuation voltage can be observed in Figure 3.5 (a) where the minimum initial contact time occurs just after the first natural frequency and before the region of larger bounces mentioned above. Other regions where improvements in the initial contact time, t_i can be achieved using the harmonic perturbations are observed between the first and the second natural frequencies; however, in these regions the initial contact time is not minimal but other performance parameters such as BH and NB have smaller values than those obtained using the step voltage alone.

Based on the above discussion, it is worth noting that reduction in all performance parameters which leads to better switch response can be achieved close to the first natural frequency. For example, at harmonic dither frequency of $180.5 \times 10^3\ rad/s$ which is just above the first natural frequency and with a dither amplitude of 15% of the actuation step voltage, the initial contact time t_i, has been reduced by 15.5% while the permanent contact time t_p, height of major bounce BH and the number of bounces NB are reduced by 43%,

100%, and 100% , respectively. Figure 3.6 demonstrates, via the bounce responses, the superior performance of the optimal mitigation condition when compared with pure step actuation with no dither. It may be noted that the horizontal colored lines in Figure 3.6 represent the substrate and the bounce height thresholds.

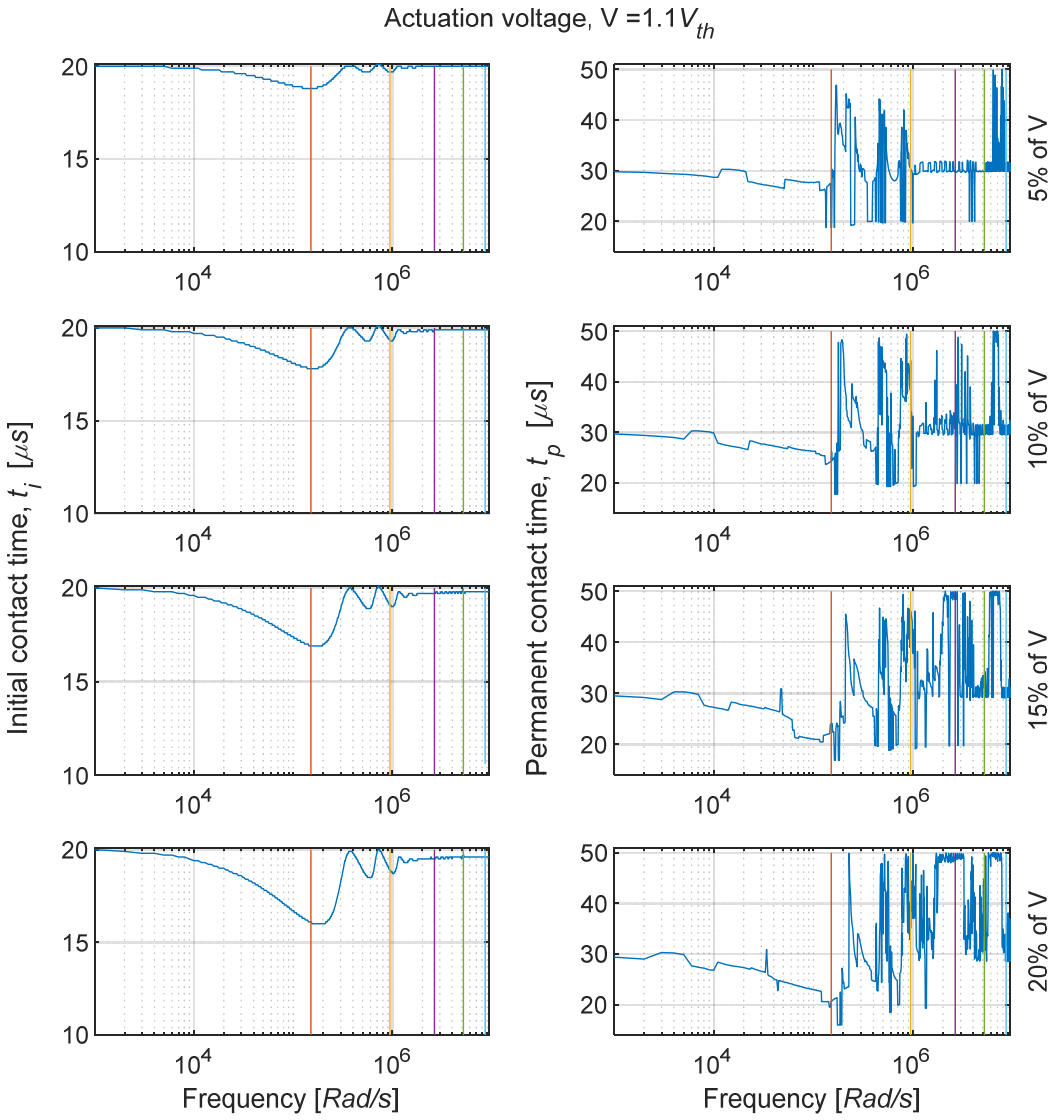

Fig. 3.5 (a). Influence of frequency and amplitude of harmonic dither in electrostatic voltage on initial contact time and permanent contact time for $V = 1.1\, V_{th}$.

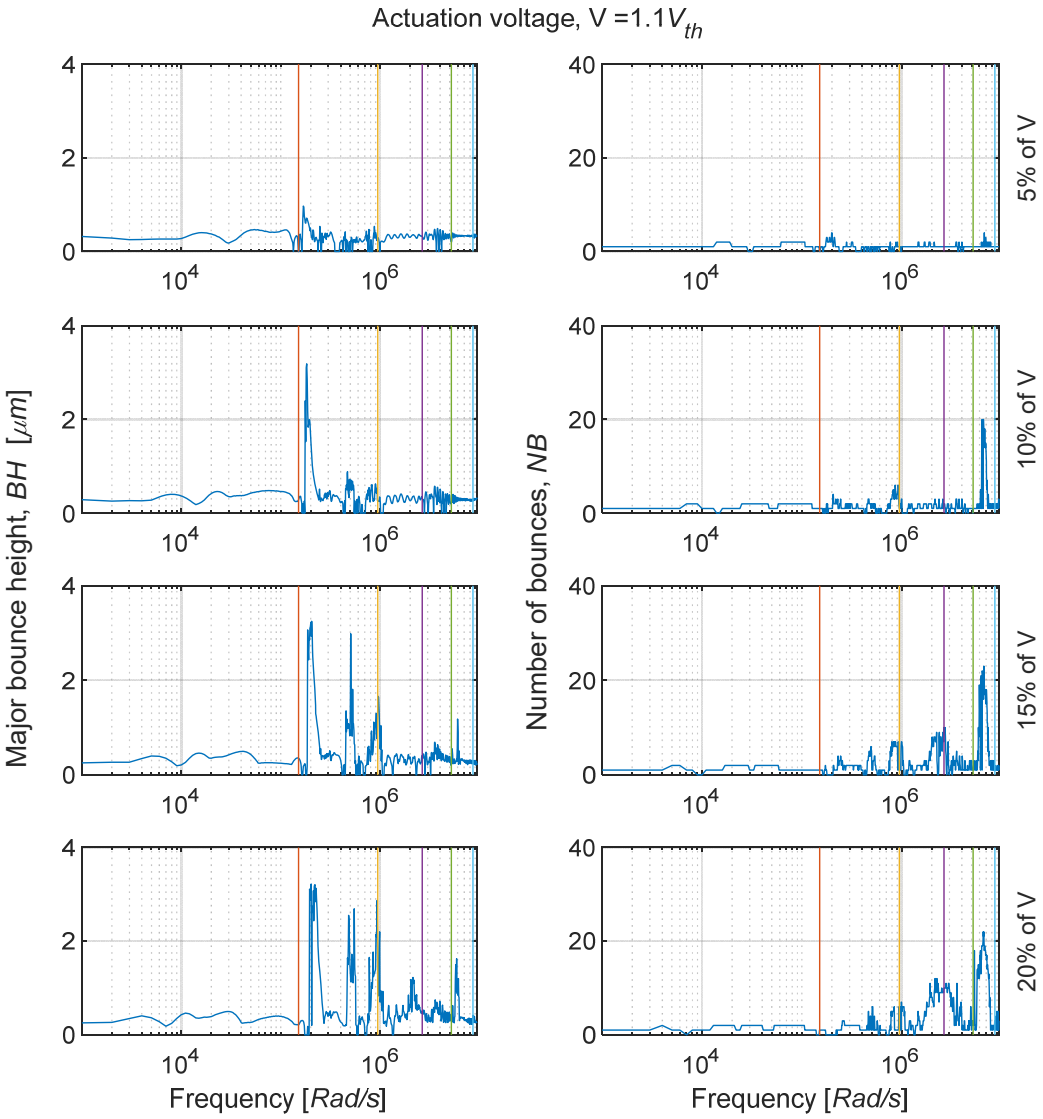

Fig. 3.5 (b). Influence of frequency and amplitude of harmonic dither in electrostatic voltage on major bounce height and number of bounces for $V = 1.1\ V_{th}$

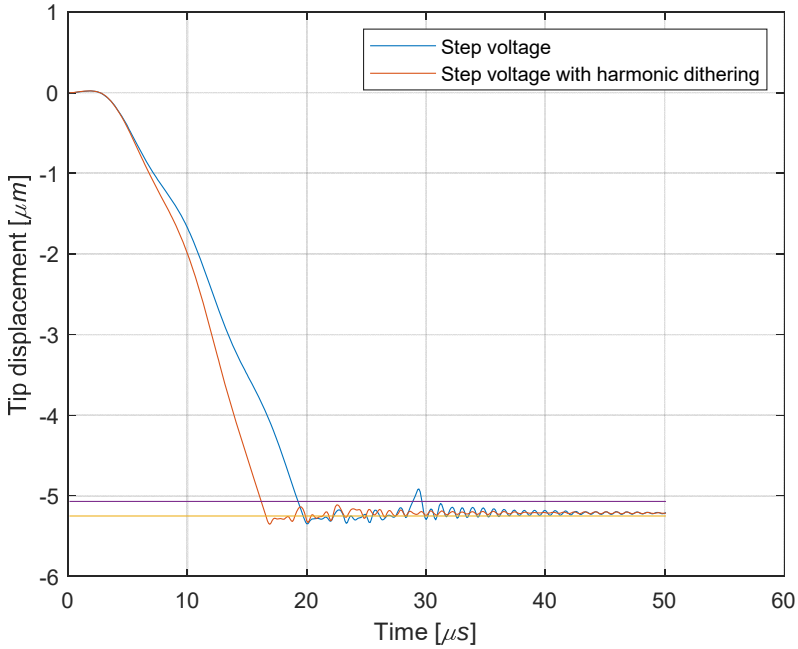

Fig. 3.6. Responses of step voltage and step voltage with harmonic dither of 15% amplitude, $180.5 \times 10^3\ rad/s$ frequency at $V = 1.1\ V_{th}$.

The influences of frequency and amplitude of harmonic perturbations on the switch bouncing behavior at moderate actuation voltage, $V = 1.25V_{th}$, are demonstrated in Figure 3.7 (a) and 3.7 (b) where some similarities in behavior to the case of low actuation voltages have been observed. The initial contact time t_i generally tends to decrease or stays the same for varying frequency and the harmonic dither amplitude. Variations in other performance parameters such as the permanent contact time t_p, height of major bounce BH and the number of bounces NB are apparent with the increase of the amplitude and frequency of the harmonic perturbations. However, in contrast to low actuation voltage where weak attractive electrostatic force is attributed to allowing larger bounces as seen in Figure 3.5 (b), at this moderate actuation voltage no such larger bounce height has been observed as depicted in Figure 3.7 (b). Multiple bounces with relatively moderate height can be seen in Figure 3.7 (b) at the third natural frequency when the amplitude of the harmonic dither is high while multiple bounces with smaller heights are observed in the region between the fourth and the fifth natural frequencies with a tendency to increase bounce height for higher

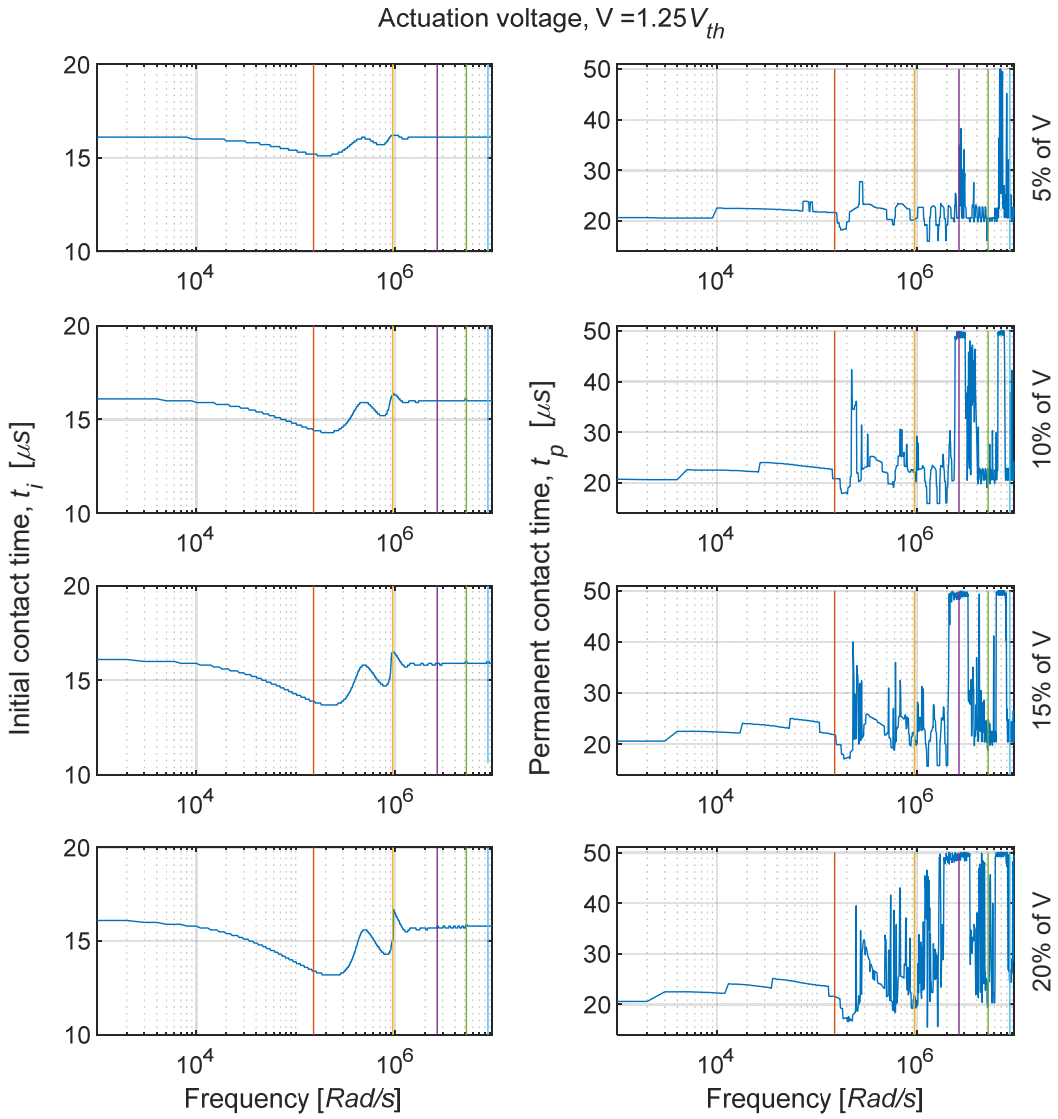

Fig. 3.7 (a). Influence of frequency and amplitude of harmonic dither in electrostatic voltage on initial contact time and permanent contact time for $V = 1.25\, V_{th}$.

amplitudes of harmonic dither. The initial contact time has its minimum value in the region closer to the first natural frequency and in between the first and second natural frequencies; however, parameter such as bounce height has no minimum in this region which limits the achievable improvement in this region. An example of such behavior at frequency just after the first natural frequency is demonstrated in Figure 3.8 where the frequency and amplitude of the harmonic perturbations are $180.5 \times 10^3\ rad/s$ and of 15%, respectively. It is

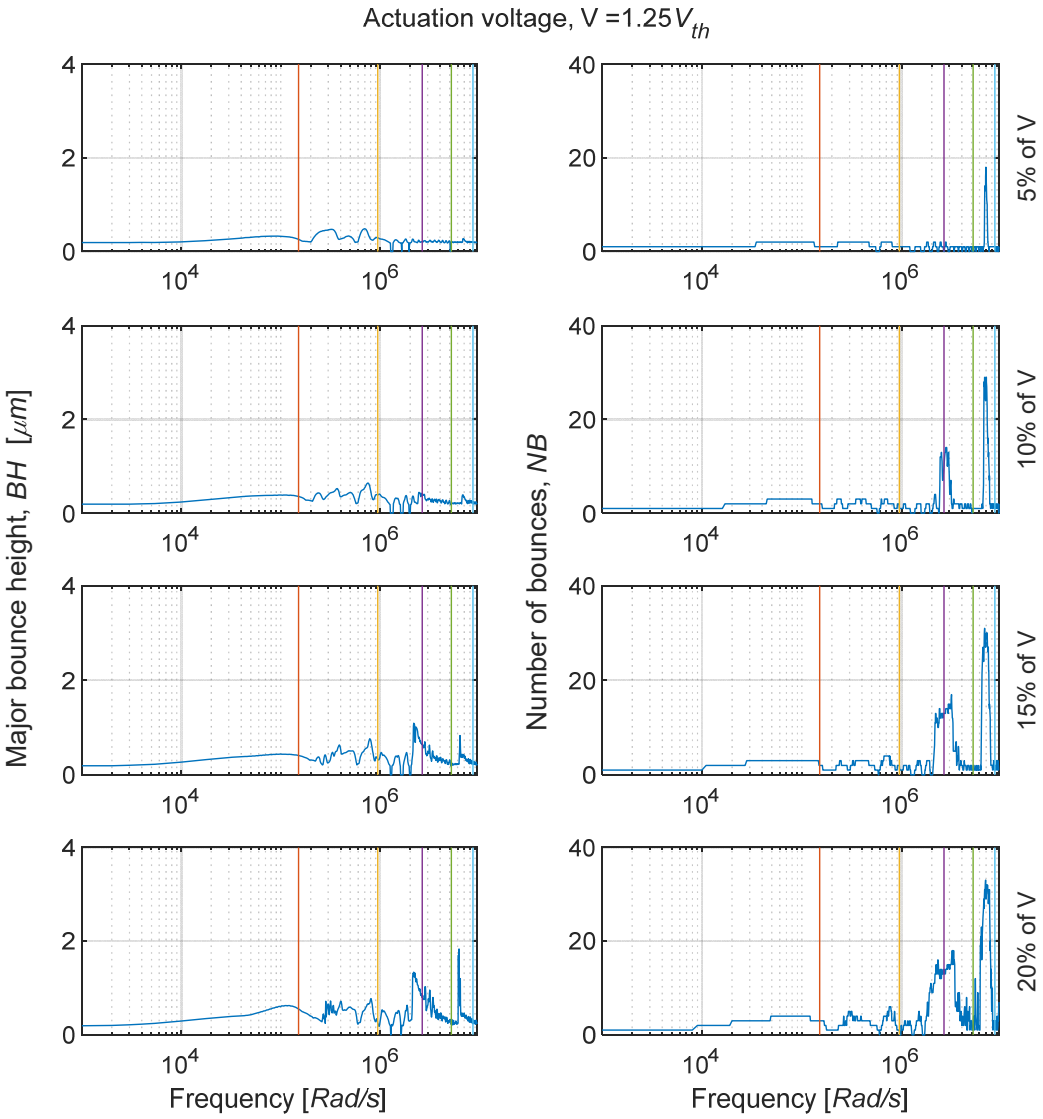

Fig. 3.7 (b). Influence of frequency and amplitude of harmonic dither in electrostatic voltage on major bounce height and number of bounces for $V = 1.25\, V_{th}$.

obvious from the figure that improvement has been achieved in initial contact time and permanent contact time by 19% and 13%, respectively. However, this improvement comes in the expense of bounce height which is increased by 94% while the number of bounces remain constant. This inability in achieving significant improvements can be clearly attributed to the operating condition which is already near the optimal step voltage level based on the predictions made in section 3.2. It is also worth noting that the region

between the second and the third natural frequency has multiple frequencies where both the bounce height and number of bounces are minimum; however, the initial contact time at these frequencies can be observed to be non-minimal and this condition may be of value if bounce heights and the number of bounces are given higher priority.

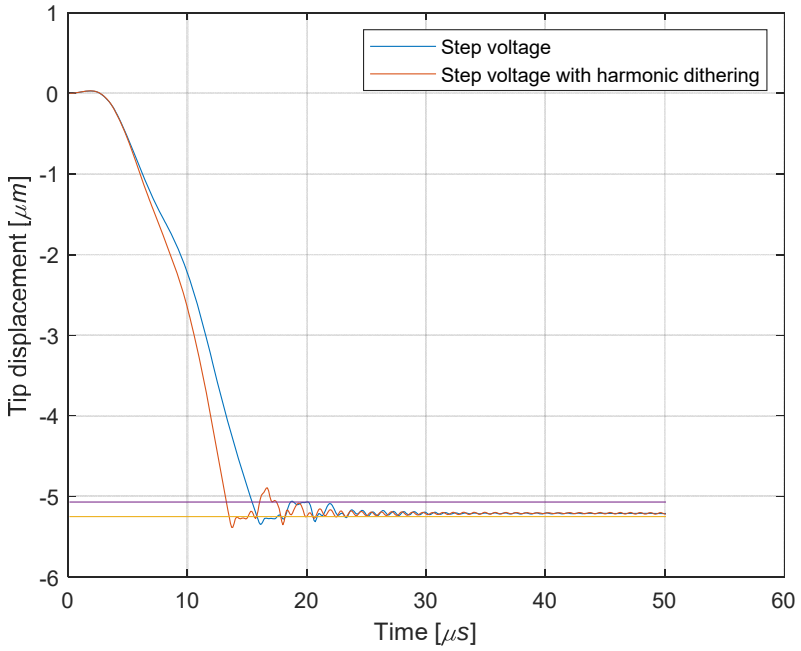

Fig. 3.8. Response of step voltage and step voltage with harmonic dither of 15% amplitude, $180.5 \times 10^3\ rad/s$ frequency at $V = 1.25\ V_{th}$.

Actuation of a switch at the relatively high voltage magnitude of, $V = 1.5V_{th}$, along with harmonic perturbations in the actuation voltage, although results in variation of initial contact time t_i as the frequency and dither amplitude increase, but the variation in t_i has significantly lower values when compared with the low/moderate step voltage. Variation in other performance parameters also tends to have similar behavior as in the t_i variation. This behavior can be seen in Figures 3.9 (a) and 3.9 (b) where improvements in performance can be seen at relatively low frequencies between the first and the second natural frequencies. Unlike the low voltage actuation, no large bounces are observed at this high level of actuation voltage as seen from Figure 3.9 (b). In the figure, multiple bounces of moderate height can be seen around the third natural frequency while multiple bounces with small heights are observed in the region between the fourth and the fifth natural

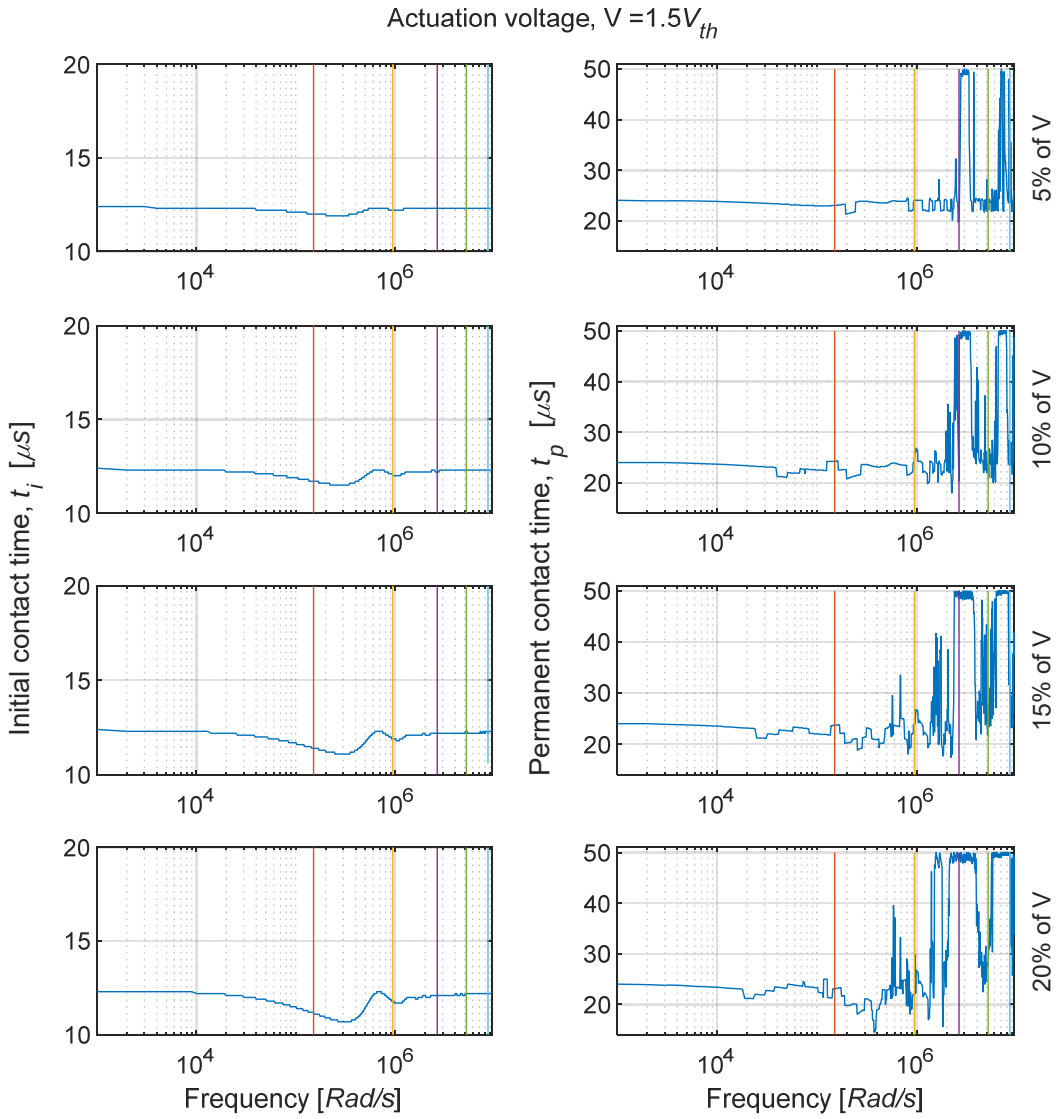

Fig. 3.9 (a). Influence of frequency and amplitude harmonic dither in electrostatic voltage on initial contact time and permanent contact time for $V = 1.5\, V_{th}$.

frequencies and the number of these bounces increase as the dither amplitude increases. In the region between the first and the second natural frequencies where both the initial contact time and the bounce height are minimal, an improvement in the switch bounce parameters can be achieved. For instance, at a dither frequency of $380.3 \times 10^3\ rad/s$ which lies between the first and the second natural frequencies and a dither amplitude of 20% of the actuation step voltage, all the performance measures appear to be improved.

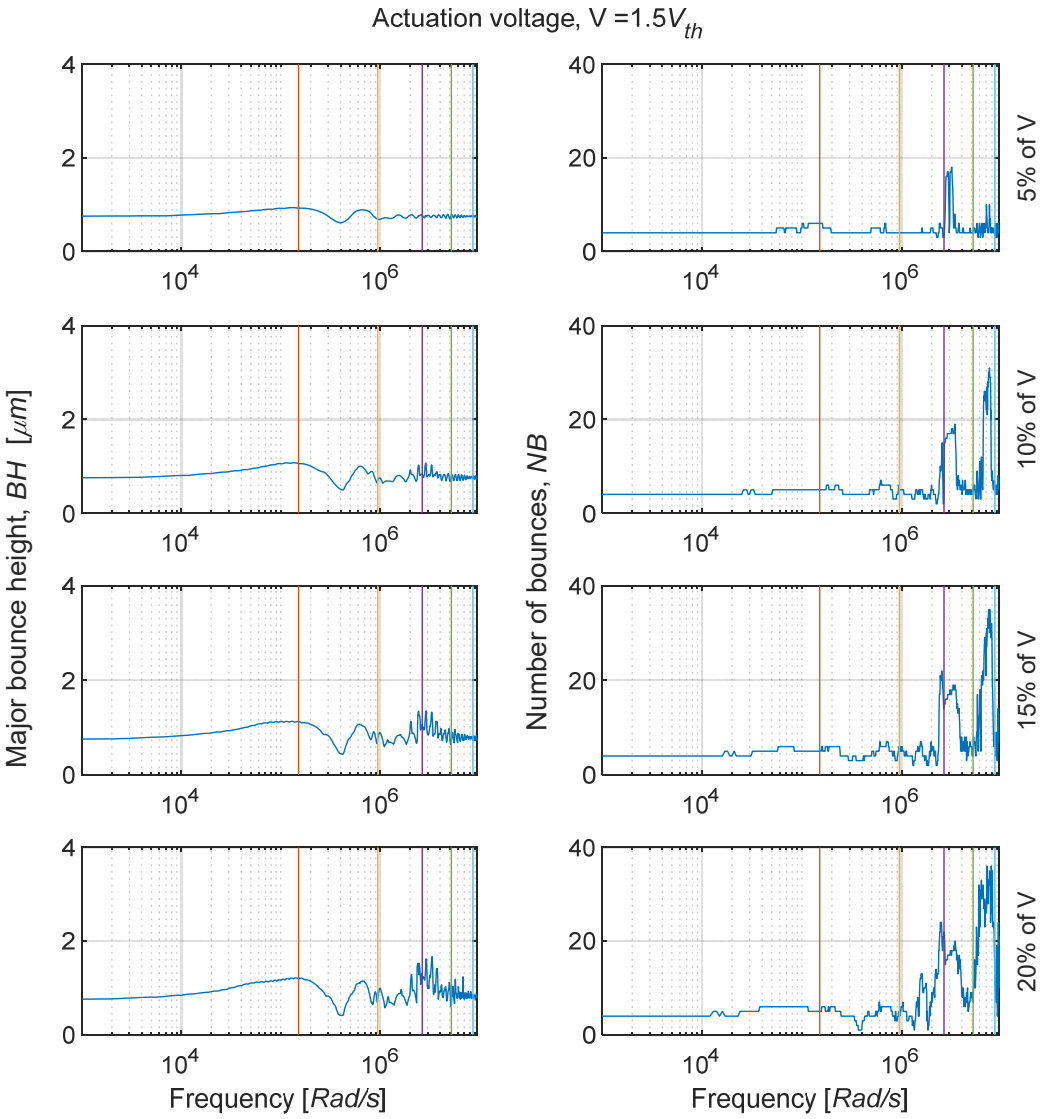

Fig. 3.9 (b). Influence of frequency and amplitude of harmonic dither in electrostatic voltage on major bounce height and number of bounces for $V = 1.5\ V_{th}$.

The initial contact time t_i, and the permanent contact time t_p, have been improved by 19% and 39%, respectively, while the height of major bounce BH and the number of bounces NB have been improved by 41%, and 75% , respectively. Figure 3.10 demonstrates, via the bounce responses, the superior performance of the most desirable mitigation condition for this level of actuation when compared with a pure step actuation with no dither.

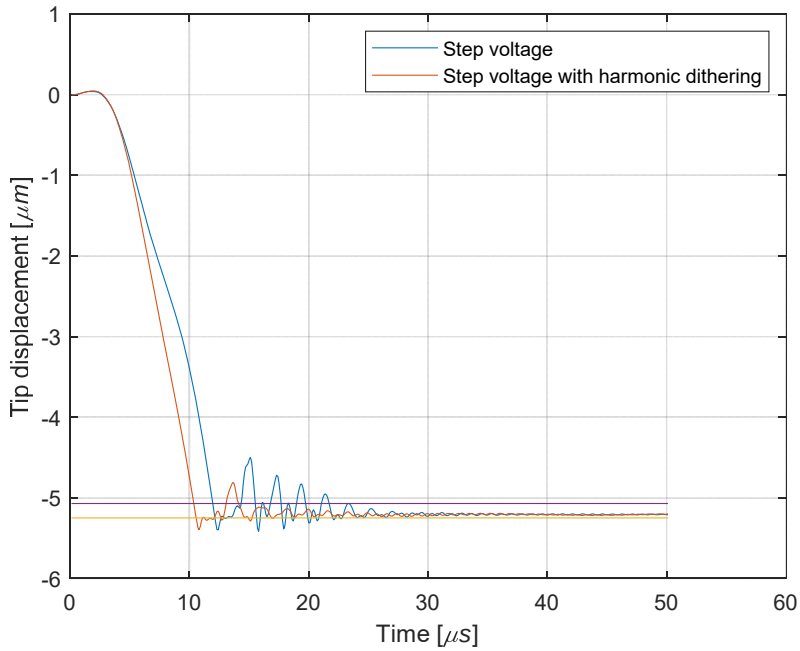

Fig. 3.10. Responses of step voltage and step voltage with of harmonic dither of 20% amplitude, $380.3 \times 10^3\ rad/s$ frequency at $V = 1.5\ V_{th}$.

3.4 Switch performance under combined actuation of electrostatic step voltage and harmonic dither in the secondary actuator voltage

Using harmonic dither in electrostatic actuation voltage has shown improvement in the bounce behavior at some combination of frequency and amplitude of the harmonic dither; however, these harmonic perturbations in the electrostatic voltage is only capable in providing attractive nonlinear action on the switch with fluctuations in the magnitude. The electrostatic force has a nonlinear inverse proportionality to the gap between the electrodes and directly proportional to the square of applied voltage. Employing actuation that has a different linear actuation principle such as alternating bending action may prove to be useful. Such actuation can be physically realized using a piezoelectric layer actuator so that the control of the bouncing behavior can be achieved if this force is used as control force in conjunction with the attractive nonlinear electrostatic actuation.

To this end, a switch with a primarily electrostatic electrode and a secondary piezoelectric actuator has been chosen for the purposes of investigating the influence of the harmonic perturbations in the secondary PZT actuator on the switch bouncing behavior. This type of combined actuation method has been previously proposed by Liu and Liu (2014) to investigate the nonlinear response of an electrostatically actuated switch. For the purposes of validation of the piezoelectric switch, the material and geometric properties of the micro-switch that was used in a study by Zhang *et al.* (2005) have been employed. Their model which included the PZT layers was validated using the natural frequency and deflection predictions using the proposed mathematical model used in the present study. This analysis provided confidence in using the present model for simulation predictions. The current model is then extended to include the electrostatic electrode which is validated previously with a switch investigated by Wang (2009) as demonstrated in section 3.3. The employed switch with the secondary PZT actuator is described in section 2.2. The piezoelectric actuator layer is made of Lead Zirconate Titanate $Pb(Zr_{\mathrm{x}}\, Ti_{1-\mathrm{x}})O_3$ or (PZT) and has dimensions and properties which are listed in Table 3.3 while the ones not listed are the same as those given in Table 3.1.

Table 3.3. PZT actuator parameters and properties

Parameter	**Value**
Layer width, a_p	$30\ \mu m$
Layer thickness, b_p	$0.25\ \mu m$
Starting point of PZT layer, L_3	$30\ \mu m$
Ending point of PZT layer, L_4	$60\ \mu m$
Young's modulus for PZT material, E_p	$139\ GPa$
Material mass density of PZT, ρ_p	$7500\ kg/m^3$
Piezoelectric constant, d_{31}	$123 \times 10^{-12} m/\mathrm{v}$

Other dimensions and material properties of the switch are similar to those of the electrostatically actuated switch described in section 3.3. It is worth noting that in the present study the dimensions and the location of the piezoelectric actuator are taken without any optimization process for shaping the response and hence more research is needed to obtain the optimal parameters of secondary actuator for bounce reduction; however, the proportionality between the present switch structure and the one used in the study by Zhang *et al.*, (2005) is used for choosing the actuator parameters and recommended location. The predicted natural frequencies of the switch with a PZT actuator are shown in Table 3.4. It may be noted that these frequencies differ from the natural frequencies of the switch employed in section 3.3 by not more than 1.04%.

Table 3.4. Predicted natural frequencies of the MEM switch with PZT layer

Mode	1	2	3	4	5
Natural frequency $[rad/s]$	152.5×10^3	950.3×10^3	2651.4×10^3	5182.6×10^3	8553.2×10^3

In the present study, harmonic dither in the piezoelectric actuator voltage along with the step actuation voltage for the electrostatic electrode are employed to investigate the influences of the harmonic perturbations on the bouncing characteristics of the switch. For these purposes, different electrostatic actuation voltages along with harmonic perturbations in the PZT voltage with different frequencies and amplitudes have been employed. Three values of step actuation voltage are chosen at $1.1V_{th}$, $1.25V_{th}$ and $1.5V_{th}$ which represent actuation voltage at or below/above the optimal voltage predicted in section 3.2. Four dither harmonic amplitudes of 5%, 10%, 15%, and 20% of the step voltage magnitude are taken to investigate the influence of dither amplitude on the bouncing behavior. The harmonic perturbation frequency is swept from zero to a value beyond the fifth natural frequency of the MEM switch with linear incremental steps. For mitigation purposes, harmonic dither in the PZT actuator voltage is considered to be applied just before the contact. As a consequence, under this condition, significant improvement in the initial contact time is

not expected. Therefore, this model is used mainly to investigate the mitigation of remaining performance parameters such as the permanent contact time t_p, height of major bounce BH and the number of bounces NB. The results show improvement in the bounce behavior at specific regions of frequencies and dither amplitudes which can be achieved without prior extensive knowledge of the switch parameters. This feature clearly is advantageous when compared to other mitigation techniques which require measurement of responses and/or knowledge of system parameters. Figures 3.11 through 3.16 show the effects of using harmonic dither in PZT voltage along with the step actuation voltage on the switch performance parameters.

Influences of frequency and amplitude of harmonic perturbations in the secondary PZT actuator voltage along with electrostatic actuation voltage on performance parameters are shown in Figures 3.11 (a) and 3.11 (b) at relatively low actuation voltages, $V = 1.1V_{th}$. As previously mentioned expectations, the variation in initial contact time is absent in the low to moderate frequencies and minimal at high frequencies and this is evident in Figure 3.11 (a). Fluctuating trend in performance parameters with increase of both the frequency and amplitude of harmonic dither is obvious from Figures 3.11 (a) and (b). It may be seen from Figure 3.11 (b) that at this low actuation voltage and at frequencies beyond the first natural frequency multiple regions in which the bounce height is large with a relatively higher number of bounces have been observed and this region extends to the third natural frequency with the increase of the harmonic dither amplitude. The bounces around the third natural frequency are characterized by a greater number of bounces compared to the numbers that appear in the region between the first and the second natural frequencies. The region near the fifth natural frequency is characterized by large bounce height with increased number of bounces as the amplitude of the harmonic dither increases. The phenomenon of larger bounce may be attributed to the weak attracting force at this low actuation voltage which permit larger bounces to occur at these frequencies. As mentioned previously, the increase of number of bounces or the height of bounces leads to longer permanent contact time, as seen in Figure 3.11 (a); therefore, exciting at frequencies beyond the first natural frequency at low actuation voltage can be risky if not carefully chosen. However, the region between the first and the second natural frequencies has

multiple frequencies where the performance can be improved at low or moderate dither amplitudes. An example of improved response is demonstrated in Figure 3.12 where 10% of the actuation voltage magnitude is taken as dither amplitude for the piezoelectric actuator at a frequency of $647.4 \times 10^3\ rad/s$. It is clear from this figure that the initial contact time has not improved since the harmonic dither is made to commence just prior to contact while the permanent contact time has been decreased by 38%. In this example, both number of bounces and bounce height is decreased by 100%. This example shows

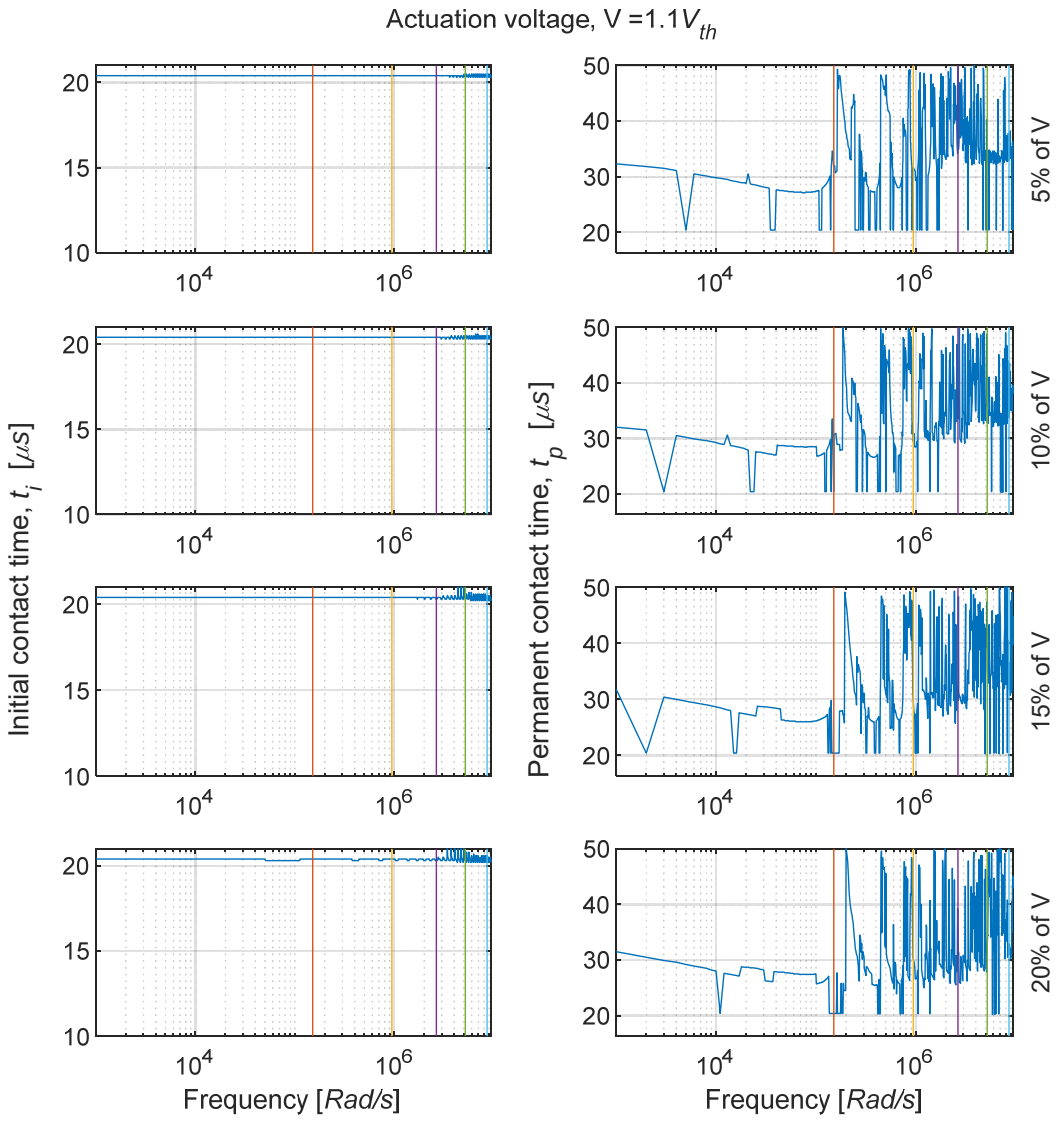

Fig. 3.11 (a). Influence of frequency and amplitude of harmonic dither in the PZT voltage on initial contact time and permanent contact time for $V = 1.1\ V_{th}$.

the improved bounce response of the desirable mitigation condition when compared with pure step actuation with no dither.

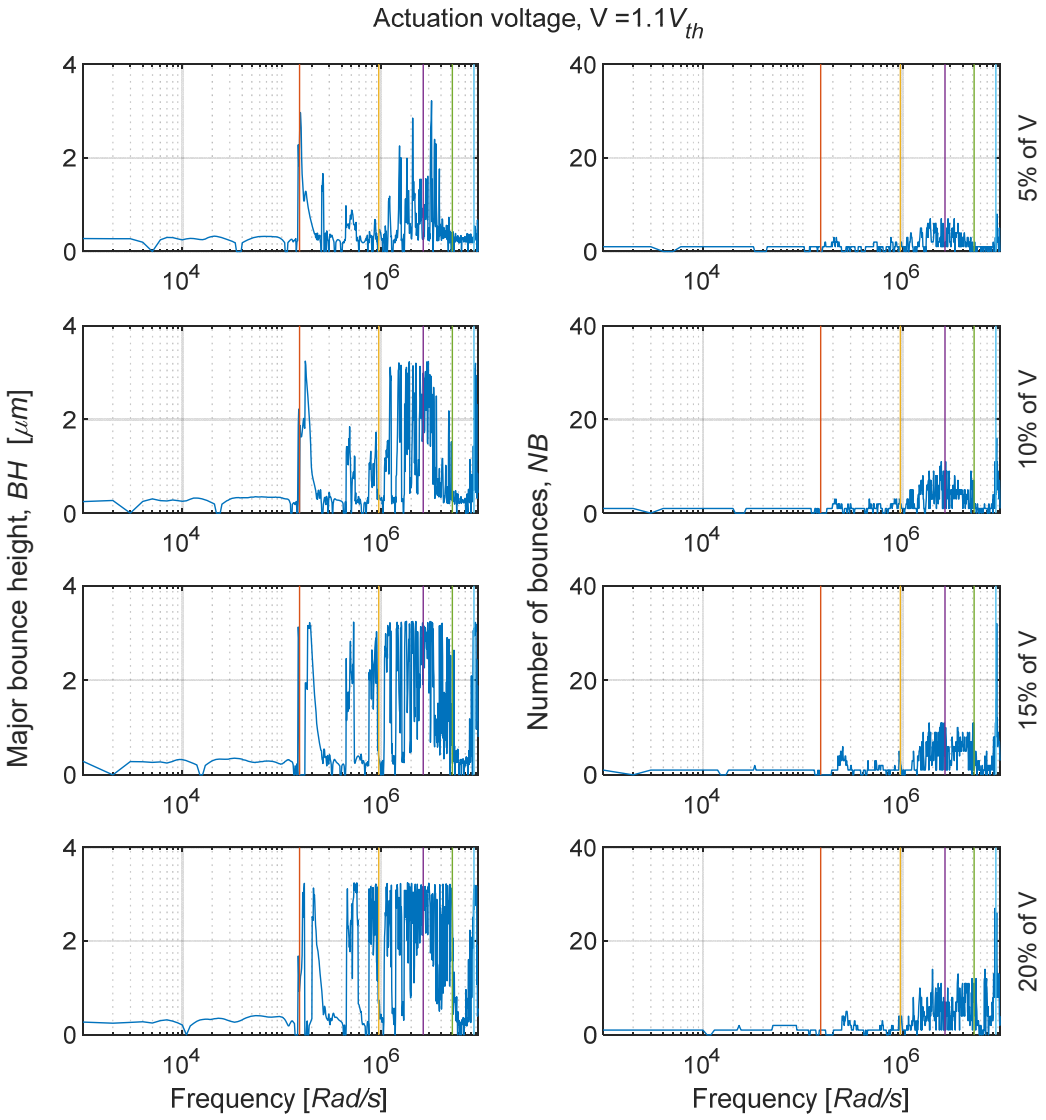

Fig. 3.11 (b). Influence of frequency and amplitude of harmonic dither in PZT voltage on major bounce height and number of bounces for $V = 1.1\ V_{th}$.

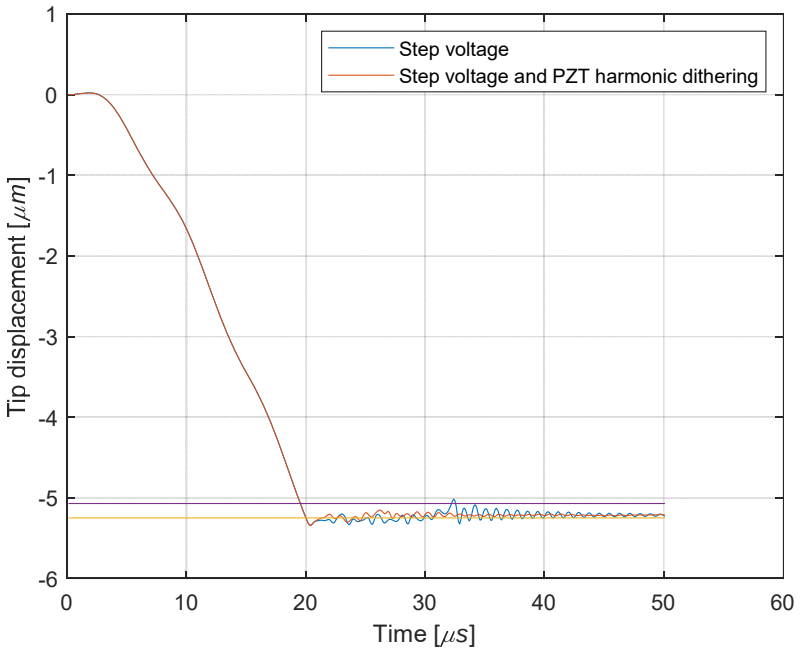

Fig. 3.12. Responses of step voltage and step with harmonic dither in PZT harmonic voltage of 10% amplitude, $647.4 \times 10^3\ rad/s$ frequency at $V = 1.1\ V_{th}$.

At $1.25\ V_{th}$ electrostatic step actuation voltage, variations in performance parameters such as the initial contact time t_i is still small since the harmonic dither commences just before the contact; however, fluctuation trend in parameters such as permanent contact time t_p , height of major bounce BH and the number of bounces NB with the increase of the amplitude and frequency of harmonic dither has been demonstrated in Figures 3.13 (a) and 3.13 (b). Large bounces, such as those observed at low actuation voltage as seen from Figure 3.11 (b), appear to have disappeared at this moderate actuation voltage due to relatively strong attraction of the electrostatic force as seen in Figure 3.13 (b). In the figure, multiple bounces with relatively moderate height has been observed around the third natural frequency and, tend to take higher values when the harmonic dither amplitude is high. Region between the first and the second natural frequencies contains few frequencies where bounce height and number of bounces have minimal values at relatively low dither magnitude. Between the second and the third natural frequencies, a frequency where both bounce height and the number of bounces is minimum close to the second natural frequency can be observed. Improved response at these conditions is possible, for example,

when the frequency and magnitude of harmonic dither are $1205 \times 10^3\ rad/s$ and of 15%, of the actuation voltage, respectively. The initial contact time and the number of bounces remain unchanged at their original no dither condition while permanent contact time and heights of bounces have been reduced by 16% and 100 % , respectively. Figure 3.14 shows the switch response at this operating condition together with the response for pure electrostatic step actuation voltage. As previously noted in the case of harmonic dither

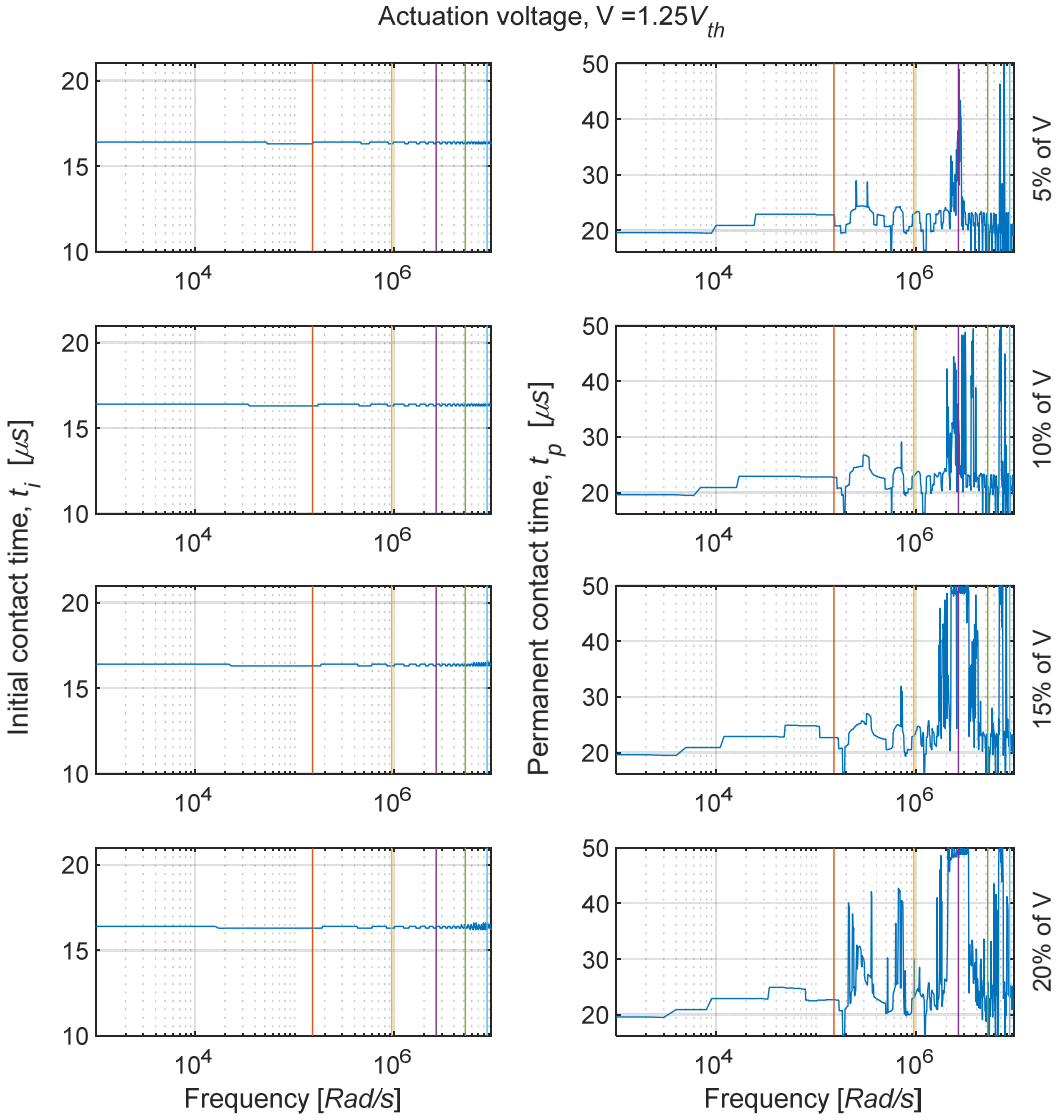

Fig. 3.13 (a). Influence of frequency and amplitude of harmonic dither in the PZT voltage on initial contact time and permanent contact time for $V = 1.25\ V_{th}$.

in electrostatic actuation voltage, the improvement at this optimal voltage is limited since the operating condition is already at the optimal voltage level.

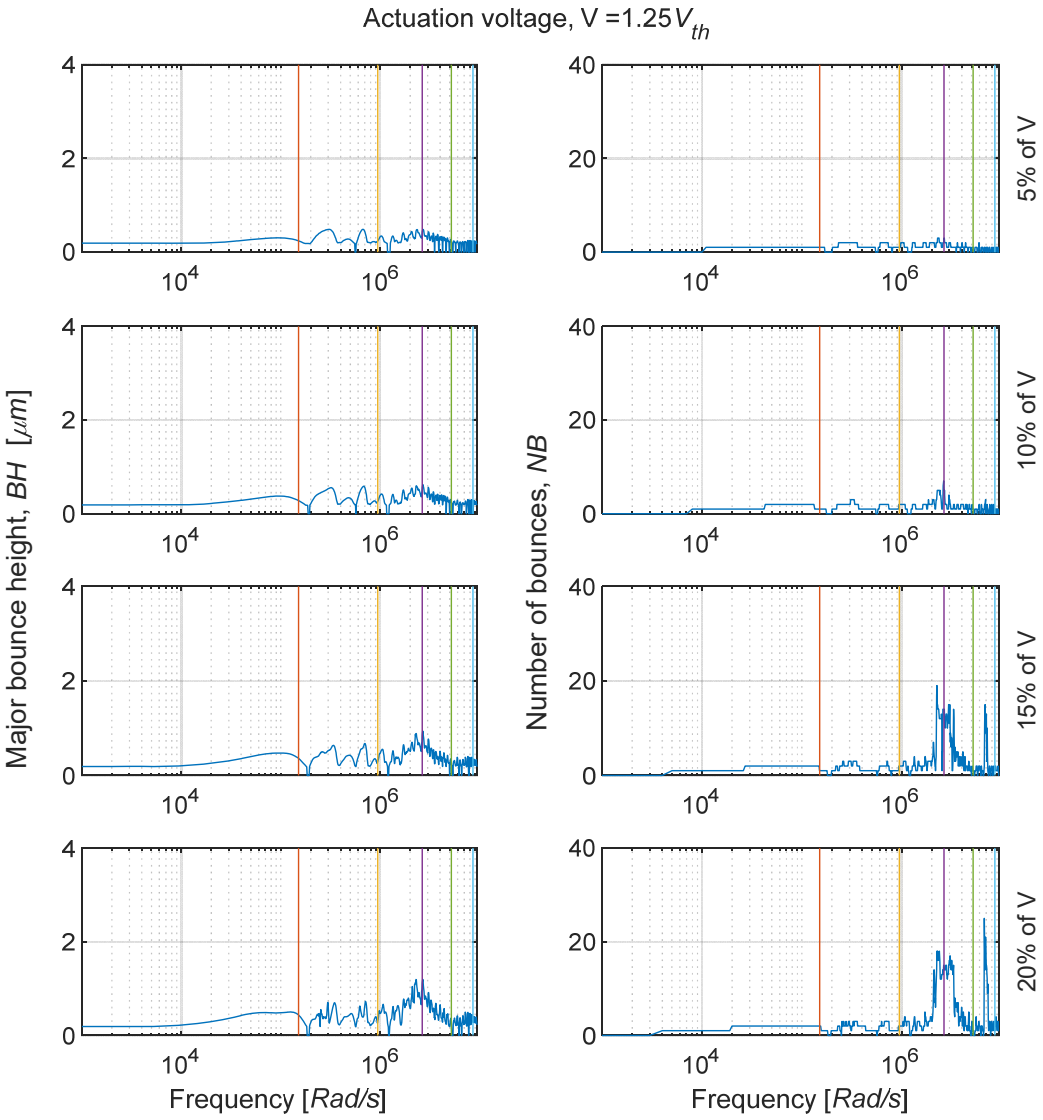

Fig. 3.13 (b). Influence of frequency and amplitude of harmonic dither in PZT voltage on major bounce height and number of bounces for $V = 1.25\, V_{th}$.

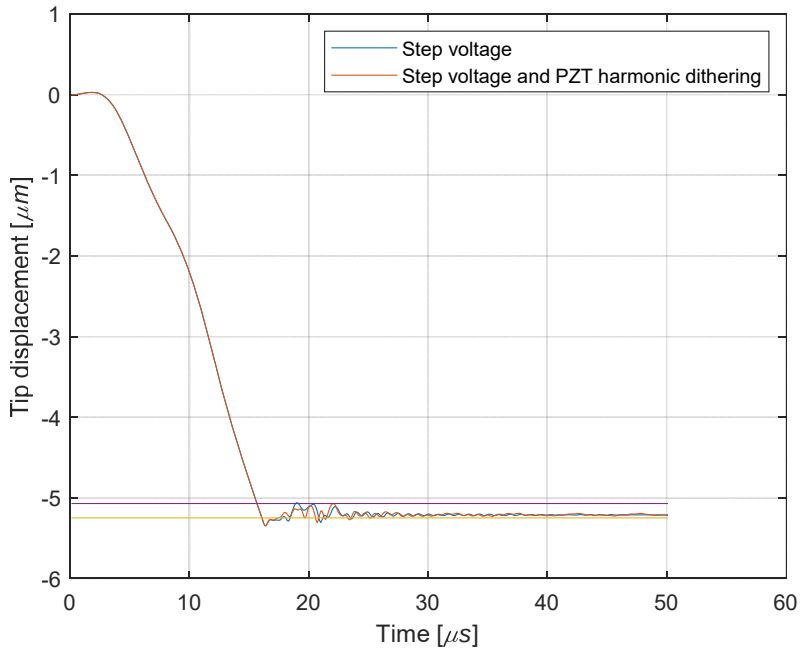

Fig. 3.14. Responses of step voltage and step with harmonic dither in PZT harmonic voltage of 15% amplitude, $1205 \times 10^3\ rad/s$ frequency at $V = 1.25\ V_{th}$.

When the electrostatic actuation voltage is increased to $V = 1.5V_{th}$ and harmonic perturbation is applied to the piezoelectric actuator voltage, the responses are depicted in Figures 3.15 (a) and 3.15 (b). Initial contact time remains constant at low frequency and its variation is minimal at high frequency since the harmonic dither voltage is applied just before the contact. As in the moderate voltage case, no large bounces are observed as seen in Figure 3.15 (b) when compared with the case with low voltage actuation. At high frequencies that are close to the third natural frequency and at lower dither amplitudes, small bounce heights with relatively large number of bounces are observed and the height tends to increase to moderate height with the increase of dithering amplitude as seen in Figure 3.15 (b). Further, multiple small bounces tend to appear in the region between the fourth and the fifth natural frequencies only at higher dither amplitudes. Figures 3.15 show that improvements in performance can be achieved at frequencies between the first and the third natural frequencies. For example, when the dither harmonic voltage in the PZT actuator is set at a frequency of $1681.8 \times 10^3\ rad/s$ and at an amplitude of 20% of the actuation voltage, improvements in the performance measures except for the initial contact

time are achieved as depicted in Figure 3.16. The permanent contact time t_p, the height of major bounce BH, and the number of bounces NB are decreased by 12%, 44% and 25%, respectively.

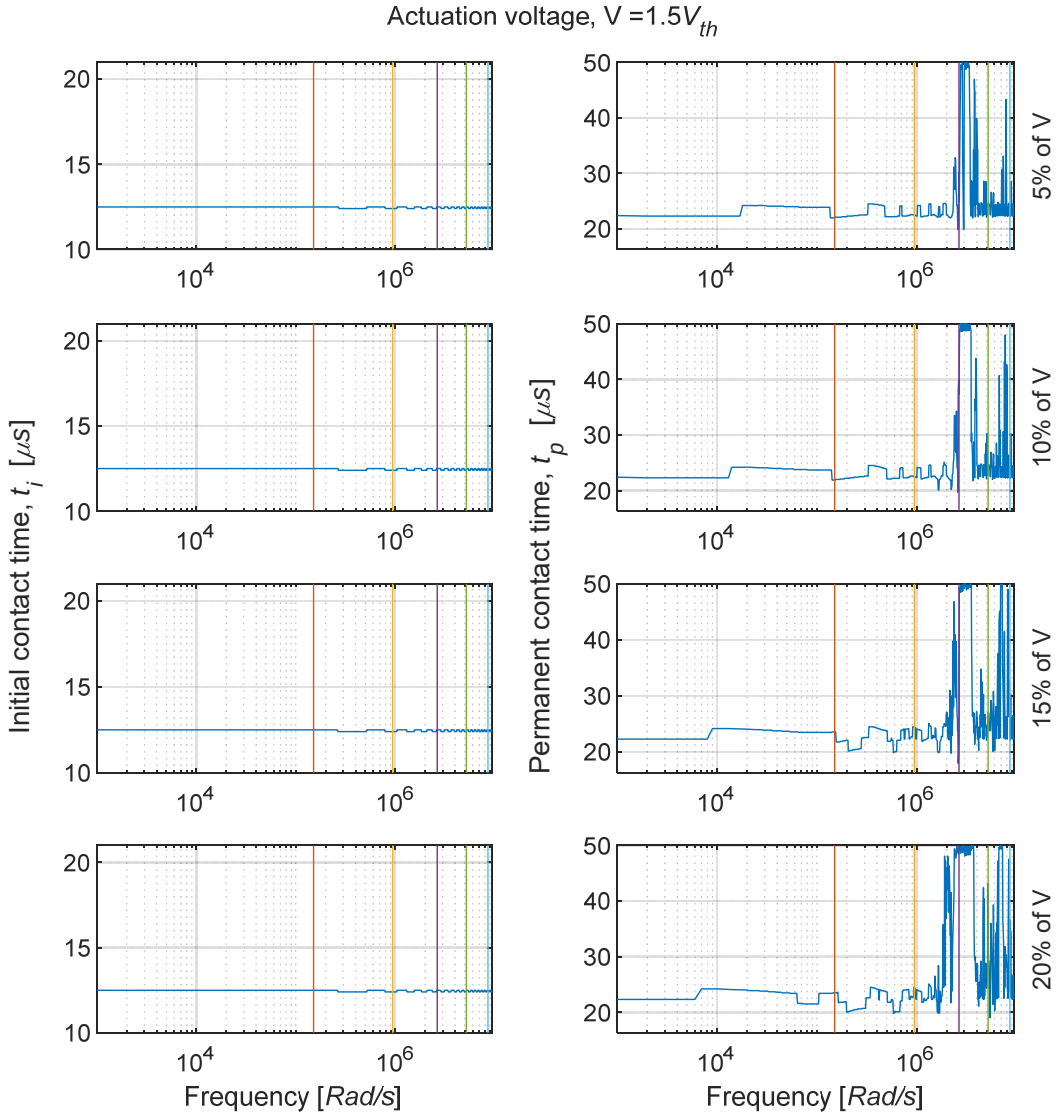

Fig. 3.15 (a). Influence of frequency and amplitude of harmonic dither in the PZT voltage on initial contact time and permanent contact time for $V = 1.5\, V_{th}$.

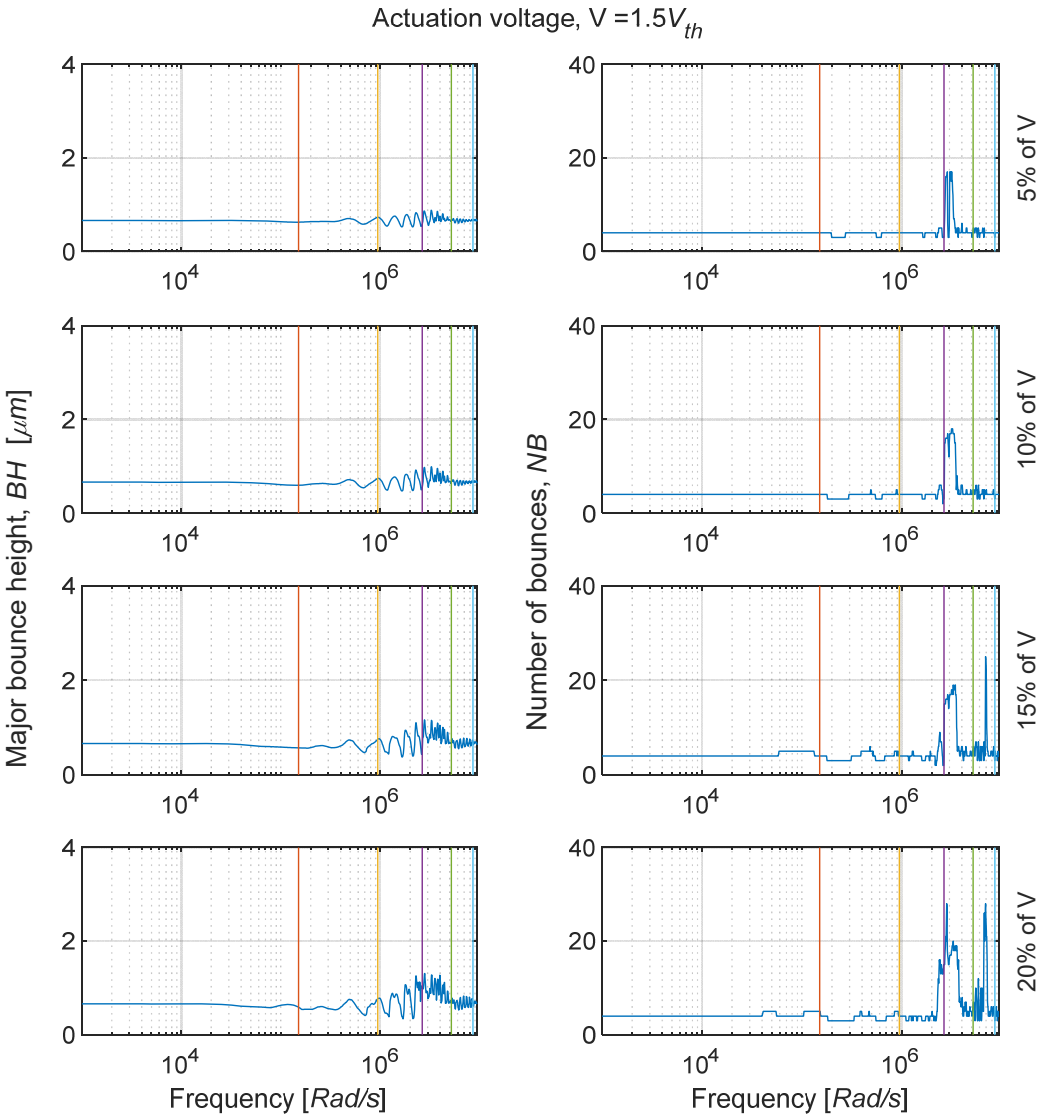

Fig. 3.15 (b). Influence of frequency and amplitude of harmonic dither in PZT voltage on major bounce height and number of bounces for $V = 1.5V_{th}$.

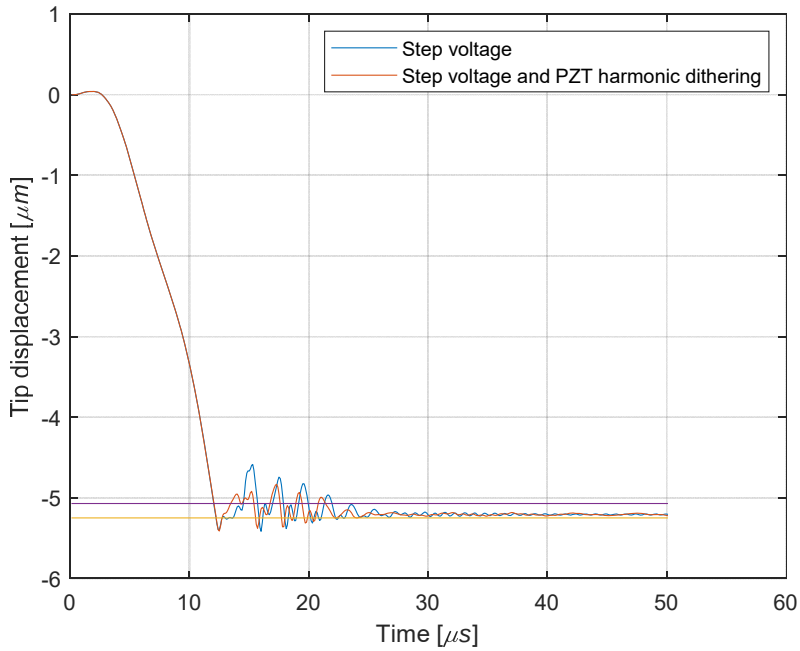

Fig. 3.16. Responses of step voltage and step with harmonic dither in PZT harmonic voltage of 20% amplitude, $1681.8 \times 10^3\ rad/s$ frequency at $V = 1.5\ V_{th}$.

3.5 Conclusions

The derived models of cantilever-type switches along with the proposed numerical scheme are employed to predict the switch dynamic response. In the present study, two switches namely an electrostatically actuated switch and a switch of combined electrostatic and piezoelectric actuation are considered. The latter model was developed and used only for bounce mitigation purposes. Although both methods could be employed for useful bounce mitigation, it appears that the electrostatic dither offers simplicity due to the absence of an additional actuator component. Performance parameters such as initial contact time, permanent contact time, major bounce height, and the number of significant bounces have been quantified based on the predicted response. Using harmonic dither in the step actuation voltage for switch under an electrostatic actuation or harmonic dither in the piezoelectric actuator voltage has been shown to improve the bouncing behavior for certain frequencies and dither amplitudes. Regions where such improvements could be made have been identified for both type of switches. For the switch with electrostatic dithering

considered in the study, most improvements are found to be achieved at low dither frequencies below the second natural frequency of the switch either at high or low actuation voltages. On the other hand for the switch with secondary PZT dithering considered in the study, most improvements are found to be achieved at low dither frequencies below the third natural frequency of the switch either at high or low actuation voltages. Both methods are shown to be less effective when the switch is actuated at a moderate voltage. It has been shown that both dither methods could potentially be employed for bounce mitigation, in practice, using the present simulation study as a basis. It may be noted that the methods used were not optimized and as a result direct quantitative comparisons could not be made based on the present study. However, it is shown that depending on the mitigation parameter(s) of interest, suitable choice of actuation voltage as well as dither frequencies and amplitudes could be predicted based on the simulation study. These selections could then be used for the purposes of initial experimental tuning. Further, the present study demonstrates the existence of favorable actuation and dither conditions which gives confidence in applying this approach for bounce mitigation. It is worth noting that opportunities exist for several structure/actuator optimization for improving the performance which can open further research work in this area.

CHAPTER 4

UNCERTAINTY QUANTIFICATION BASED ON MEM SWITCH TIP BOUNCING

4.1 Introduction

Despite the improvements of design, analysis and fabrication of micro-switches, the tolerances in MEMS fabrication process are notoriously poor. Therefore, batch fabrication processes employed to produce MEM systems are prone to uncertainties in the geometrical and contact parameters as well as material properties. These uncertainties affect the device performance and life time and are difficult to control or predict. Moreover; the effects that parameter variations have on device behavior are poorly understood. Since the common design method for these systems is typically based on precise deterministic assumptions, it is necessary to get more insight into their variations. To this end, understanding the influences of uncertainties accompanied by these processes on the system performance and reliability are warranted. This chapter focuses on predictions of uncertainty measures for MEM switches based on the transient dynamic response, in particular, the bouncing behavior. To understand and quantify the influence of pertinent parameters on the bouncing effects, suitable mathematical models that capture the bouncing dynamics as well as the forces that are dominant at this micron scale are employed. Measure of performance in terms of second order statistics is performed, particularly for the beam as well as beam tip parameters since excessive tip bounce is known to degrade switch performance. Thus, the present work focusses on the influence of uncertainties in the beam tip geometry parameters such as beam tip length/width as well as contact asperity variables such as the area asperity density and the radius of asperities on the bouncing behavior. In addition to beam tip parameters, this study quantifies the effects of uncertainties in Young's modulus, beam thickness as well as actuation voltage. These influences on significant switch performance parameters such as initial contact time and major bounce height have been quantified in the presence of interactive system nonlinearities.

As mentioned in previous chapters 2 and 3, during the switch closure stage, the beam bounces several times before making a permanent contact with the drain. This behavior is likely to result in significant performance degradation. In order to obtain a quantitative understanding of this phenomenon, it is essential to characterize the uncertainty effects of geometrical, contact parameters and material property as well as the operation conditions. This chapter focusses on gaining an understanding the bouncing dynamics via numerical simulations due to uncertainties in system parameters/properties of significance as well as due to uncertainty in the operation conditions. To date, only limited studies are available in the literature on the topic of parameter uncertainties associated with switch dynamics, particularly with consideration given for bouncing.

In the interest of investigating the effects of system uncertainties on output responses of the system and for comprehensive understanding of these effects, randomness in the dimensional/material properties as well as operational conditions is introduced to the developed model. Based on response predictions, quantifications of second order statistics for significant performance parameters are derived from system output. Switch response needs to be predicted from a comprehensive model that captures the dynamic response. It is obvious that these effects, in general are difficult to predict intuitively, owing to the manner in which they affect the multi-modal system dynamics with several nonlinearities.

The results from this investigation are expected to provide insights into each parameter's contribution to the variability present in the model output. It is envisaged that the quantitative understanding of the effects of uncertainty of system parameters facilitate identifying of significant design parameters that affect system response, which can then be further improved in the design and fabrication processes and hence improve the device's performance and reliability.

4.2 Uncertainty quantification analysis

For the purposes of reader convenience, the switch material and geometric properties are provided again in this section in Table 4.1. In this study, the values used for E, b, L_T, a, R and η have been taken as the nominal mean values in the uncertainty quantification

predictions. In addition, a value for area density of asperities, η, is also chosen as 45 $asperity/\mu m^2$ to demonstrate measures at lower values of density as reported in literature (Majumder *et al.*, 2001). Response predictions made via numerical simulation of the switch model have been used to evaluate the significant design parameters.

Table 4.1. MEM switch parameters and properties

Parameter	**Value**
Beam length, L	130 μm
Beam width, a	30 μm
Beam thickness, b	1.25 μm
Beam tip contact gap, d_T	1.5 μm
Air gap, d	2.5 μm
Starting point of electrostatic electrode, L_1	55 μm
Ending point of electrostatic electrode, L_2	95 μm
Beam tip length, L_T	10 μm
Young's modulus of beam material, E	78 GPa
Poisson's ratios of contact surfaces, v	0.44
Material mass density of the beam, ρ	19300 kg/m^3
Radius of sphere asperity, R	100 nm
Area density of asperities, η	150 $asperity/\mu m^2$

The switch tip bounce response computed for a set of nominal switch parameters has been depicted in Figure 4.1. This figure shows two important parameters that characterize the switch performance as follows:

- Initial contact time, t_i, is the time taken for the first contact.
- Major bounce height, BH.

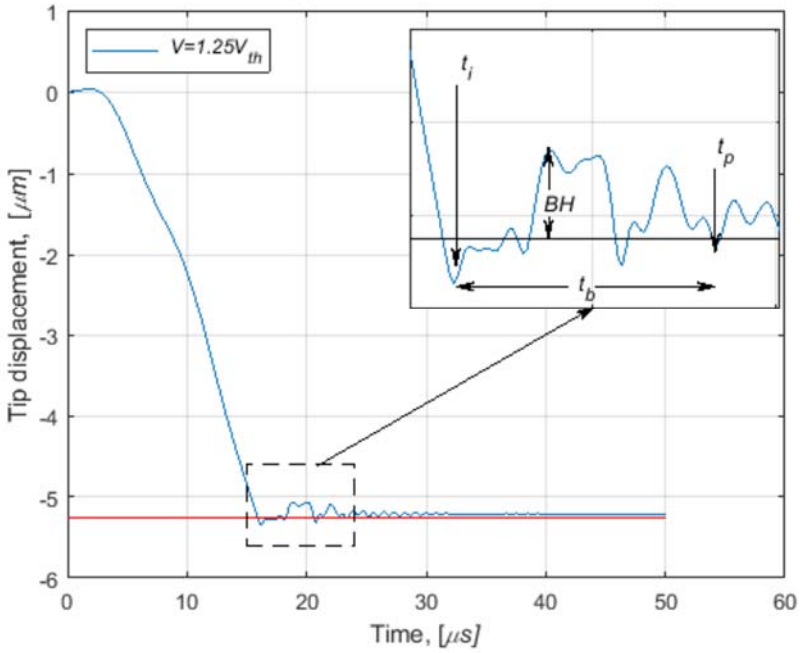

Fig. 4.1. Typical switch tip-end response for $V = 1.25\, V_{th}$.

As mentioned in chapter 3, this model has been used to evaluate the dynamic pull-in voltage, V_{th} and this model has been validated with pervious experimental switch data by Wang (2009). In this section the model will be employed to investigate the effects of uncertainty switch material/geometric properties, switch tip properties, actuation voltage and tip asperity contact parameters on the switch bounce performance.

For analysis purposes, input uncertainties are specified with nominal mean values as presented above and varying standard deviations. All quantifications presented in the present study consider the major bounce height, BH and the time for initial contact, t_i as output performance parameters. These measures have been examined employing thirty random samples with the chosen nominal mean and varying values of standard deviations for two different actuation voltages namely $V = 1.25\, V_{th}$ and $V = 1.50\, V_{th}$. In addition, a study is also performed for varying actuation voltage standard deviations. The effects of uncertainties in beam tip parameters are depicted in Figures 4.2, 4.3 and 4.4 while the effects of uncertainty in beam parameters are illustrated in Figures 4.5, 4.6 and 4.7. Figure

4.8 shows the influence of uncertainties in the actuation voltage on the chosen performance parameters. It may be noted that beam parameters such as the modulus of elasticity and the beam width are also relevant to beam tip parameters.

The effects of uncertainty in the asperities contact parameters are illustrated in Figures 4.2 and 4.3. Figures 4.2 depict the quantification of second order statistics when uncertainties in values of radius of the spherical asperity, R, are specified. Significantly a lower influence of uncertainties in the asperity radius, σ_R, on the major bounce height uncertainty is demonstrated by the σ_{BH} values for both voltages. Figure 4.2(a) also demonstrates clear linear behavior and shows relatively larger effects for the higher voltage. A noticeable effect of asperity radius uncertainty on the initial contact time is evident in figure 4.2(b) when compared with the behavior for the bounce height shown in Figure 4.2(a). The influence of uncertainty in area density of asperities, σ_η, is depicted in Figures 4.3 for two nominal areas of asperity densities at two operation voltages.

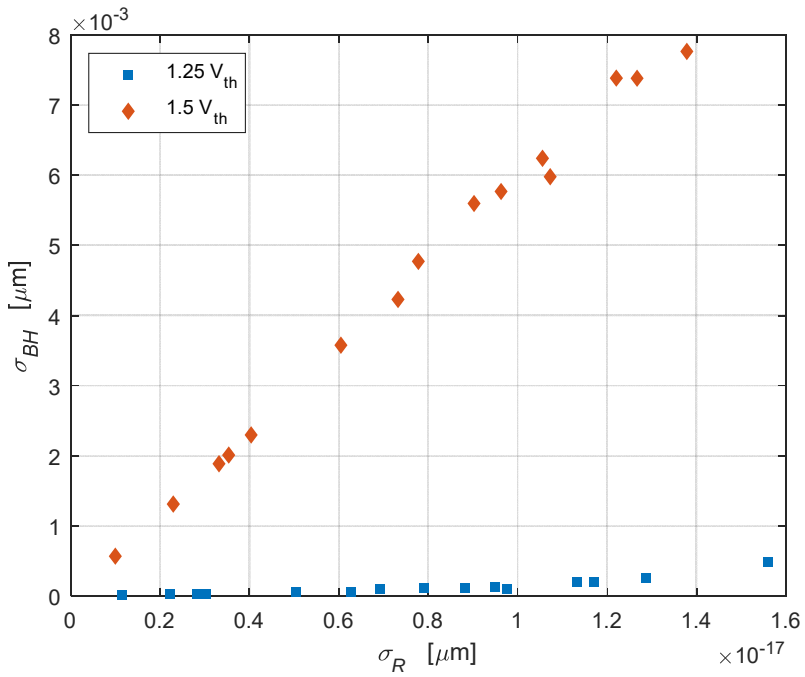

Fig. 4.2 (a). Uncertainties in asperity radius R on major bounce height BH for actuation voltages $1.25\,V_{th}$ and $1.5\,V_{th}$.

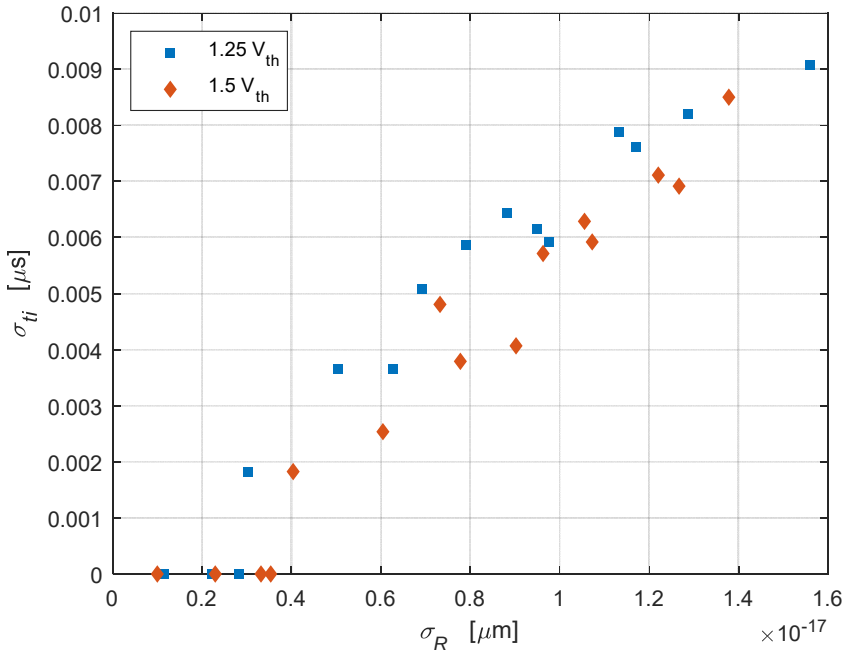

Fig. 4.2 (b). Uncertainties in asperity radius R on initial contact time t_i for actuation voltages 1.25 V_{th} and 1.5 V_{th}.

The dimensionless uncertainty in area of asperity density with respect to the nominal area of asperity density values is used in Figures 4.3. It may be noted from the figures that an approximately linear trend for all the cases is evident with larger effects on the output parameters for a smaller area density of asperities than for the denser one. A drop in the gradient for lower voltages is noticed in Figure 4.3 (a) for the major height uncertainty at both densities, while the opposite behavior is observed at lower density for the initial contact time uncertainty as shown in Figure 4.3 (b).

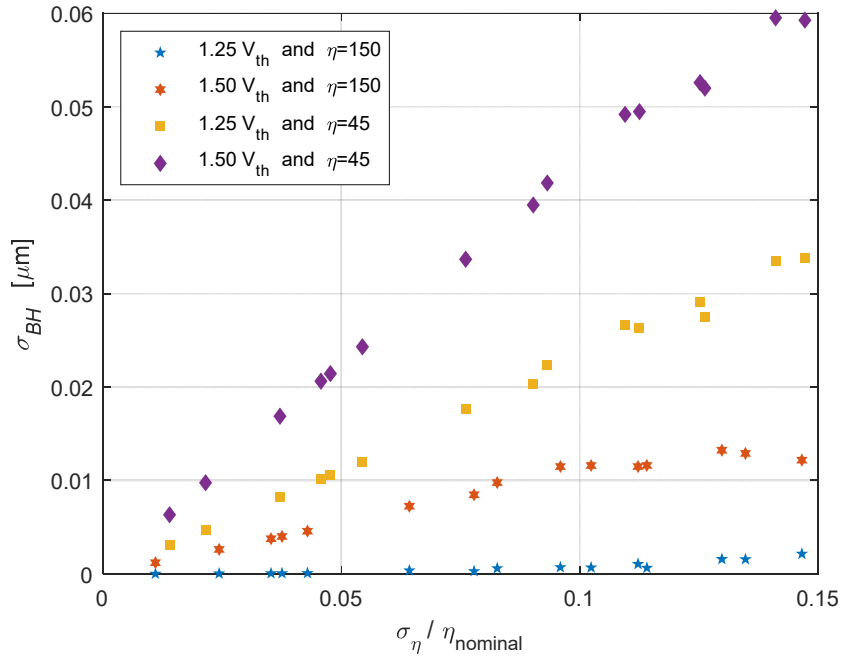

Fig. 4.3 (a). Uncertainties in area density of asperities η on major bounce height BH for actuation voltages 1.25 V_{th} and 1.5 V_{th}.

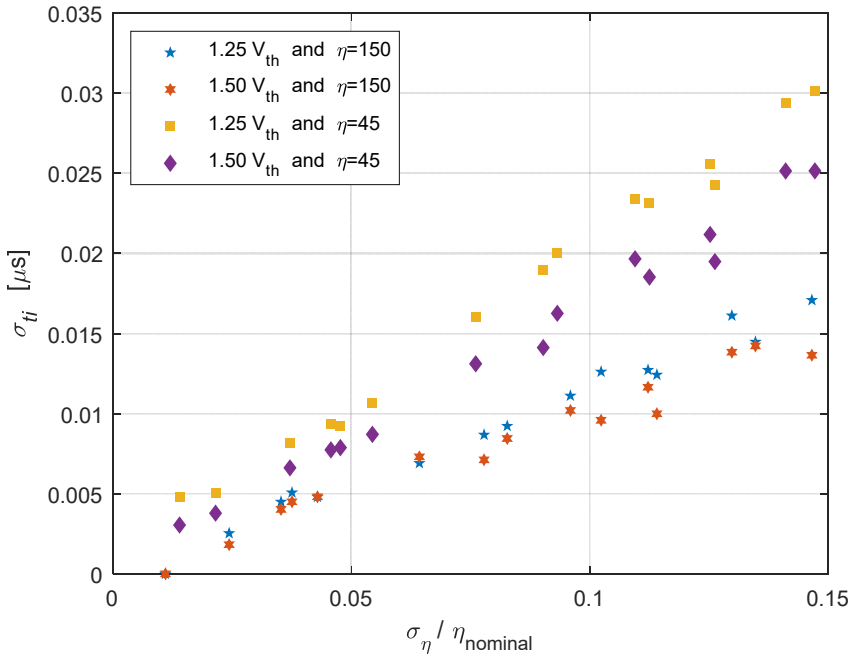

Fig. 4.3 (b). Uncertainties in area density of asperities η on initial contact time t_i for actuation voltages 1.25 V_{th} and 1.5 V_{th}.

Figures 4.4 depict the quantification of second order statistics when uncertainties in values of beam tip length, σ_{L_T}, are specified. An approximately linear behavior for the uncertainty in major bounce height σ_{BH} at both lower and higher voltage values with a drop in the gradient for lower voltages as shown in Figure 4.4(a) is evident. The effect of uncertainty in the beam tip length on the initial contact time seems to be significantly lower at lower and higher voltages with softening type nonlinear behavior as can be seen in Figure 4.4(b). The influence of uncertainty in the beam tip length, σ_{L_T}, appears to be slightly higher for lower voltage.

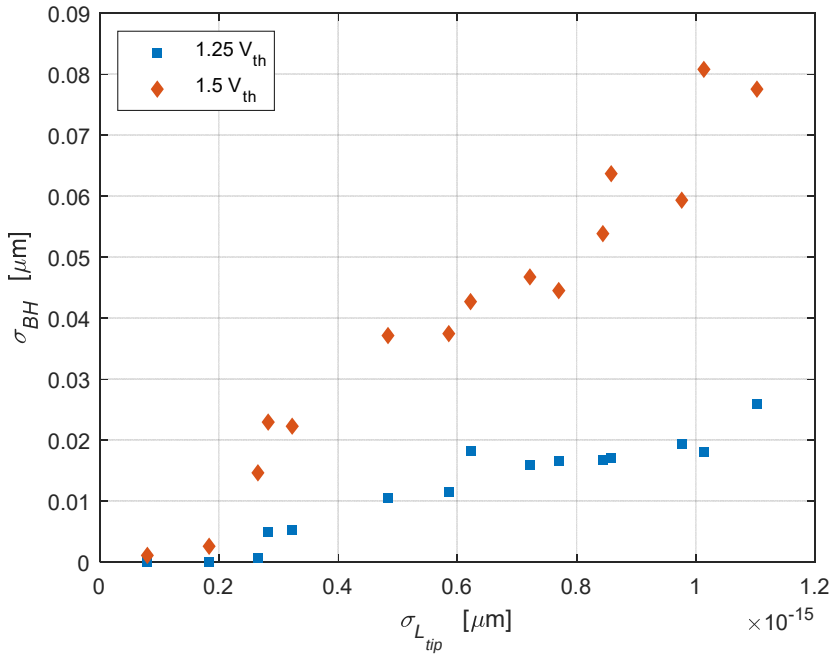

Fig. 4.4 (a). Uncertainties in in beam tip length l_T on major bounce height BH for actuation voltages $1.25\,V_{th}$ and $1.5\,V_{th}$.

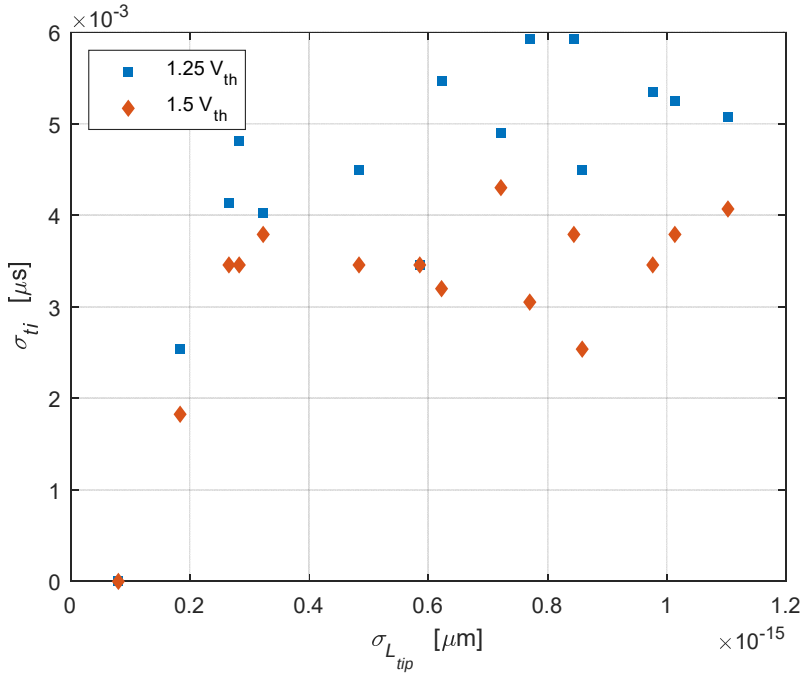

Fig. 4.4 (b). Uncertainties in beam tip length l_T on initial contact time t_i for actuation voltages $1.25\,V_{th}$ and $1.5\,V_{th}$.

The cases when uncertainties in the form of second order statistics are specified for Young's modulus, the beam width, and beam thickness are demonstrated in Figures 4.5, 4.6 and 4.7. Figures 4.5 depict the quantification of second order statistics when uncertainties in values of Young's modulus E are specified. At lower voltage a saturation behavior in uncertainties is observable in Figure 4.5(a) for σ_{BH} while a stiffening type nonlinear behavior is observable for σ_{ti} from Figure 4.5(b). In Figures 4.5(a) and 4.5(b), a more linear trend for both H and t_i at higher voltage can be noted with less effect of the uncertainties in Young's modulus on the initial contact time and greater influence on the major height compared with the corresponding behavior at a lower voltage. Further, at lower values of σ_E, the standard deviation σ_{BH} is greater than that of the higher voltage while an opposite behavior is observed for higher values of σ_E. When uncertainties in the form of second order statistics are specified for the tip width a, the output measures demonstrate a linear behavior for both H and t_i with the latter being less affected for the higher voltage by significant drop in gradient as illustrated in Figures 4.6. Uncertainties due to the variation of beam thickness b is summarized via Figures 4.7, in which a behavior

similar to that of the uncertainties in Young's modulus as depicted in Figures 4.5 is evident. It must be noted that in the case of uncertainties in thickness, the switch tends to go into a 'no contact' configuration at moderate standard deviations and hence relatively lower values for σ_b have been chosen to demonstrate the quantification.

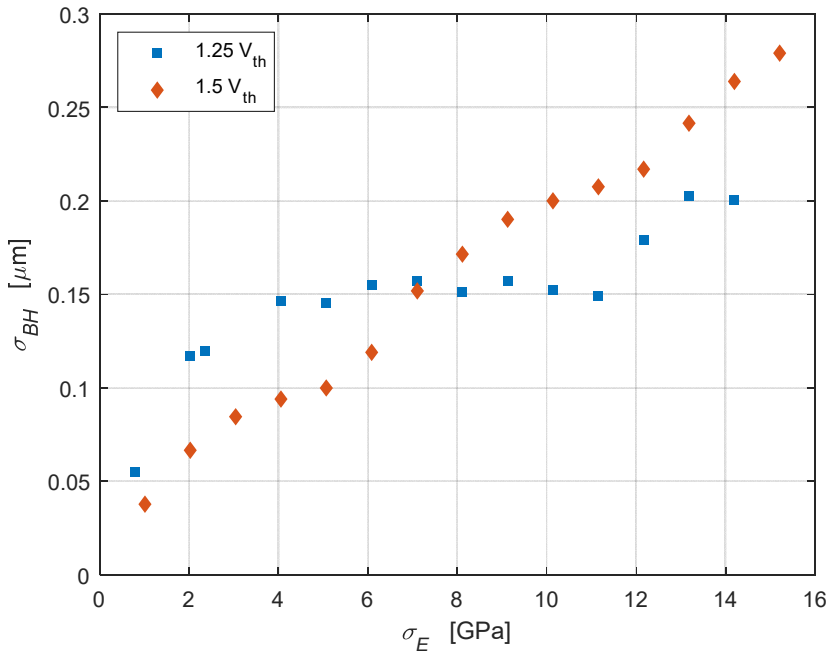

Fig. 4.5 (a). Uncertainties in Young's modulus E on major bounce height BH for actuation voltages 1.25 V_{th} and 1.5 V_{th}.

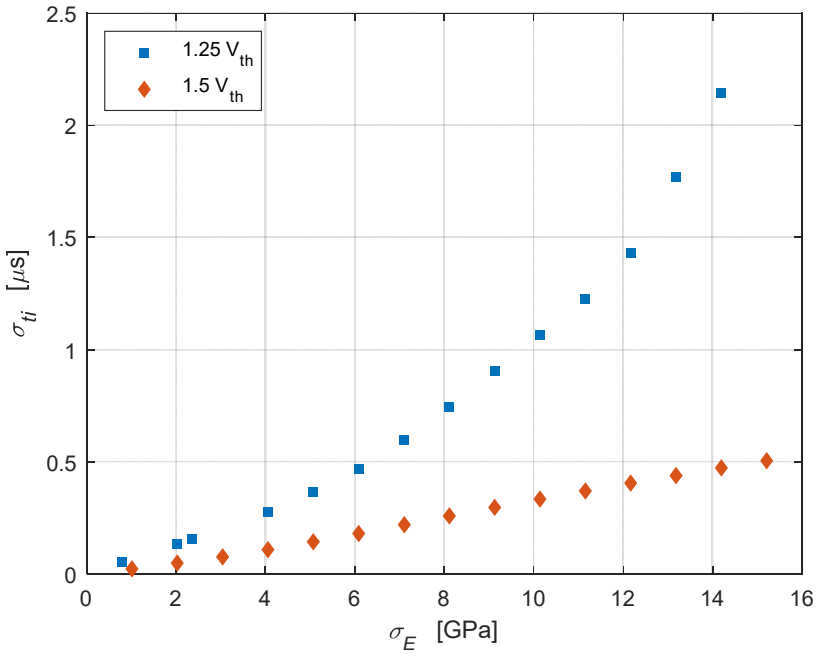

Fig. 4.5 (b). Uncertainties in Young's modulus E on initial contact time t_i for actuation voltages $1.25\ V_{th}$ and $1.5\ V_{th}$.

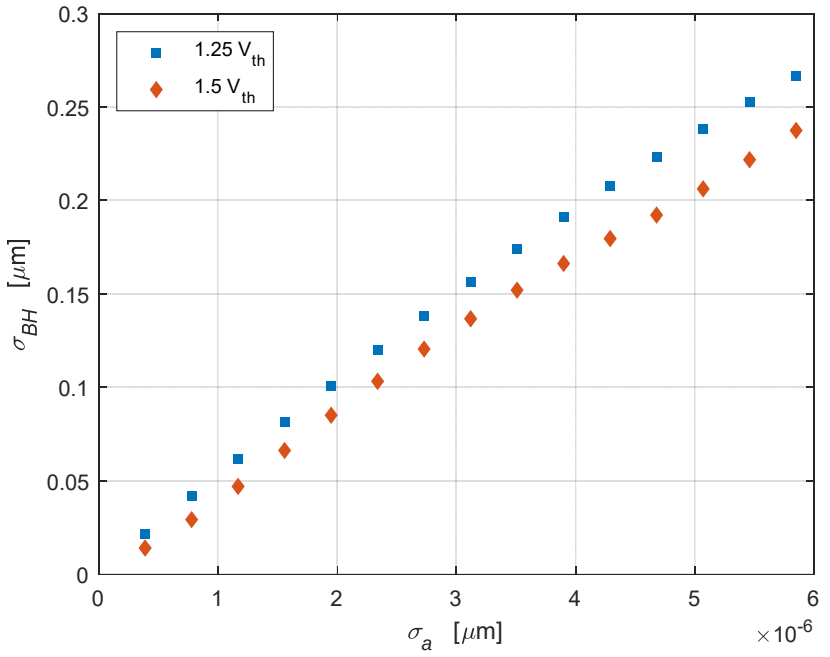

Fig. 4.6 (a). Uncertainties in beam width a on major bounce height BH for actuation voltages $1.25\ V_{th}$ and $1.5\ V_{th}$.

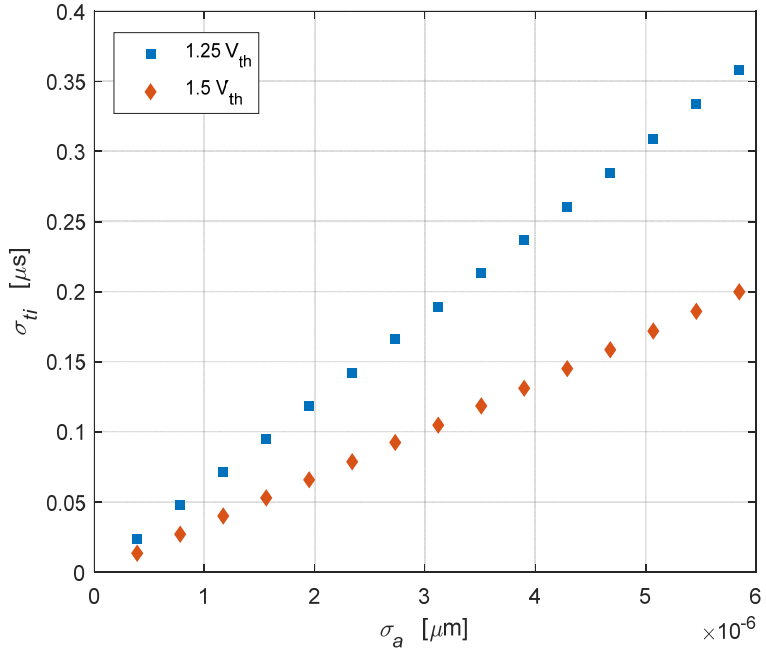

Fig. 4.6 (b). Uncertainties in beam width a on initial contact time t_i for actuation voltages $1.25\ V_{th}$ and $1.5\ V_{th}$.

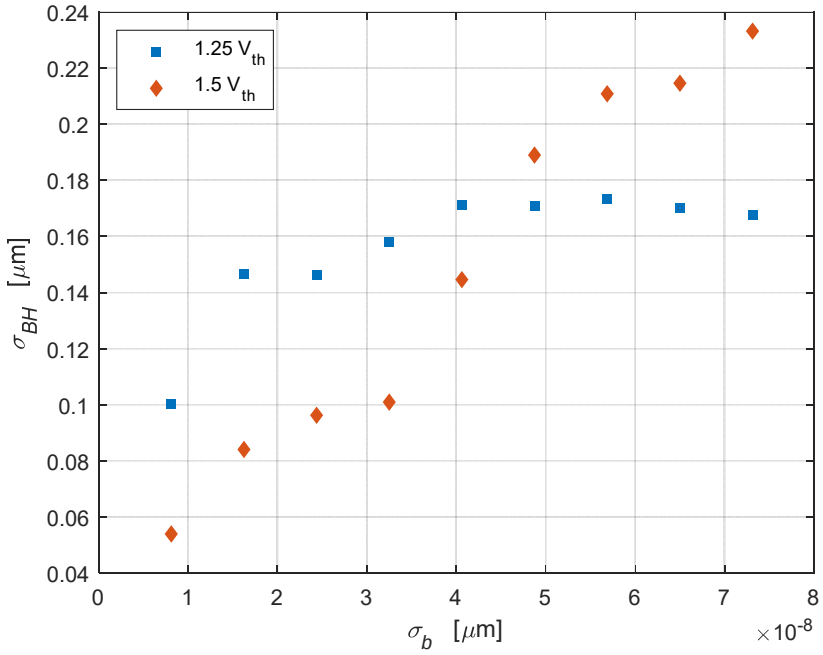

Fig. 4.7 (a). Uncertainties in beam thickness b on major bounce height BH for actuation voltages $1.25\ V_{th}$ and $1.5\ V_{th}$.

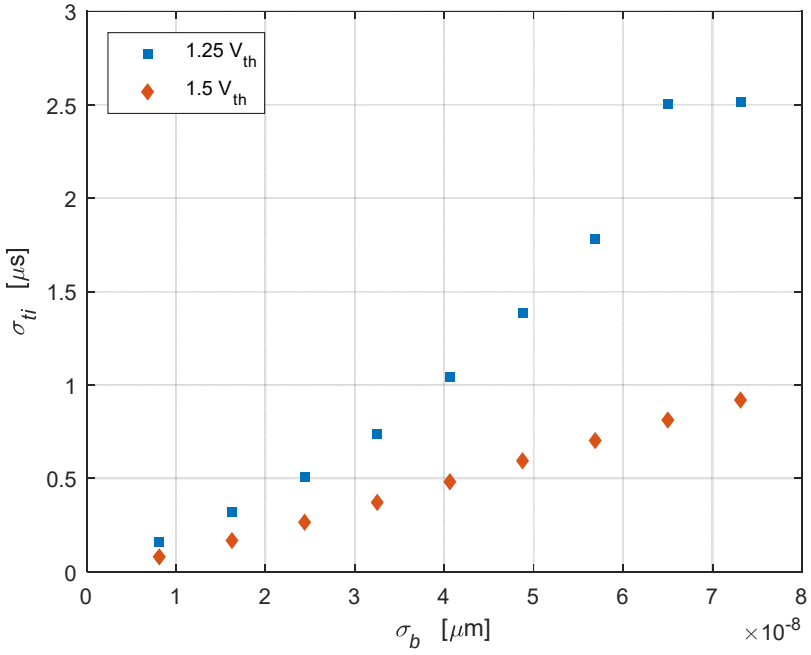

Fig. 4.7 (b). Uncertainties in beam thickness b on initial contact time t_i for actuation voltages $1.25\ V_{th}$ and $1.5\ V_{th}$.

Further, to demonstrate the effects of uncertainties in the actuation voltage, two mean voltages, namely $1.25\ V_{th}$ and $1.5\ V_{th}$ have been considered. A behavior similar to those exhibited for the cases of uncertainties in Young's modulus and beam thickness has also been observed in this case and is depicted in Figures 4.8. It is worth noting that in the case of uncertainties in the actuation voltage a 'no contact' configuration also occurred at moderate standard deviations and hence the analysis has been limited to relatively lower values for σ_V .

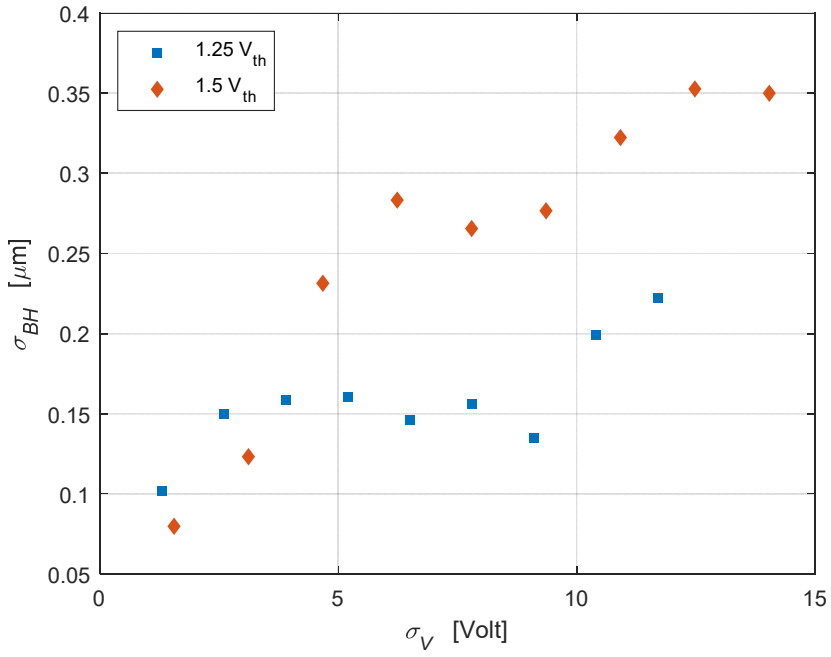

Fig. 4.8 (a). Uncertainties in actuation voltage V on major bounce height BH.

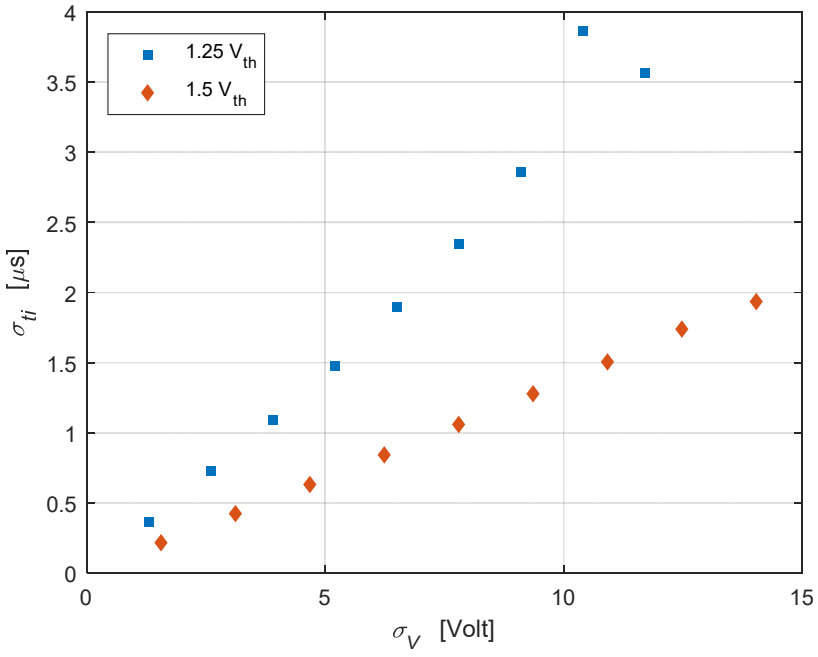

Fig. 4.8 (b). Uncertainties in actuation voltage V on initial contact time t_i.

It may be noted that, from the uncertainty point of view, using a higher actuation voltage reduces the uncertainty in the initial contact time for the tip geometry and contact surface

parameters and increases the uncertainty in the major bounce height except in the case of the uncertainty in the tip width. Moreover, the benefit of using high voltage to reduce the uncertainty in the bounce height uncertainty is limited by most of the studied parameters except for the uncertainty in the beam width. This result confirms the deterministic results in chapter 3 that pointed out the limitation of using higher actuation voltage to improve switch performance. It is acknowledged that the present study has been limited to single parameter effect assessment. However, it is worth noting that multiple parameter variation to characterize the mutual effects of these parameters on the switch performance may prove to be beneficial and it is recommended for further investigation.

4.3 Conclusions

A micro switch model that includes the relevant forces and a suitable numerical scheme for providing an insight into the switch nonlinear transient dynamics is employed as a basis for characterizing the influence of uncertainties in system parameters. An asperity-based contact model which represents the nonlinear contact mechanics is included in the model. Euler-Bernoulli beam theory and an approximate approach based on Galerkin's method have been employed for predicting transient dynamic responses which takes the bouncing behavior into consideration. The model and the scheme developed are capable of accurately predicting responses and are employed for the assessment of uncertainty measures due to important beam material/geometric properties, beam tip properties, actuation voltage and tip asperity contact parameters. The quantitative predictions reveal several varying patterns as well as similar trends for output measure second order statistics. The study also points out the advantages in operating the switch at higher voltages to gain some performance improvements while emphasizing the limitations based on the bounce height. It is envisaged that this quantitative understanding of uncertainties will lead to more exact identification of critical design parameters, which can then be controlled during fabrication, in order to improve the device performance and reliability.

CHAPTER 5

MODELING OF A NEM SWITCH

5.1 Introduction

In this chapter, mathematical models of cantilever-based NEM switches under electrostatic as well as pure Casimir actuation have been employed to study the switch dynamics. Other forces and effects related to nano structures, such as intermolecular forces, surface effects and rarefication effects are included in the model. As discussed in the literature review section, modeling of NEM devices that uses conventional theories available in mechanics may not accurately predict the behavior when the characteristic sizes shrink to nanometers; therefore, continuum models for MEMS need to be modified to accommodate these effects for nano scale. As the dimensions shrink to nano level, intermolecular forces, such as van der Waals force (Israelachvili, 1992) and the Casimir force (Lamoreaux, 2004, Mostepanenko & Trunov, 1997), may play an important role in predicting the behavior of NEM switches. These intermolecular forces are usually neglected in MEM applications since the strength of these forces are negligible compared to other forces. However, the magnitudes of these forces grow rapidly with decreasing separation distance, which is a character of NEM switches, and hence such forces have comparable magnitudes. Moreover, NEM devices have large surface area to volume ratio, due to typical nanoscale structures, and the surface energy becomes a significant part of the total elastic energy. Therefore, surface effects of nanostructured materials such as surface stress and surface elasticity have also significant effects on the NEM device dynamic behavior. In addition to the importance of intermolecular forces and surface effects in modeling, a rarefied condition in gas damping should be also incorporated in the modeling. This rarefaction is caused by either the small characteristic length scales and/or operating in a vacuum condition which exists in NEM applications. Typically, the nano switches are electrostatically actuated but with the emergence of Casimir force alteration, a new method of actuation could open a new avenue to develop nanoscale self-switching without electrostatic actuation. In order to develop a continuum model of a NEM switch, these

forces and effects need to be accommodated in the model to accurately predict the dynamic response. The following sections describe the mathematical modeling of these forces and effects followed by a comprehensive mathematical model of the switch under both electrostatic and pure Casimir actuation.

5.2 Intermolecular forces

As discussed earlier, the intermolecular forces, which include the Casimir force and the van der Waals force, between two separated electrodes may play a significant role in the performance of NEM switches. The origin of both the van der Waals and Casimir forces are related to the existence of quantum fluctuation of the electromagnetic fields (Lamoreaux, 2004). The generic name of these forces is dispersion forces. When the gap between two surfaces is much smaller than the plasma (for metals) or characteristic absorption (for dielectrics) wavelength, that is between a few angstroms and a few nanometers, the retardation effects are not negligible. At this separation level, the dispersion force is usually called the van der Waals force. At relatively large atomic separations, retardation effects play an important role and at such separations the dispersion forces are usually called Casimir-Polder for atom-atom and atom-wall interactions or Casimir for interaction between two macroscopic bodies forces (Klimchitskaya *et al.*, 2009).

The well-known Lennard-Jones potential that describes interaction between two atoms is usually used to formulate a continuum model of the van der Waals force. The attractive and the repulsive parts of the Lennard-Jones potential should be taken into account when the gap between two surfaces is smaller than few nanometers; however, the repulsive part of the potential decays extremely fast with separation and plays an important role only after the contact of surfaces takes place. The total van der Waals energy (or force) can be found by integrating the energy between all pairs of molecules existing in the two bodies. The attractive and repulsive van der Waals force magnitudes are proportional to the inverse cube and ninth power of the separation, respectively, and this force is affected by material properties and falls off rapidly at distances larger than the plasma wave length. When the separation between the two surfaces increases further and lies in a range around $100\ nm$,

the interaction between two surfaces is described by the Casimir force, which is proportional to the inverse fourth power of the separation and is not affected by material properties. It is obvious that van der Waals and Casimir forces describe the same physical phenomenon but at two different length scales, hence they may not be considered simultaneously in most cases moreover the repulsive part of van der Waals force is considered when contact occurs. In the following sections, detailed mathematical modeling of the intermolecular forces will be introduced.

5.2.1 Casimir force

As mentioned in section 5.2, the Casimir force is connected with the existence of the quantum fluctuations in the zero-point electromagnetic field. Modern physics assumes that a vacuum is full of fluctuating electromagnetic waves that can never be eliminated and the existence of these electromagnetic waves with all possible wavelengths implies that empty space contains a certain amount of energy. When two plates are placed very close together facing each other in a vacuum, some waves will be trapped between the plates and bouncing back and forth while other waves cannot fit. As the gap between the plates decreases, a larger number of longer waves can not fit between them. Thus, the energy between the plates becomes less than the energy in the surrounding vacuum. The waves (energy) from outside pushes the plate together. Therefore, the plates will attract each other due to the pressure from outside. This pressure represents a Casimir attraction force. In the literature, the parallel plate concept is employed for beams if the gap is very small as in NEM switches. In this case, the Casimir force per unit length of the beam is given in a study by Farrokhabadi *et al.* (2016) as,

$$f_{CA} = \frac{1}{240}\frac{\pi^2\,\bar{h}\,c\,a}{[d - y(x)]^4}\ , \tag{5.1}$$

where $\bar{h} = 1.055 \times 10^{-34}\,J$ represents the Planck's constant divided by 2π while $c = 2.99810^8\,ms^{-1}$ denotes the speed of light.

Reduction of both power consumption and size of devices is a goal in previous research and it would be beneficial in this regard to develop nano-switches which can be switched by using new stimuli that contribute to power saving or size reduction. Hence, emergence of Casimir alteration attracted many researchers to utilize this force as alternative method for actuation. The techniques that can successfully control Casimir force are summarized in studies (Chen *et al.*, 2007, Esquivel-Sirvent *et al.*, 2009, Chen *et al.*, 2006, Torricelli *et al.*, 2010) in literature review section 1.2.2. For example, the latter reference increased Casimir force experimentally by 20% to 25% via controlling the dielectric properties of materials by laser heating a thin film made of Ag-In-Sb-Te (AIST). Heating this film changes the phase reversibly from a crystalline to an amorphous state. Eq. (5.1) can be modified by including a parameter k to represent the change in Casimir force. Thus, the Casimir force per unit length of the beam as given in the paper by Ma *et al.* (2010) utilized in the present study:

$$f_{CA} = \frac{1}{240}\frac{\pi^2\,\bar{h}\,c\,a}{[d-y(x)]^4}\,(1+k)\,, \tag{5.2}$$

where a parameter k represents the actuation gain. Hence, this parameter can be considered to essentially represent the controllable part of the Casimir forces. A low Casimir force associated with a non-actuated switch is represented by $k = 0$, while a value of $k = 0.25$ for a corresponding actuated switch.

5.2.2 Van der Waals force

The van der Waals force described by the Lennard-Jones potential is determined per unit length of the beam as,

$$f_{VDW} = \frac{A_h\,a}{6\pi}\left[\frac{1}{[d-y(x)]^3} - \frac{\varepsilon^6}{[d-y(x)]^9}\right], \tag{5.3}$$

where A_h is the Hamaker constant and ε is the equilibrium distance at which f_{VDW} becomes zero (see, e.g., Hariri *et al.*, 2004, Yu & Polycarpou, 2004). The Hamaker constant depends on the material properties and its typical values are in the range of $(0.4 - 4) \times 10^{-19} J$ for most polar molecules (Ma, 2011) while the equilibrium distance varies around 2A^0 for most materials. The cubic term in Eq. (5.3) represents long range van der Waals attraction forces and the ninth order term describes the short range Born repulsion (Yu & Polycarpou, 2004). It is worth noting that the Casimir force and the van der Waals force cannot be considered to act simultaneously since they describe the same physical phenomenon and both act at different gap separation. In the present study, a separation of $20\ nm$ as suggested in the study by Ramezani *et al.* (2007) has been employed in the simulations to distinguish between the ranges of dormancy of each force. Thus, van der Waals force acts when the electrode separation is below $20\ nm$ while the Casimir force dominates beyond $20\ nm$ of gap separation. It should also be noted that the repulsive part of the van der Waals force will participate during contact phase in addition to asperities-based contact force. Figure 5.1 shows a graphical representation of the dominant range of the intermolecular forces.

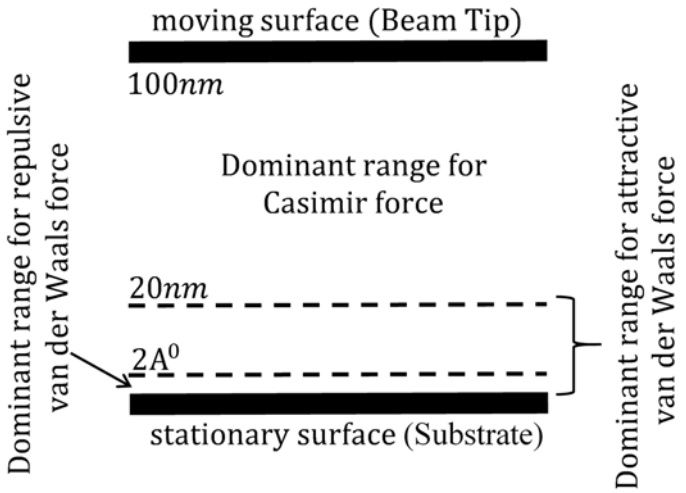

Fig. 5.1. Schematic representation of active range for intermolecular forces.

5.3 Force due to surface effects and equivalent bending elasticity

In general, the mechanical properties of macroscopic materials are independent of the structure size. However, when the size of the structure is reduced to nano scale, such as for nano-switches, the surface becomes relatively large compared the volume and hence the surface may play crucial role in characterizing the properties. Surface effects such as surface stress (or surface tension) and surface elasticity are ignored in macro and micro structures. For instance, when the sizes of MEMS structures greater than $100\ nm$, the effective properties are mainly governed by classical bulk elastic strain energy in which the influence of surface stress can be neglected. However, these effects have been considered in nano structures and the properties have been found to be proportional to the increase in surface area to volume ratio. In nanomaterials, surface effects arise due to the fact that atoms which are at the material free surfaces have a different bonding configuration as compared to bulk atoms. Atoms at a surface are not at an energy minimal-state and surface stresses try to cause these atoms to deform to minimize their energy. The different bonding environment of atoms at a surface and in bulk makes the elastic properties of surfaces differ from those of bulk material and the effect of the difference magnifies with an increase of the surface to volume ratio (Park, 2008). Thus, for accurate prediction of dynamic behavior, consideration of surface effects in modeling of nano-structures, such as nano switches in the present study, is essential.

The continuum modeling of nanostructures with the consideration of surface effects is based on linear surface elastic theory developed by Gurtin and Murdoch (1975) and the generalized Young–Laplace equations. In the surface elasticity model, the surface consists of a thin layer with negligible thickness perfectly bonded to the bulk material and slipping between the surface and bulk materials is not allowed. The properties of the surface are different from those for the bulk materials. The constitutive relations for the surface and the bulk of the nanostructures are different since the atoms in these two domains experience different surrounding environments. The generalized Young-Laplace equations govern the equilibrium of the surface. It should be mentioned that the material properties of the surface can be determined from experiments or atomistic simulations. In the present study, the

surface elasticity model and the generalized Young-Laplace equations are employed to model the surface effects in the switch.

A surface-layer-based model constitutes the foundation for continuum modeling of nanostructures with the consideration of surface effects. In this model, the nanostructure is assumed to be composed of a bulk and a surface, i.e., a nanostructure = bulk + surface. A thin layer with an elastic modulus E^1 and with negligible thickness, t^s, beneath the surface represents the surface layer of a cantilever nanobeam with rectangular cross section as shown in Figure 5.2. As mentioned previously, the constitutive equation for the surface is

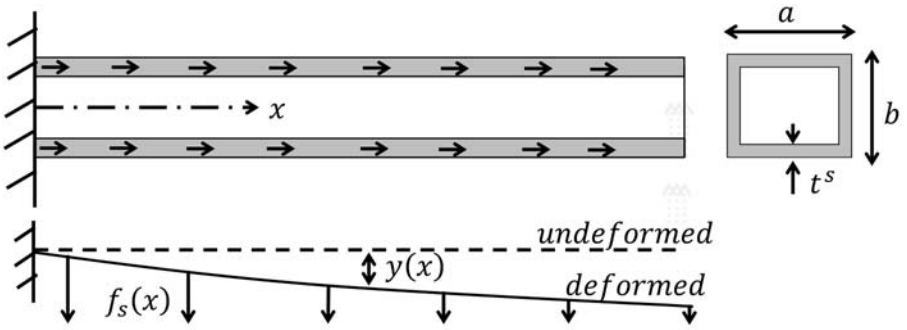

Fig. 5.2. Schematic of a bending NEM switch with surface effects (Ma, 2011).

different from the bulk due to different local environments present around the atoms. For a bending beam, the relation between the surface stress, τ, and the longitudinal strain ϵ_x, as given in study by Miller an Shenoy (2000), is

$$\tau = \tau^0 + E^s \epsilon_x \,, \tag{5.4}$$

where τ^0 is the residual surface stress along the beam longitudinal direction and E^s represents the surface elastic modulus. The relationship between $E^1$and E^s is expressed as $E^s = E^1 t^s$. By using the composite beam theory under the assumption that the thickness of the surface layer t^s, is much smaller than the beam thickness b, the effective bending rigidity, $(EI)_{eff}$, for a beam with rectangular cross-section is derived as,

$$(EI)_{eff} = EI + \frac{1}{2}E^s ab^2 + \frac{1}{6}E^s b^3. \tag{5.5}$$

The last two terms in Eq. (5.5) contribute to the surface elasticity. The generalized Young-Laplace equation gives a mathematical description of the out-of-plane stresses induced from in-plane stresses of curved interface surfaces (He & Lilley, 2008). According to the generalized Young-Laplace equation, the residual surface stress results in a jump of the normal stress $\langle \sigma_{ij}^{+} - \sigma_{ij}^{-} \rangle$ across the interface surface between the surface layer and the bulk volume, i.e.,

$$\langle \sigma_{ij}^{+} - \sigma_{ij}^{-} \rangle \, n_i n_j = \tau^0 \, \kappa, \tag{5.6}$$

where σ_{ij}^{+} and σ_{ij}^{-} represent the stresses above and below the surface, respectively. The parameter n_i is the unit normal vector to the surface and κ is the curvature of the beam. For a beam with small deformation, the curvature is approximated by the second derivative $\mathrm{y}''(x)$ of the beam deflection. For a deformed beam, Eq. (5.6) predicts that the stress jump due to the residual surface stress will generate a distributed transverse load $f_S(x)$ along the longitudinal direction of the beam and this load is given in study by He and Lilley (2008) as:

$$f_S(x) = 2\tau^0 a \, \frac{d^2 y(x)}{dx^2}. \tag{5.7}$$

Equation (5.7) indicates that surface stress comes into effect once the beam is bent with a non-zero curvature, as shown in Figure 5.2. This distributed transverse force may stiffen or soften NEM switches during its bending process depending on the sign of the surface stress. In the present study, the surface effects will be incorporated into the nonlinear model of the NEM switch to investigate dynamic bouncing behavior. It is worth noting that in the modeling of a NEM switch, the contact force will take a similar form as in the MEM switch as presented in section 2.1.3 with the consideration of surface effects discussed in this section.

5.4 Damping force

NEM devices usually work under a dry and clean environment and require vacuum packaging for these purposes. In the dynamics of NEM devices, the gas damping has a significant influence on the device behavior since the surface is large compared to the volume. However, under these conditions of low pressure and the smallness of characteristic gaps, the rarefied damping effect needs to be considered in the modelling. If the dimensions of the structure contained the gas is comparable to the mean free path of the gas molecules, the fluid can no longer be regarded as continuum flow and the rarefaction will occur. The ratio between the mean free path and the characteristic dimension of the flow geometry, d , is commonly referred as the Knudsen number, K_n, and this ratio is given by:

$$K_n = \frac{\lambda}{d}. \tag{5.8}$$

In the beam case, d represents the gap between the beam and the substrate. For gases, the mean free path of the molecule, λ, can be related to the temperature, T, and pressure, P, via

$$\lambda = \frac{\mu}{P}\sqrt{\frac{\pi K_B T}{m_m}}, \tag{5.9}$$

where $K_B = 1.38066 \times 10^{-23}\, J\, K^{-1}$, is the Boltzmann's constant, T represents the temperature, P denotes the pressure and m_m is mass of the molecules (Sumali, 2007). The value of the Knudsen number determines the degree of rarefication of the gas and the validity of the continuum flow assumption. For $K_n \leq 0.001$, continuum flow is applicable, and the Navier-Stokes equations can be used. When $0.001 \leq K_n \leq 0.1$ rarefication effects start, and Navier-Stokes equations can be used along with slip-velocity boundary conditions. Beyond $K_n = 0.1$, the continuum assumptions of Navier-Stokes equations are not appropriate. In this case alternative simulation techniques such as particle based DSMC (Direct Simulation Monte Carlo) is used. For $K_n \geq 10$ the continuum approach breaks down completely and the flow refers as free molecular flow (Barber & Emerson, 2002). As mentioned in the literature review in section 1.2.2, several models

have been developed that are valid for high Knudsen number. Gallis and Torczynski (2004) developed a molecular-dynamics-based model by the direct simulation Monte Carlo method for squeeze-film damping on a rigid beam. Then Parkos (2013) further improved Gallis and Torczynski's model and validated experimentally. In Parkos' model, a variable damping coefficient C_f is defined as:

$$C_f = \frac{f_D}{(dy/dt)}, \tag{5.10}$$

where f_D represents the damping force per unit length. The velocity of the beam, dy/dt, varies with lengthwise location as well. Based on this formulation, the near-contact damping coefficient is assumed to be of the form:

$$C_f = A_1 \left[\frac{a}{d - y(x)}\right]^{\gamma} + A_2 \tag{5.11}$$

for $[a/(d - y(x))]$ values less than a certain cut-off value z_c. Beyond this cut-off value, the damping coefficient takes the form

$$C_f = \frac{\mu \left[\frac{a}{d - y(x)}\right]^{-3}}{(1 + 6\chi K_n)} \left[1 + 6\eta \frac{a}{d - y(x)} + 12\zeta \frac{a}{d - y(x)}\right]. \tag{5.12}$$

The cut-off value z_c is used to extend the near contact model to a model that is not applicable near the contact developed by Gallis and Torczynski (2004). Suggestions for typical parameter value for γ are determined via simulations while the constants $A_1$and A_2 in Eqs. (5.11) are shown to depend on the Knudsen number. The suggested values of the coefficients $A_1$and A_2 are

$$A_1 = \frac{-3\mu_G}{(1 + 6\chi K_n)} \left(\frac{1}{z_c^4} + \frac{4\varphi}{z_c^3} + \frac{4\zeta}{z_c^2}\right) a^{-1} \; z_c^{1-a}, \tag{5.13}$$

$$A_2 = \frac{\mu_G}{(1 + 6\chi K_n)} \left(\frac{1}{z_c^3} + \frac{6\varphi}{z_c^2} + \frac{12\zeta}{z_c}\right) - z_c^a \, A_1, \tag{5.14}$$

where $\mu_G = 0.84\mu$ and μ is the air viscosity. The coefficients χ, φ, and ζ are calculated as functions of the Knudsen number by Gallis and Torczynski (2004). Their values may be obtained from

$$\chi = \frac{1 + 8.834\, K_n}{1 + 5.118\, K_n}\ , \tag{5.15}$$

$$\varphi = \frac{0.634\ +\ 1.572\, K_n}{1\ +\ 0.537\, K_n}\ , \tag{5.16}$$

$$\zeta = \frac{0.445\ +\ 11.20\, K_n}{1\ +\ 5.510\, K_n}. \tag{5.17}$$

Based on the above discussion on effects and forces that need to be considered in the modeling of nano structures, the governing equation of motion of the switch with consideration of these effects can now be introduced in the following section.

5.5 Equations of motion for a switch under electrostatic/pure Casimir actuation

Figure 5.3 shows a typical cantilever switch that has length L, beam tip gap d_T, beam initial gap d, beam thickness b , beam tip length L_T , and beam width a. The electrostatic force is considered to act on the beam segment between lengths L_1 and L_2. An asperity-based contact model which represents the nonlinear contact mechanics along with consideration

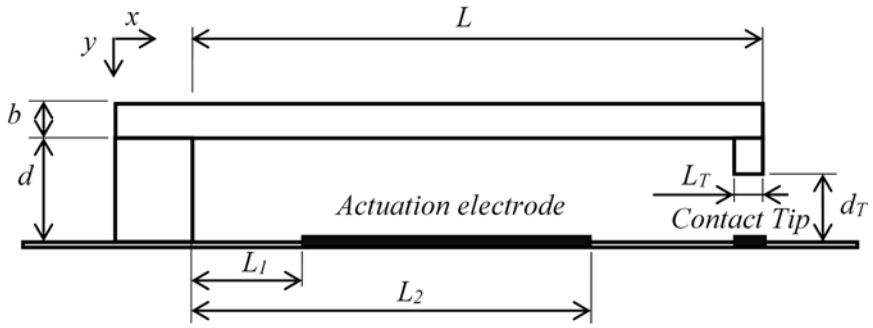

Fig. 5.3. Typical cantilever beam type nano-switch with electrostatic electrode.

of intermolecular forces are incorporated for the purposes of capturing the bouncing dynamics and for actuation purposes. In addition, rarefied damping forces, surface effects due to surface stress, surface elasticity are incorporated in the model. Euler-Bernoulli beam theory is used to develop the equation of motion that governs the flexural dynamics of the switch. When these forces and effects are incorporated in the modeling, the equation of motion takes the form (Liu, 2016):

$$\frac{\partial^2}{\partial x^2}\left((EI)_{eff}\ \frac{\partial^2 y(x,t)}{\partial x^2}\right) + \rho A \frac{\partial^2 y(x,t)}{\partial t^2} = f_E + f_{CA} + f_{VDW} + f_s + f_D - f_C\ , \qquad (5.18)$$

where $y(x,t)$ is the transverse displacement of the beam, $(EI)_{eff}$ represents the effective bending rigidity of the beam with the consideration of surface elasticity, and ρ is the beam material mass density per unit volume, while A denotes the area of the beam's cross-section. f_E represents the actuation electrostatic force, while f_{CA} and f_{VDW} denote, respectively, the Casimir force and van der Waals force. f_s represents a load force due to surface stresses. f_D denotes the dissipating damping force due to the squeezed air film damping effect between the beam and the substrate. f_C is the contact force. It may be noted that all applied forces are expressed per unit length of the beam.

Detailed expressions for forces such as the Casimir force, van der Waals force, dissipating damping force and the force that represents surface stress effect, in addition to the expression for the effective bending rigidity, are provided in previous sections. Detailed expressions for forces such as the electrostatic force, and contact force were presented in chapter 2 and they have similar forms as for MEM switches and are not repeated in this section. Moreover, the solution procedures including the determination of mode shapes, natural frequencies of the beam, the discretization method and the prediction of the response are similar to those presented in chapter 2 for the MEM switch. The reader recommended to refer to chapter 2 for details. The system of ordinary equations is solved in MATLAB using the numerical integrator ode45 which is based on an explicit Runge-Kutta (4, 5) formula (The MathWorks, 2013).

It may be noted that the electrostatic force, as well as the intermolecular forces for nanoscale switches, are inversely proportional to different powers of electrode separation.

The contact force has nonlinear characteristics due to its discontinuity definition as well as due to fractional proportionality of the interface of the asperities. Hence NEM switches exhibit inherent nonlinear behavior, which makes the prediction on the dynamic rather challenging. Moreover, surface effects and damping for nanoscale switches further complicate the analysis. Exact solution for the resulting nonlinear beam equation is difficult to obtain and an approximate numerical approach based on Galerkin's method is employed in the present study to predict the responses.

To the best of the author's knowledge, it appears that the influence of the surface effects as well as incorporation of both van der Waals force and the multi asperity contact model as described in section 2.1.3 as contact model on the behavior of NEM switches has not been investigated thus far. Moreover, the bouncing dynamic behavior under pure Casimir actuation has also not been covered in literature. Hence, the objective of the current work is to present a general mathematical model for NEM switches by incorporating the electrostatic force, the intermolecular forces, surface effects, tip-contact under electrostatic or pure Casimir actuation to characterize bouncing dynamic behavior. The presented comprehensive model which incorporates these forces and effects is expected to accurate prediction of dynamic behavior which is considered necessary for developing new NEM devices and for controlling/improving their performances.

5.6 Conclusions

The mathematical model representing the dynamic behavior of NEM switches that are actuated electrostatically or via the Casimir force has been derived. Euler-Bernoulli beam theory has been used for the modeling of the cantilever beam. Influences of intermolecular forces, surface effects and the rarefied squeeze film damping have been taken into consideration in the mathematical model in order to provide more accurate response prediction for the NEM switches. In addition to repulsive van der Waals force, a more realistic asperity-based contact model has also been incorporated in the model in order to capture the contact force between the beam tip and the substrate. Surface effects including surface stress and surface elasticity have been incorporated in the governing equation of the models based on the linear surface elasticity theory and the generalized Young-Laplace

equation. The derived distributed parameter model is inherently nonlinear due to the influence of nonlinear forces involved in the model. Since no closed form solution is available for the resulting nonlinear partial differential equation, Galerkin's method is employed to discretize the equation motion of the beam and the resulting system of ordinary differential equations is solved numerically for the purposes of response prediction. It is expected that such comprehensive model of NEM switch yields accurate dynamic responses which are necessary for developing new NEM devices and improving their performances.

CHAPTER 6

BOUNCING DYNAMICS OF NEM SWITCHES UNDER ELECTROSTATIC AND PURE CASIMIR ACTUATION

6.1 Introduction

In this chapter, the dynamic behavior of NEM switches actuated by an electrostatic force and by a pure Casimir force is investigated. Performance parameters such as initial contact time, permanent contact time, major bounce height, and the number of significant bounces have been quantified to investigate the influences of some effects on the switch performance. For electrostatically actuated NEM switches, in the presence of the Casimir force, the influence of surface effects on the dynamic behavior has been studied by comparing the results for cases with/without surface effects at different low-pressure vacuum conditions. The dynamic pull-in voltage is determined for such switches and verified with previous work. A significant improvement in switching time is gained when the applied voltage takes a value of about 1.3 times the dynamic pull-in voltage; however, beyond this voltage bouncing deteriorates the performance and limits the advantage of using higher voltages. Surface effects seems to have non-consistent effect on various parameters during the bouncing stage due to the curvature changes of the beam deflection but it tends to underestimate the performance parameters if ignored at high voltages. Light vacuum pressures although not realistic, seems to improve the bouncing switch performance. For purely Casimir actuated NEM switches, pull-in as well as bouncing dynamic behavior have been investigated in the presence of surface effects at different vacuum conditions. Combinations of lengths and gaps associated with pure Casimir force actuation of the switch have been quantified. The predicted simulation responses show that the beam tip bounces then makes a final contact with the substrate. The results reveal that using short beams with smaller gaps provide better bouncing performance. It was also demonstrated that the elastic forces due to asperities had negligible or no influence on the bouncing behavior. Hence, the van der Waals force is instrumental in governing the tip

contact dynamic behavior. Therefore consideration of van der Waals force is considered sufficient for understanding the bouncing dynamics of NEM switches. The present study is expected to yield greater insight into the design and performance predictions of nano switches and help improve the performance predictions of such switches.

6.2 NEM switch under electrostatic actuation

The switch employed in this analysis is depicted in Fig. 5.3 and dynamically the switch is governed by Eq. (5.18). Transient response simulation of nano switch has been performed to quantify important switch design parameters based on the predicted response with consideration of contact bouncing phenomenon. To validate the model, a silver cantilever NEM switch as considered in the paper by Ma *et al.* (2010) has been chosen in the present study. The dimensional and material properties of the switch are listed in Table 6.1. It may be noted that for all predictions, five normal modes have been used, i.e. $n = 5$. The nano-switch beam from the study by Ma *et al.* (2010) is used for verification of the proposed model. Although the current study focuses on the dynamic behavior of a nano-switch, the static deflections of a similar beam under electrostatic force is used to validate the current model via static deflection. A good agreement is achieved when the electrostatic force is applied very slowly providing a confidence of the current model. It may be noted that the simulations carried out to investigate the bouncing behavior considered all forces including the Casimir as well as the asperity contact forces. However, it was found that in the nano-scale, the asperity contact forces made negligible or no contribution to the bouncing dynamics and hence it was ignored in all of the simulations associated with tip substrate contact. Hence, the bouncing due to the repulsive part of the van der Waals force has been given importance at the contact phase since it governs the bouncing behavior.

Table 6.1. NEM switch parameters and properties

Parameter	**Value**
Beam length, L	$1\ \mu m$
Beam width, a	$250\ nm$
Beam thickness, b	$50\ nm$
Beam tip contact gap, d_T	$0.70L$
Air gap, d	$50\ nm$
Starting point of electrostatic electrode, L_1	$0.25L$
Ending point of electrostatic electrode, L_2	$0.85L$
Beam tip length, L_T	$0.10L$
Young's modulus of beam material, E	$76\ GPa$
Poisson's ratios of contact surfaces, v	0.37
Material mass density, ρ	$10490\ kg/m^3$
Radius of the sphere asperity, R	$100\ nm$
Area density of asperities, η	$0.004\ asperity/\mu m^2$
Residual surface stress, τ^0	$0.89\ \mu N\ \mu m^{-1}$
Surface elastic modulus, E^s	$1.22\ \mu N\ \mu m^{-1}$
Hamaker constant, A_h	$16.4 \times 10^{-20} J$
Equilibrium distance, ε, at which $f_{VDW} = 0$	$1.84\ A^o$
Near contact damping cut-off value, z_c	0.0197
Near contact damping exponent, γ	-0.9373

Figure 6.1 shows a typical switch response when all the relevant forces are included in the model. When a sufficient voltage is applied between the electrodes, the beam switches on and its tip touches the substrate then it bounces several times before it makes the permanent

contact. The figure shows some of the important parameters that characterize the switch performance as follows:

- Initial contact time, t_i, is the time taken for the first contact.
- Permanent contact time, t_p, is the time taken for the switch to maintain permanent contact.
- Bouncing time, t_b, is the time from the instant of making first contact to the instant when the single significant bounce ends.
- Major bounce height, BH.
- Number of significant bounces, NB.

For the set of parameters used in the study, a dynamic pull-in voltage, V_{th} has been determined using the NEM switch model. For the present switch configuration, value of $7.3\ V$ for the dynamic pull-in voltage has been obtained. At this voltage, the NEM switch collapses as the electrostatic force and other attractive forces overcome the elastic restoring force with the consideration of inertia effect and other relevant effects. An increase in the dynamic pull-in voltage to a value of 7.5 V is observed when the surface effects are ignored.

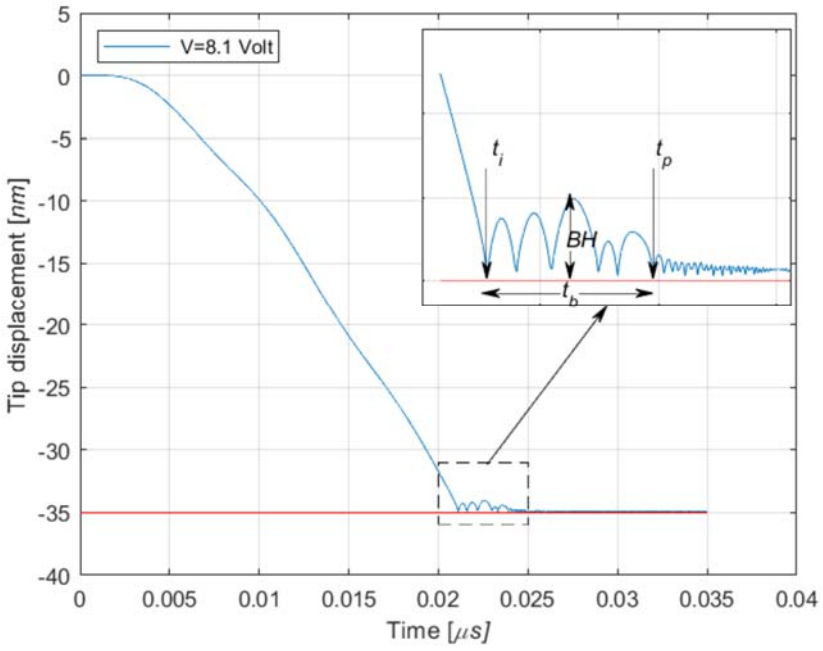

Fig. 6.1. Typical time response of the switch tip.

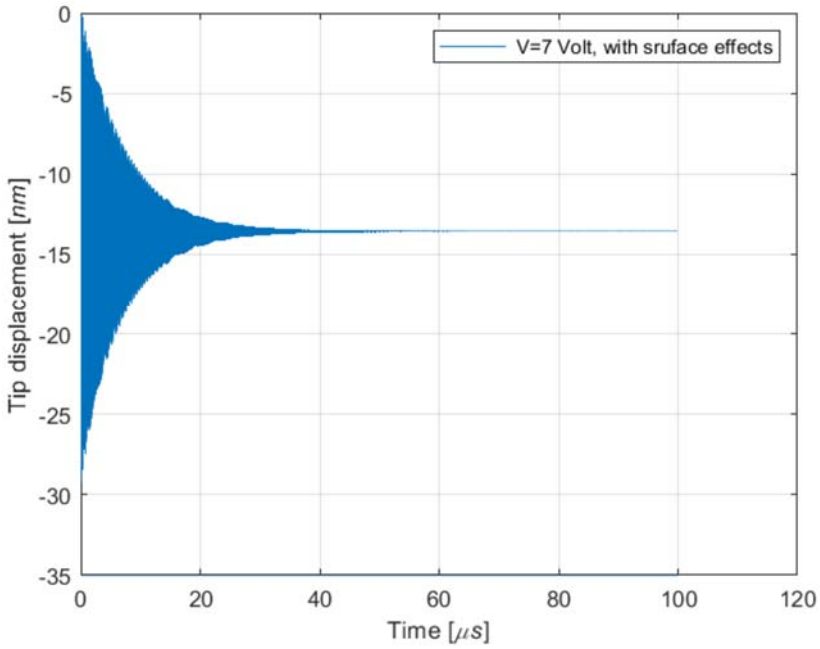

Fig. 6.2. Damped oscillatory motion of nano switch under voltage less than the dynamic pull-in voltage.

An oscillatory damped motion is predicted for voltages less than the dynamic pull-in voltage associated with cases of with and without the consideration of surface effects. As an example, this behaviour is illustrated in Figure 6.2 for a voltage of 7 V. This oscillatory motion eventually settles to an equilibrium position and the beam deflects but do not touch the substrate. For the purposes of comparison, the dynamic behavior of switch is predicted under different vacuum pressures namely at 0.1 $mTorr$,1 $mTorr$, and 100 $mTorr$. It is worth noting that Casimir force has been measured experimentally in a study by Chan *et al.* (2001) at 1 $mTorr$. Having determined the dynamic pull-in voltage V_{th}, the influence of surface effects on the switch performance parameters at different actuation voltages and different pressures have been quantified and are shown in Figures 6.3 through 6.7. Figure 6.3 shows the influence of surface effects on the initial contact time t_i for increasing actuation voltages while Figures 6.4 show the influences of surface effects on the permanent contact time t_p at different pressure as well as voltage values. An overall reduction in the switching time with increasing actuation voltages can be observed from Figures 6.3 and 6.4 which indicates a performance improvement with higher actuation

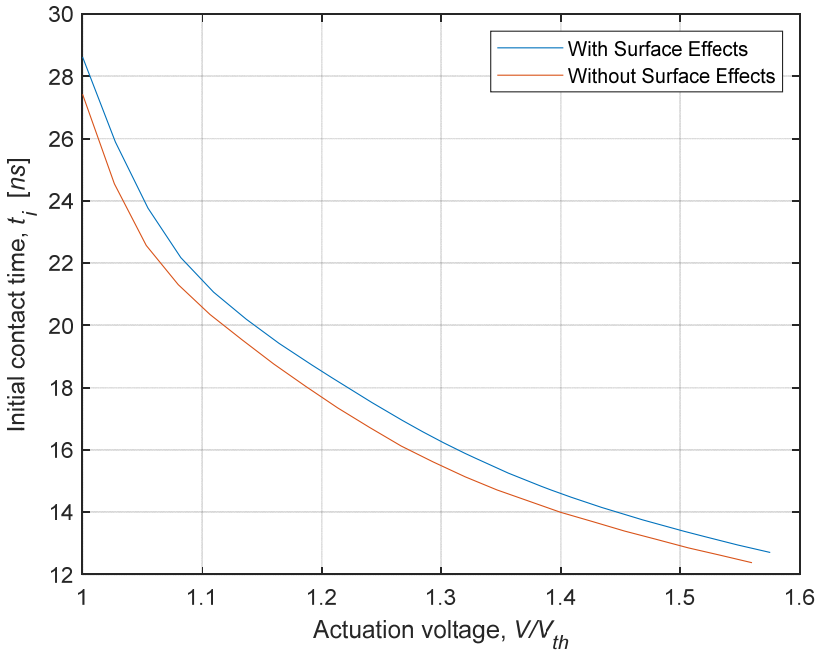

Fig. 6.3. Influence of surface effects on initial contact time t_i at various actuation voltages.

voltage. It is also obvious from the figures that the reduction in the initial contact time, t_i, is greater than the reduction in the permeant contact time due to the bouncing. Increasing the pressure improves t_p but it has no significant effects on t_i and hence not provided. This may be attributed to the low damping values associated with the rarefication. An under estimate of the initial contact time t_i is obvious when the influence of surface effects is ignored. Also, the trend of the variation of t_i as seen in Figure 6.3 may be attributed to the absence of any curvature sign change during the beam flight stage, ie. prior to actual contact; however, when the beam touches the substrate and starts bouncing, the beam curvature sign changes along different regions of beam length, and these curvature sign changes lead to stiffening and softening effects along different segments of the beam. As a result, in general, a non-consistent variation of the permanent contact time t_p at different actuation voltages are evident in Figures 6.4. This may be attributed to the effects of bounce induced curvature changes that influence surface effects as well as other bounce related forces. In general, there is an under estimation of t_p at lower voltages when the surface

effects are not considered at low and high pressures, but it overestimates the performance parameters at medium pressures for high voltage. Figures 6.4 also show reduction in t_p with increasing pressure due to an increase in damping which depress the bouncing.

It is worth noting that the improvement in the switching time by increasing the actuation voltage is seen to be gained at the expense (increase) of other bouncing parameters and

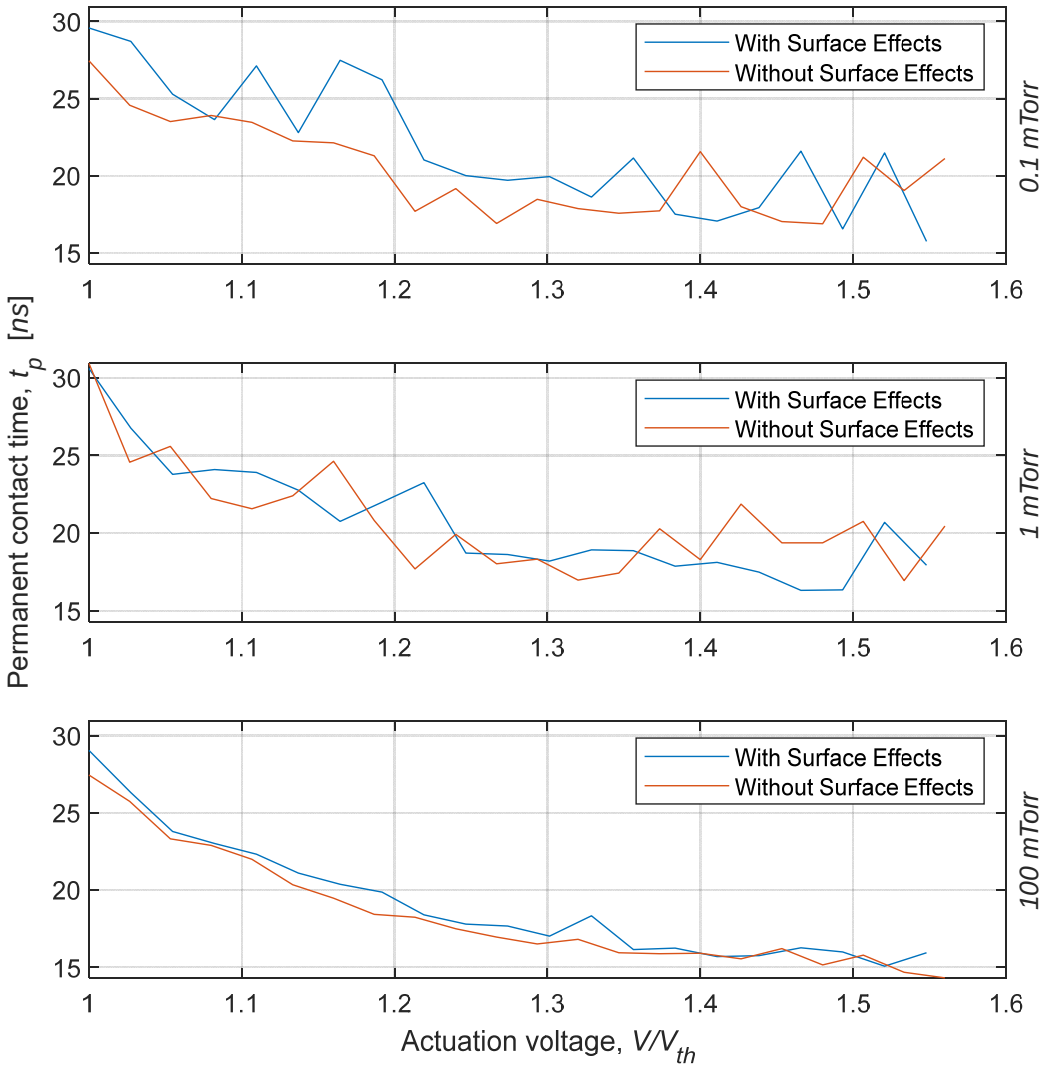

Fig. 6.4. Influence of surface effects on permanent contact time t_p at various actuation voltages and pressures.

these limitations are illustrated in Figures 6.5, 6.6, and 6.7. In addition to the drawback of actuating the switch at higher voltages, the figures show the influence of surface effects at different pressures on the pertinent performance parameters. Figures 6.5 show the influence of surface effects at different pressures on the bouncing time for different actuation voltages. These figures illustrate a general increasing trend of switch bouncing time t_b with the increase of actuation voltage at lower pressures. However, at higher pressure, bouncing

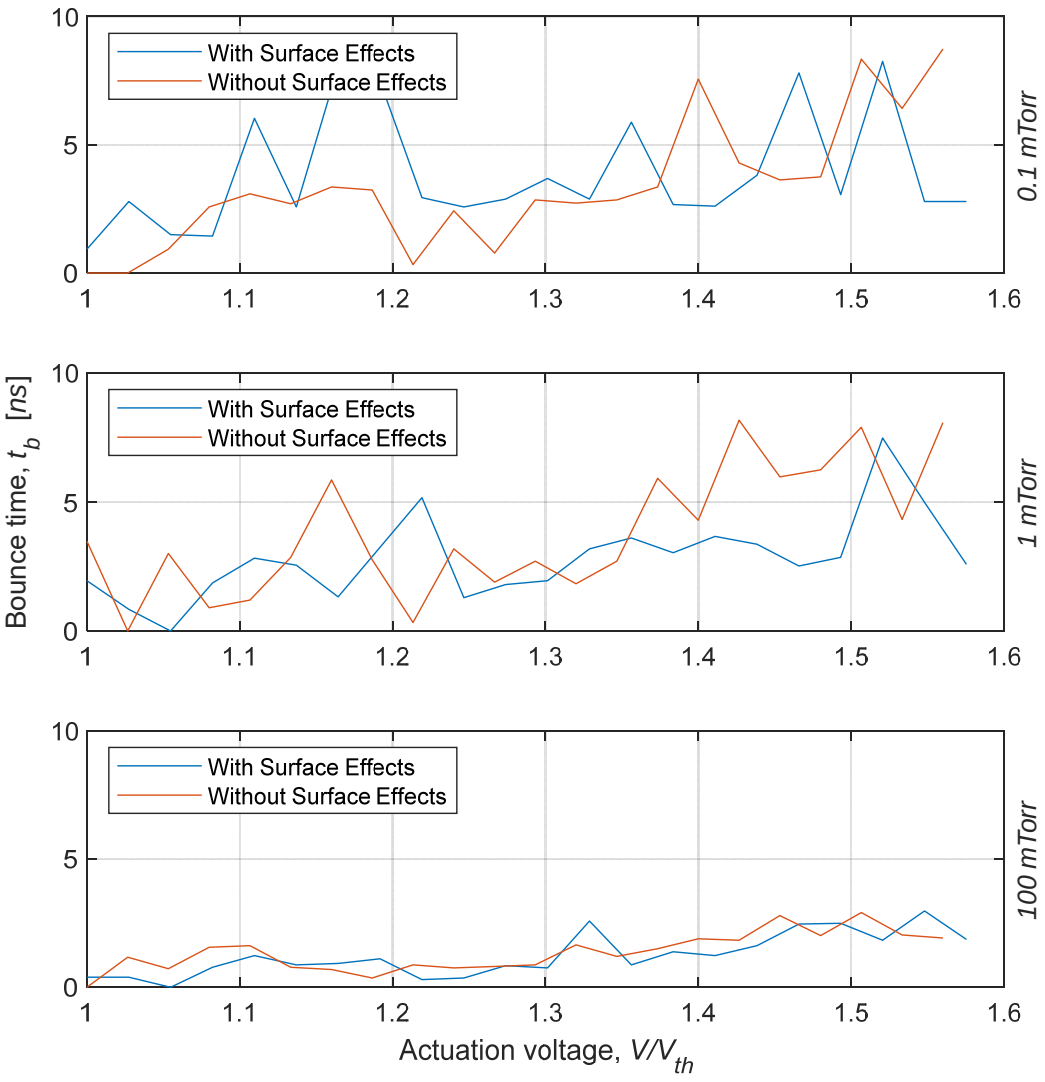

Fig. 6.5. Influence of surface effects on bounce time t_b at various actuation voltages and pressures.

time improves significantly compared with performance at lower pressures. As in the contact time behavior, surface effects lead to a non-consistent trend since the bouncing time is considered during the beam bouncing stage with various stiffening/softening behavior. Also, in general an over estimate of bounce time can be seen at higher voltages when the surface effects are ignored. Similar performance degradation behavior can be observed from Figures 6.6 and 6.7 with increasing the actuation voltage for other performance parameters such as major bounce height, BH, and number of significant bounces NB. Figures 6.6 show a general increasing trend of major bounce height with increasing actuation voltages at all pressures while a relatively smaller increase can be seen in major bounce height for higher pressure. An over estimation of the major bounce height BH at higher voltages is evident in these figures when surface effects are ignored. The disadvantage of using higher actuation voltage to improve the switching time is also limited by the increase of the number of bounces. Figures 6.7 show such behavior where an increase of the number of bounces is associated with increasing actuation voltages. Also, an observation that a slight reduction of NB with increasing pressure is evident. Further, ignoring the surface effects appear to over estimate NB at higher voltages. It may be noted that relatively larger rates of increase in major bounce height BH and the bounce time $t_p$with actuation voltages is evident when the actuation voltage exceeds 1.3 V_{th}. Applying voltages higher than $1.3V_{th}$ causes multiple bounces with larger heights compared to the voltages below 1.3 V_{th}. The increase in these performance parameters limits the use of high voltages to improve the switching time. Thus, more favorable bounce behavior may be obtained when the voltage is less than this voltage. In these cases, a significant improvement in the switching time is attained prior to reaching the severe bouncing stage which will certainly have a detrimental effect on the switch performance. It is worth noting that increasing the pressure is shown to improve the above mentioned performance parameters owing to the increased damping levels; however, NEM devices are usually operated at low pressures and, it is known that the Casimir force cannot be considered at higher pressures since this force is reported in literature only at low pressures. Thus, situations where the pressure is higher as discussed above are not realistic in NEM applications and they are reported here for comparison purposes only.

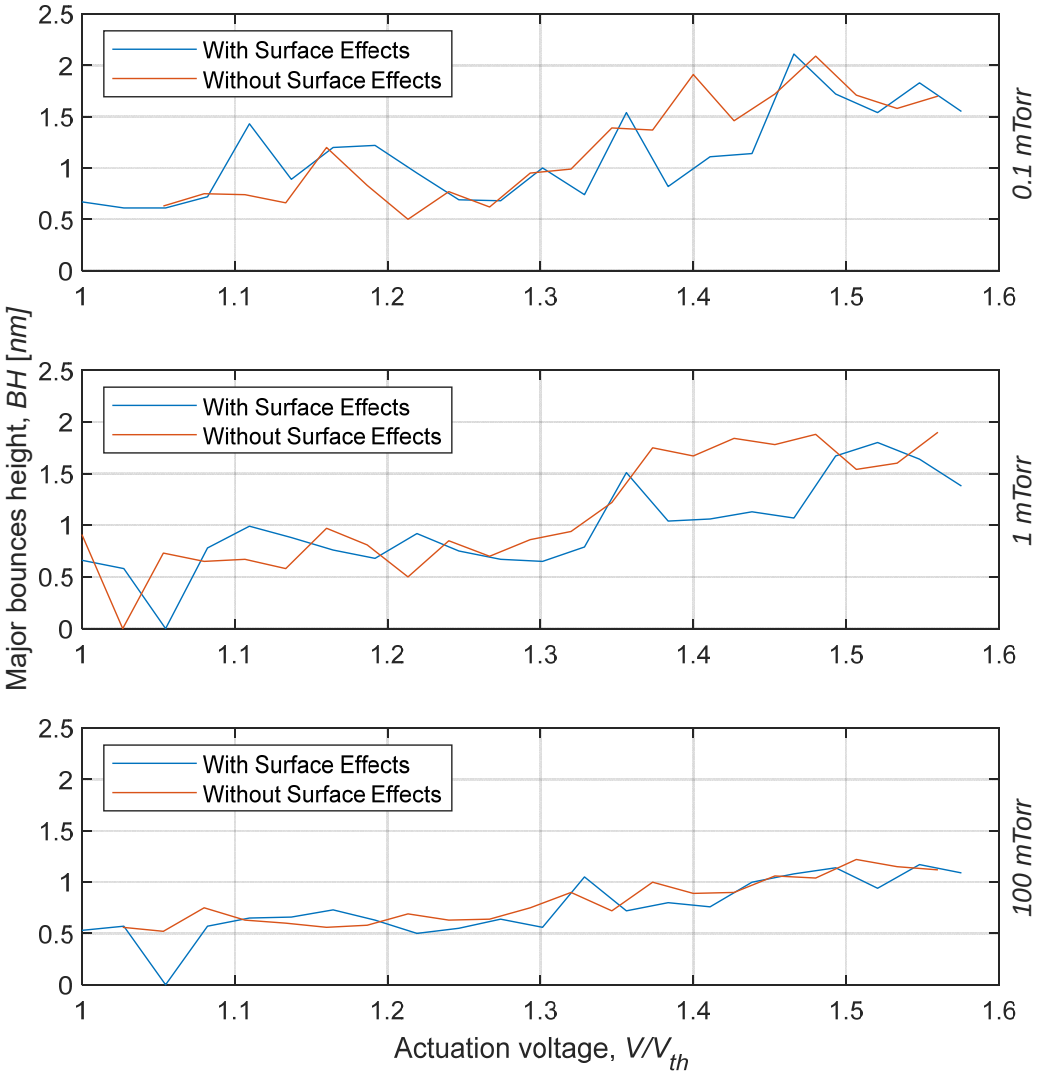

Fig. 6.6. Influence of surface effects on major bounce height BH at various actuation voltages and pressures.

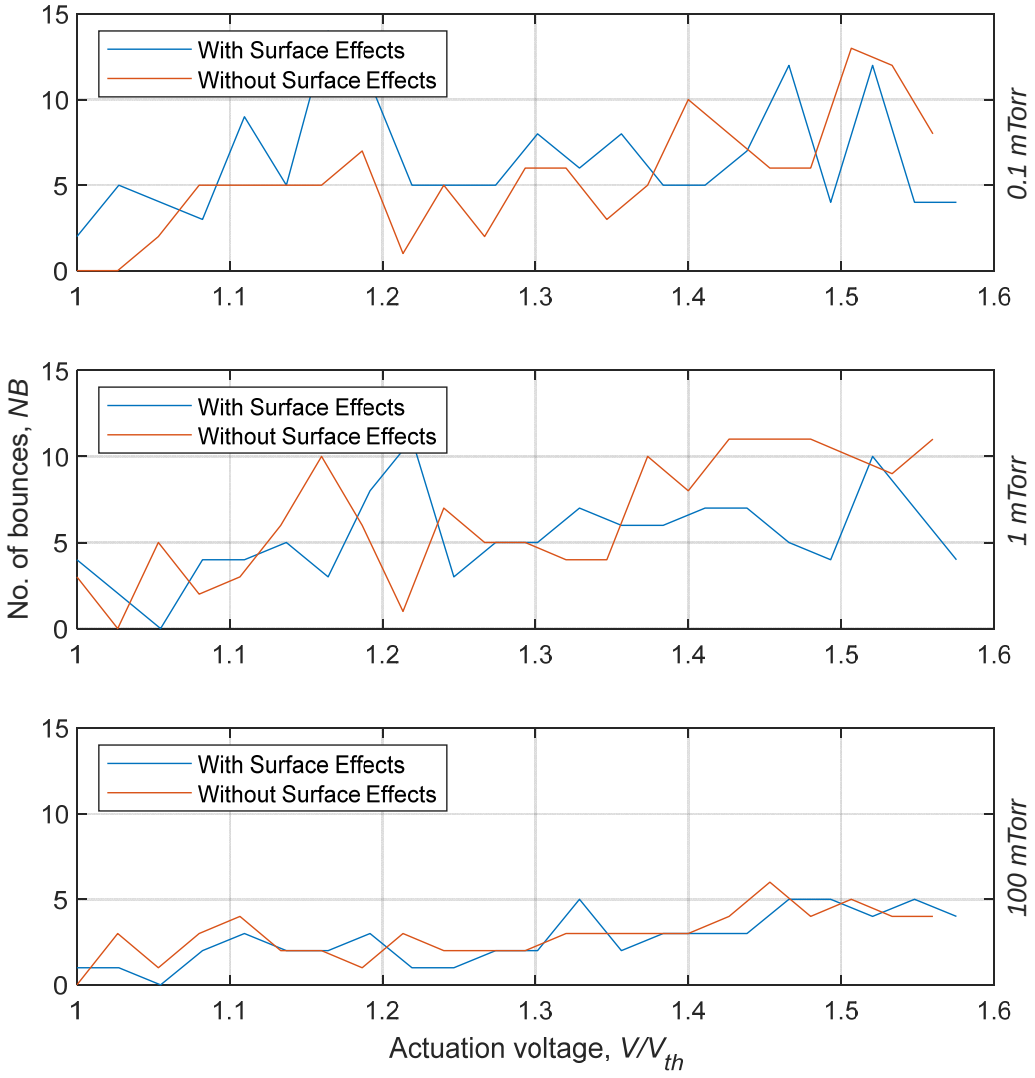

Fig. 6.7. Influence of surface effects on number of bounces NB at various actuation voltages and pressures.

6.3 NEM switch under pure Casimir actuation

The switch employed for pure Casimir actuation is similar to the one used in the electrostatically actuated switch in section 6.2, but with no electrostatic actuation. Hence, the chosen parameters and the material proprieties are similar to the electrostatically

actuated switch for comparison purposes. Transient response simulation of a Casimir actuated nano switch has been performed to quantify important switch design parameters based on the predicted response. Although the current study focuses on Casimir force actuation, the electrostatic force is used to validate the current model by comparing the static deflection with the electro-statically actuated switch studied by Ma *et al.* (2010). A good agreement is achieved when the electrostatic force is applied very slowly providing a confidence in the current model. For the subsequent analysis, the thickness and width of beam are fixed while length and gap are varied for the purposes of finding the critical dimensions for the actuation. The beam length is varied from 0.5 to 5 μm whereas the gap is varied from 30 to 70 nm. The dynamic behavior of the switch is predicted under different vacuum pressures namely at 0.1 $mTorr$, 1 $mTorr$, and 100 $mTorr$. As mentioned in section 6.2, the Casimir force has been measured at a vacuum pressure of 1 $mTorr$; therefore, the responses at relatively higher pressure (100 $mTorr$) are presented here for comparison proposes only. Increasing the Casimir force for some combinations of lengths and gaps do not result in pull-in of the beam but deflects the beam in a manner similar to static deflection after a phase of damped vibratory motion. Figure 6.8 shows this behavior for a specific length and a gap when the Casimir actuation gain k is set at 0.05, 0.15 and 0.20.

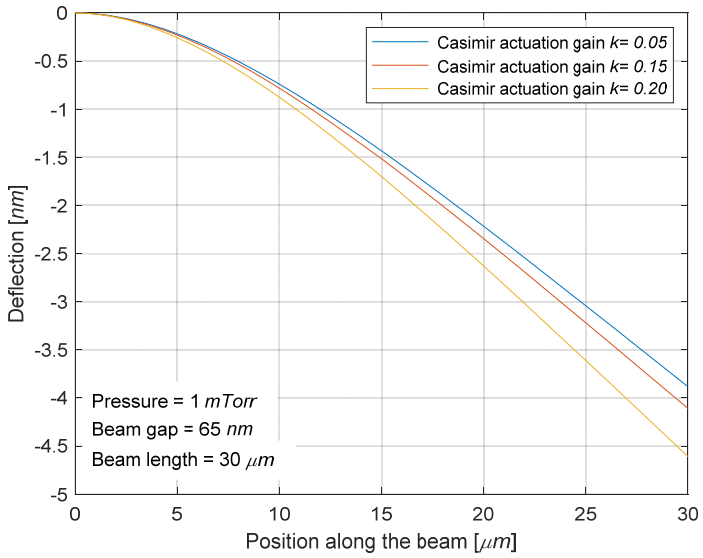

Fig. 6.8. Static deflection of the Casimir actuated nano-beam.

On the other hand, some combinations of different lengths and gaps lead to pull-in instability in the presence of the Casimir force. The beam switches on and its tip touches the substrate then it bounces several times before it makes the permanent contact. Figure 6.9 shows a typical response of a switch actuated via the Casimir force at a gain value of 0.25 in which the beam tip bounce is evident. It is worth noting that, as presented in Figure 5.1, the Casimir force is valid for large gap separation while van der Waals force is dominant at very small gap separation; hence, closer to the contact, contribution from the latter is greater in shaping the contact response.

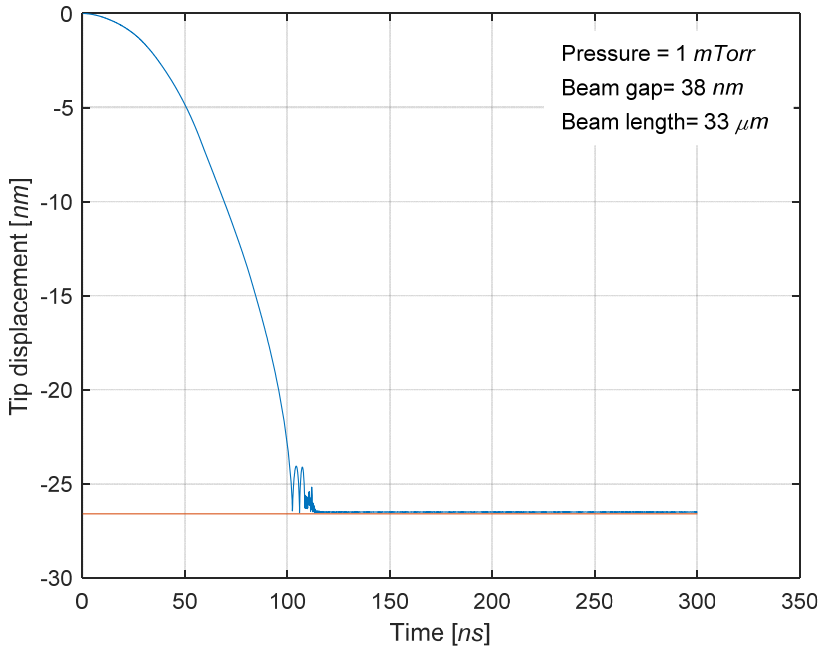

Fig. 6.9. Typical Casimir actuated NEM switch tip-end response.

Figure 6.10 shows the available combination of lengths and gaps at which the Casimir actuation takes place at $k = 0.25$. Employing this chart, for a certain gap value, the minimum length that actuates the switch can be determined. Shorter lengths or larger gap leads to damped vibratory motion and eventually makes the beam settle at an equilibrium position without pull-in instability resembling the static deflection configuration. It is worth noting that in Figure 6.10, the points indicate the calculated values while the smooth line represents the best fit curve. Performance parameters have been determined for the

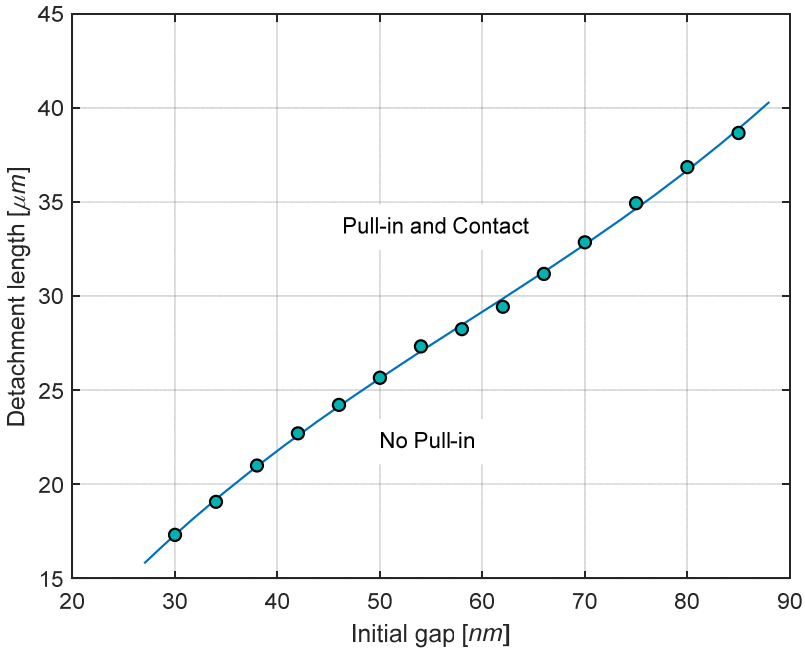

Fig. 6.10. Combination of lengths and gaps for Casimir actuation.

Casimir actuated switch from the predicted responses and the effect of vacuum pressure on the switch performance has been quantified. The initial contact time, t_i, which is one of important parameters that characterizes the switch dynamics, has been computed. Figure 6.11 shows initial contact time for various typical length-gap combinations. It is obvious from the figure that smaller gaps lead to shorter initial contact time. In general, increasing the length reduces the initial contact time at reasonable gap sizes. Although not shown in the figure, at very small gaps the initial contact time increases with length increase and this behavior may be attributed to the dominance of van der Waals effects at small gaps. It is worth noting that, like in the case of electro-statistically actuated switch, the computed initial contact time for pure Casimir actuation switches shows no dependence on the pressure at these levels of low vacuum pressure values. This may be attributed to the low damping values associated with the rarefication. Next, the permanent contact time t_p has been quantified for the pure Casimir actuated switch. The permanent contact time has a similar trend to that of the initial contact time for the length-gap combinations. This trend is illustrated in Figures 6.12 under different vacuum conditions. In general, insignificant

improvement in t_p is gained under relatively higher pressure which does not represent a realistic situation since the switch is supposed to be operated via a Casimir force which is reported only at low pressures. At these levels of low pressures, the permanent contact time appears to be not affected significantly by the very low damping as result of rarefication due to nano scale as well as the vacuum.

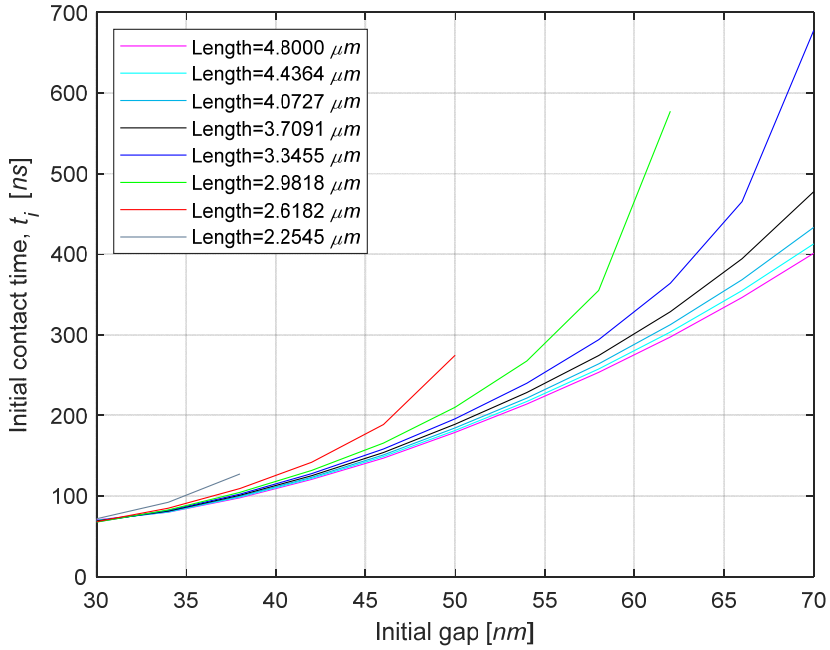

Fig. 6.11. Initial time contours t_i for length-gap combination of Casimir actuated NEM switch.

Improvement which may be gained in the switching time by using a smaller gap or a longer beam is seen to be gained at the expense of other performance parameters. Such limitations

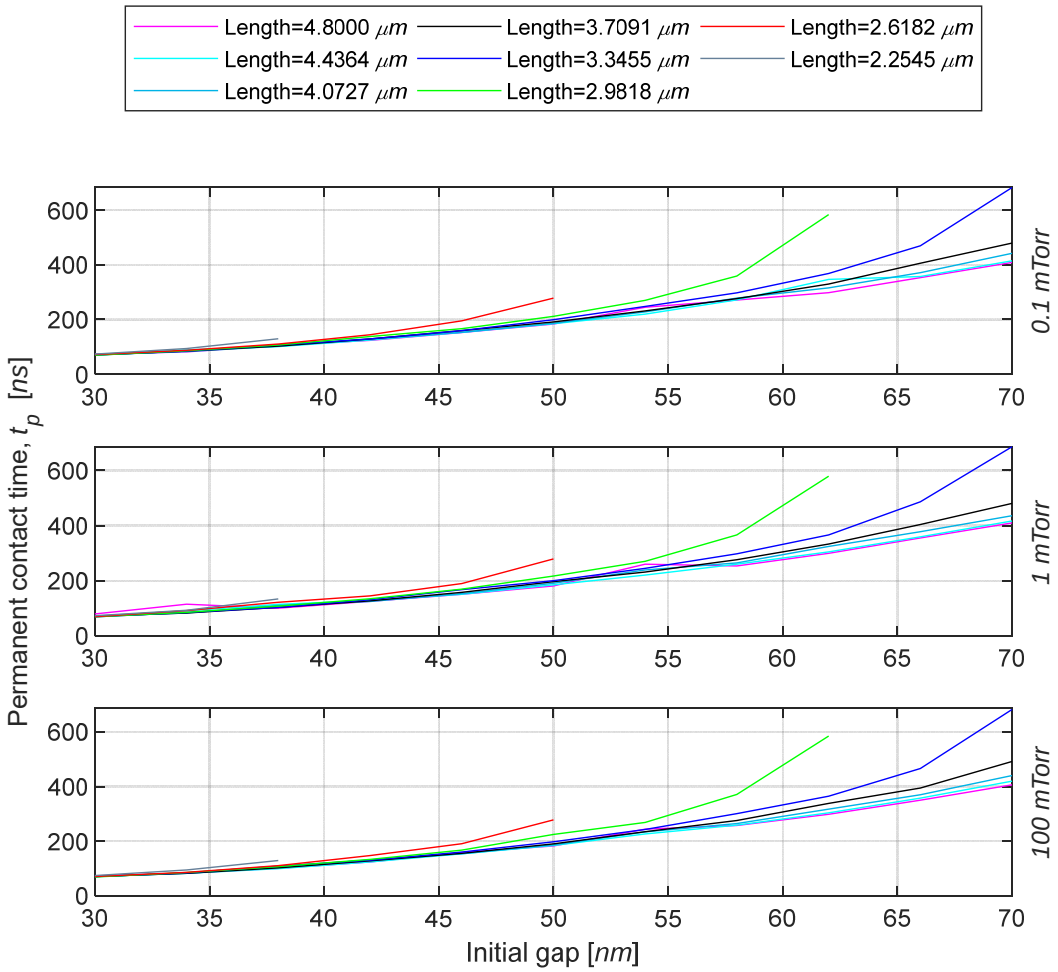

Fig. 6.12. Permanent time contours t_p for length-gap combination of Casimir actuated NEM switch at various pressures.

are illustrated in Figures 6.13, 6.14 and 6.15 for switch bouncing time t_b, major bounce height, BH, and number of bounces, NB, respectively. Figures 6.13 show the variation of switch bouncing time t_b with the increase of beam length at different pressures and gaps.

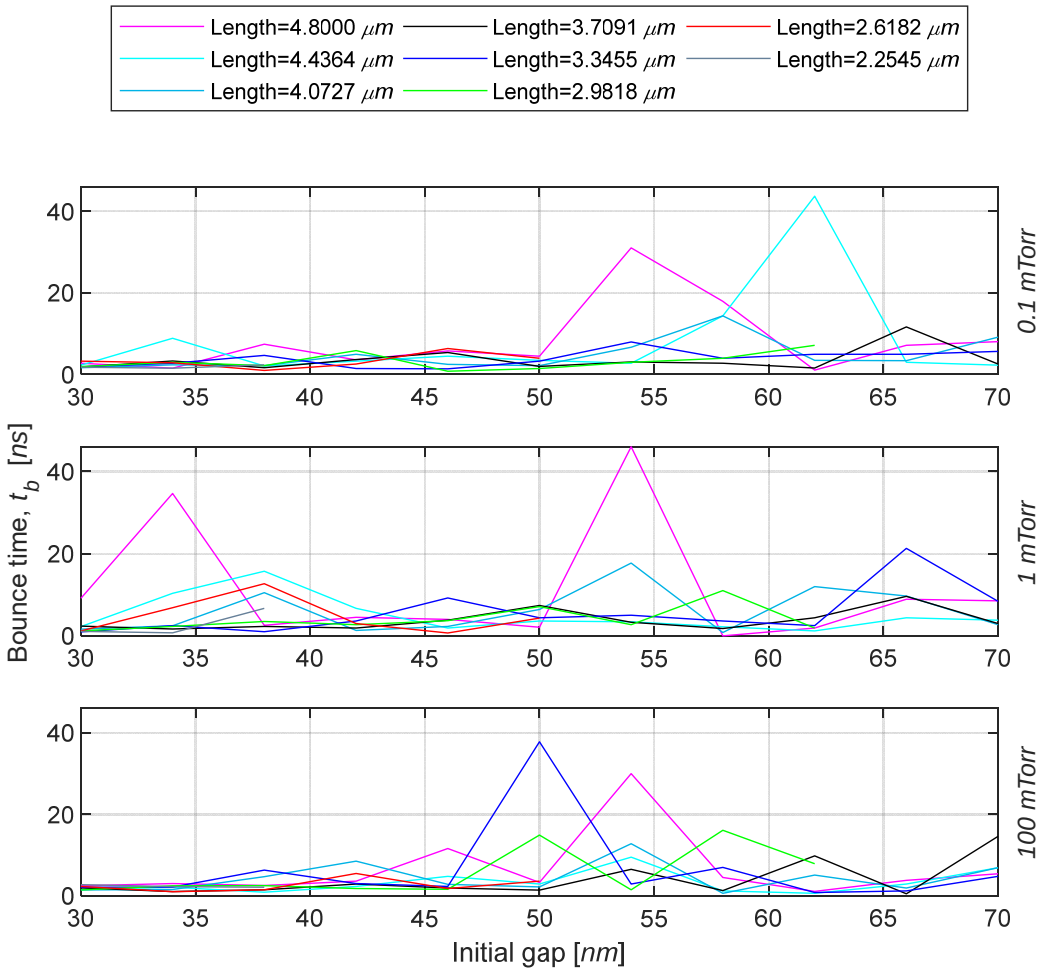

Fig. 6.13. Bounce time contours t_b for length-gap combination of Casimir actuated NEM switch at various pressures.

It is obvious from the figure that using longer beam lengths or larger gaps tends to increase the bouncing time and that the use of higher pressure is not beneficial for reducing the bouncing time and, in some cases, it leads to an increase in t_b at moderate beam lengths. Performance degradation behavior can also be noted with increasing the beam length in the case of major bounce height, BH as shown in Figures 6.14. The Figures show an increase

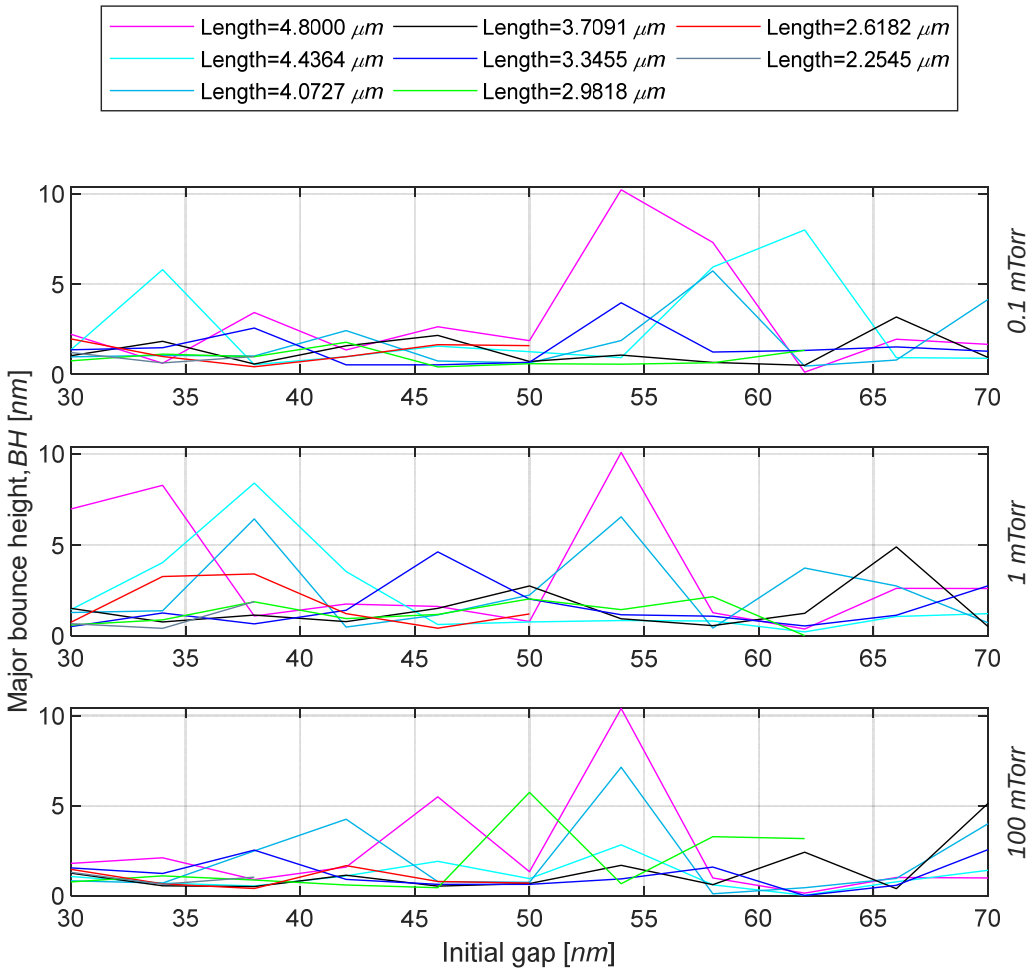

Fig. 6.14. Major bounce height BH for length-gap combination of Casimir actuated NEM switch at various pressures.

of major bounce height with increasing beam lengths or with increasing gap sizes at lower pressures while at small gaps, only a minimal improvement can be observed in major bounce height at higher pressure. The effect of choosing length-gap combinations for actuation via Casimir force on the number of significant bounces NB is illustrated in Figures 6.15. These figures reveal that a reduction in the number of bounces can be attained via shorter beam length or small gap. Moderate pressure tends to increase NB for most

length gap combinations while high pressure tends to increase the number of bounces for medium and larger gap sizes. At low pressure, it appears that degradation in NB may be made minimal, although all other bounce parameters seem to undergo significant degradation.

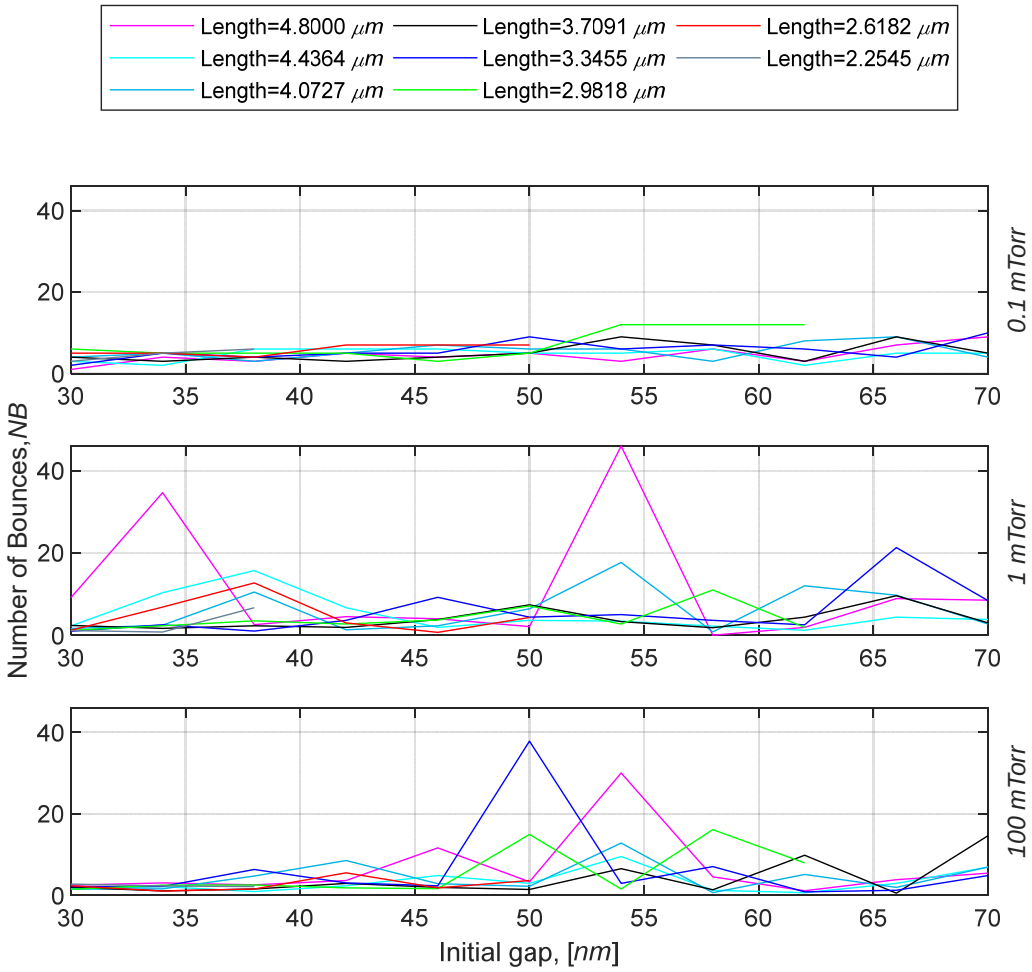

Fig. 6.15. Number of major bounce *NB* for length-gap combination of Casimir actuated NEM switch at various pressures.

It may be noted that other beam dimensional parameters such as beam thickness, beam width, and tip dimensions may also play significant roles in the actuation and dynamic behavior of the switch. However, their effects have not been investigated in the present study. Further, it is worth noting that the vacuum pressures and the rarefaction effect due to the nano scale dimensions lead to very low damping which does not affect the switch performance significantly. In general, use of shorter beam with smaller gap seems to yield better performance than the use of longer lengths and larger gaps. However, this design requirement may bring about fabrication challenges with the currently available fabrication technology.

6.4 Conclusions

The dynamic behavior of NEM switches has been investigated under electrostatic and pure Casimir actuations. A nano switch model that includes the relevant forces and effects and a suitable numerical scheme for providing an insight into the switch nonlinear dynamics is employed. Euler-Bernoulli beam theory and an approximate approach based on Galerkin's method have been employed for predicting dynamic responses. The predicted simulation responses show that the beam tip bounces then makes a final contact with the substrate. Performance parameters such as initial contact time, permanent contact time, major bounce height, and the number of significant bounces have been quantified to evaluate the switch performance and to investigate the influences of some effects and parameters on the switches performance.

The dynamic pull-in voltage is determined for an electrostatically actuated switch. Simulations show that consideration of van der Waals force is sufficient for understanding the bouncing dynamics of NEM switches. The influence of surface effects on performance of a class of electrostatically actuated nano-switches has been investigated to assist in the design and performance of switchable devices under rarefication. Switch performance parameters are determined in cases of actual contact. Significant improvement is attained when the applied voltage is about 1.3 times the dynamic pull-in voltage; however, beyond this voltage, bouncing deteriorates the performance and limits the advantage of using higher voltages. Surface effects appear to have inconsistent effects on various bounce

parameters during the bouncing stage due to the curvature changes of the beam deflection. However, in general over estimation of performance parameters at high actuation voltage is observed when the surface effects are ignored. The present study is envisaged to help the design and improve the performance predictions of electrostatically actuated nano-switches.

The idea of Casimir actuated nano-switches has been investigated to assist in the design of switchable devices that can be operated by purely altering the magnitude of the Casimir force. Combinations of lengths and gaps that actuate the switch via pure Casimir force are quantified. The predicted simulation responses show that the beam tip bounces then makes a final contact with the substrate. Some performance parameters that describe the bouncing behavior are determined in cases of actual contact while beam deflections are predicted for non-contact cases. The present study shows that using short beam length with smaller gap provide better bouncing performance. The present study is expected to yield greater insight into the design and performance predictions of Casimir actuated switches, so that these devices can become a reality in the near future.

CHAPTER 7

CONCLUSIONS AND RECOMMENDATIONS

7.1 Summary of results

In this dissertation, the bouncing dynamic behavior of cantilever type micro as well as nano switches are investigated with an aim to understand the bouncing dynamic behavior in order to improve the switches performance and reliability. The conclusions drawn from the present research are summarized as follows:

For MEM switches, the bouncing dynamic behavior of a cantilever type MEM switch has been studied in detail. Since the dynamic behavior is not adequately understood in particular the transient bouncing behavior, mathematical model that captures nonlinear contact dynamics is employed. For this purpose, a more accurate and realistic asperity-based contact model along with other forces such as force due to squeeze-film air damping, electrostatic actuation force have been incorporated in the model. In addition to the above mentioned forces, force due to piezoelectric effects is included in an alternative MEM switch model of combined actuation. Euler-Bernoulli beam theory has been used for the modeling of the cantilever beam. Galerkin's method is employed to discretize the partial differential equation that governs the flexural beam motion into a system of ordinary differential equations which is solved numerically, since closed-form solutions are not achievable. Predicted responses show that upon switch closure, the beam tip bounces several times before making permanent contact with the substrate and this behavior degrades the performance and life of the switch. Performance parameters such as initial contact time, permanent contact time, bounce height, and the number of significant bounces have been quantified from the predicted responses. Results show improvement in the initial contact time and the permeant contact time with increasing actuation voltages, but this improvement comes with the cost of increased bounce height and number of bounces.

In addition to bounce dynamic analysis, the MEM switch bounce behavior improvement has been investigated via harmonic dither in the actuation voltage of an electrostatically

actuated switch. Further, bounce mitigation using a secondary piezoelectric actuator has also been demonstrated by applying harmonic perturbations in the piezoelectric voltage along with an electrostatic step voltage. The two methods have been shown to improve the bouncing behavior for certain frequencies and dither amplitudes. Regions where such improvements could be made have been identified for both types of switches. Most improvements are achieved at higher or lower actuation voltages while the improvements at optimum actuation voltage are minimal. These improvements have been achieved at frequencies below the second natural frequency of the switch for harmonic dither in the electrostatic actuation voltage and below the third natural frequency of the switch for harmonic dither in secondary actuator. Despite the non-optimized configuration of the switches considered in the present study, simulations show that depending on the mitigation parameter(s) of interest, suitable choice of actuation voltage and dither parameters could be predicted. These approaches could be further improved to achieve better bounce mitigation in the future via optimization techniques for the switch configurations.

Owing to the fact that MEM switches are prone to uncertainties due to the presence inaccuracy in fabrication processes, the above-mentioned comprehensive MEM switch model has also been employed to investigate the influence of uncertainties in system parameters on the bouncing behavior. The accurately predicted responses are used to evaluate the uncertainty performance measures in terms of second order statistics due to important beam material/geometric properties, beam tip properties, actuation voltage and tip asperity contact parameters. These influences on significant switch performance parameters such as initial contact time and maximum bounce height have been quantified in the presence of interactive system nonlinearities. The quantitative predictions reveal several varying patterns as well as similar trends for output measure second order statistics. The study also points out the advantages in operating the switch at higher voltages to gain some performance improvements while emphasizing the limitations based on the bounce height.

This study is expected to provide useful insights for the design of MEM switches with improved performance based on bounce characteristics. Dynamic response predictions

based on the harmonic perturbations in the actuation voltage as well as harmonic dither in secondary actuator voltage are expected to aid mitigate the bouncing. The quantitative understanding of uncertainties is envisaged to help identify critical design parameters, which can then be controlled during fabrication, in order to improve device performance and reliability.

For NEM switches, the transient dynamics of a cantilever type NEM switch have been studied in detail considering the contact bouncing phenomenon. Owing to the consideration of nano effects, the contact bouncing dynamic behavior is more complicated compared to MEM switches in which these effects are not significant. In the mathematical model of nano switch, influences of intermolecular forces, surface effects and the rarefication of gas damping have been taken into consideration to provide accurate response predictions. An asperity-based model along with a repulsive van der Waals force have been incorporated in the model to capture more realistic contact dynamics between the switch tip and the substrate. The switches under consideration are under electrostatic force or pure Casimir force actuation. Euler-Bernoulli beam theory has been used for the modeling of the cantilever beam. The derived model is inherently nonlinear due to the nonlinearity of several nonlinear forces. Since no closed-form solution is available for the resulting nonlinear differential equation, an approximate solution via Galerkin's method has been employed and solved numerically. The predicted simulation responses show that the beam tip bounces then makes a final contact with the substrate. Moreover, the simulations show that consideration of the van der Waals force is sufficient for understanding the bouncing dynamics of NEM switches. Performance parameters such as initial contact time, permanent contact time, major bounce height, and the number of significant bounces have been quantified to investigate NEM switch performance.

For an electrostatically actuated NEM switch, the dynamic pull-in voltage is determined and the influence of surface effects and vacuum pressures on switch performance parameters have been demonstrated. Predicted simulation responses show improvement in the initial contact time and the permanent contact time with increasing actuation voltages; however, this improvement is limited by the deterioration of other bounce performance parameters. Significant improvement is achieved when the actuation voltage is not more

than 130% of the dynamic pull-in voltage where deteriorations in the performance are minimal. When the surface effects are ignored in the modeling, an over estimate of the bounce performance at high actuation voltages is observed. Surface effects have non-consistent influence on various parameters during the bouncing stage due to the curvature changes of the beam deflection. Higher pressure improves the switch bouncing via increased damping although it is not realistic.

The idea of a switchable Casimir-force NEM switch has also been investigated to help in the design of this class of switches that yield functionality via altering the magnitude of Casimir force. Length-gap combinations that actuate the switch have been quantified. Influence of these length-gap combinations on the switch bouncing behavior have been investigated with the presence of surface effects at different vacuum conditions. The present study shows that using short beam lengths with smaller gaps provide better bouncing performance. Vacuum pressure has been shown to have insignificant influence on the bouncing. The present study is expected to yield greater insight into the improvement of design and performance predictions of both electrostatically or Casimir actuated switches in the future.

The methodology and the theoretical model employed in the present study can also be used for analyzing other NEM/MEM switches, and the knowledge gained from the present study is considered to benefit the design and analysis of this class of NEM/MEM devices.

7.2 Thesis contributions

The original contributions of this thesis may be summarized as follows:

- A comprehensive model that accurately predicts the switch dynamic response is used to investigate the bounce behavior of the switch via numerical simulations. Predicted responses are employed for identifying pertinent bounce performance parameters and for characterizing the bounce response.
- Developed numerical schemes and MATLAB codes that accurately predict the dynamic behavior are useful for further studies related to switch bouncing

dynamics. These tools provide an insight into the switch system nonlinear transient dynamics.

- Dynamic responses of an electrostatically actuated MEM switch under harmonic perturbations in step actuation voltage as well as harmonic dither in a secondary piezoelectric actuator voltage are examined for predicting the possible performance benefits/degradation. Regions of improved responses have been identified at specific dither frequency ranges and dither amplitude levels and could have potential use in switch design as well as in achieving bounce mitigation.
- Influence of uncertainty in switch parameters and switch tip geometrical parameters, asperity contact parameters, materials properties on the bouncing behavior has been quantified for MEM switch. Second order statistical measures are used to quantify the uncertainty effects. The quantitative predictions provide a computational platform to perform uncertainty quantification for this class of switches.
- A comprehensive mathematical model of NEM switches is proposed for the purposes of characterizing bounce behavior at nano scales. The model which incorporates various forces and effects that are associated with nano scale structures has been shown to capture the switch bounce behavior. The developed model and simulation process will be of benefit to future research in the area of NEM switch dynamics.
- Influence of surface effects as well as the vacuum pressure effects on the bouncing parameters has been investigated for the purposes of providing useful insights for design of NEM switches. Predicted responses can be used for further analysis, design and achievable improvements in this class of switches.
- Bouncing behavior of Casimir actuated NEM devices as well as effects of some actuation parameters on the bouncing have been investigated in order to aid the design of switchable devices which can be operated by purely altering the magnitude of Casimir force. The proposed model can be used to study other switch parameters related to bounce dynamics for this class of switches.

7.3 Suggestions for future research

This thesis presented a systematic approach for understanding the bouncing dynamic behavior in order to improve the switch performance and reliability. The analysis presented in this thesis provides confidence in applying these schemes in practice. However, before these methods can be applied for the design of MEM and NEM switches, further research is warranted in some of the following areas:

- Adhesive force during the tip-end contact can be incorporated in the theoretical modeling of MEM switches and is expected to achieve more accurate transient response predictions for the switch contact.
- Influence of secondary actuator parameters such as thickness, length, position or use of multiple segment actuators need to be investigated via simulations. A parameter optimized model could be developed via optimization techniques such as simulated annealing, genetic algorithms, and nonlinear programming for achieving better mitigation.
- It is well known that large uncertainties exist in nano switch structural parameters due to fabrication processes; the uncertainty quantification process developed for MEM switches could also be extended to NEM switches.
- In Casimir actuated switches, parameters such as beam thickness, beam width, and tip dimensions which also play significant roles in the actuation and dynamic behavior of the switch have not been investigated in the present study and need to be considered in future research.
- Experiments on the parameter uncertainty effects of electrostatically actuated MEM switch need to be carried out to verify the findings of the present study. As well, verification experiments on the use of harmonic dither in the electrostatic actuation voltage need to be conducted. Further, to quantify the improvement due to harmonic dither in the secondary actuator, design of a MEM switch that employs a secondary actuator as well as experimental verification is warranted.

REFERENCES

Agarwal, N., & Aluru, N. R. (2009). Stochastic Analysis of Electrostatic MEMS Subjected to Parameter Variations. *Journal of Microelectromechanical Systems, 18*(6), 1454-1468. doi:10.1109/jmems.2009.2034612.

Bao, M. (2001). *Analysis and design principles of MEMS devices*. Amsterdam: Elsevier. ISBN: 9780080455624.

Barber, R.W. and Emerson, D.R. (2002). The Influence of Knudsen Number on The Hydrodynamic Development Length within Parallel Plate Micro-channels. *WIT Transactions on Engineering Sciences, 36,* 12. doi: 10.2495/AFM020191.

Bhushan B. (2005). *Micro/Nanotribology of MEMS/NEMS Materials and Devices*. In: Bhushan B. (eds) *Nanotribology and Nanomechanics*. Springer, Berlin, Heidelberg. pp 1031-1089, https://doi.org/10.1007/3-540-28248-3_21, Online ISBN978-3-540-28248-8.

Blecke, J., Epp, D., Sumali, H., & Parker, G. (2009). A Simple Learning Control to Eliminate RF-MEMS Switch Bounce. *Journal of Microelectromechanical Systems, 18*(2), 458-465. doi:10.1109/jmems.2008.2007243.

Caruntu, D. I., & Knecht, M. W. (2015). Microelectromechanical Systems Cantilever Resonators Under Soft Alternating Current Voltage of Frequency Near Natural Frequency. *Journal of Dynamic Systems, Measurement, and Control, 137*(4), 041016. doi:10.1115/1.4028887.

Chan, H. B., Aksyuk, V. A., Kleiman, R. N., Bishop, D. J., & Capasso, F. (2001). Quantum Mechanical Actuation of Microelectromechanical Systems by the Casimir Force. *Science, 291(5510),* 1941-1944. doi:10.1126/science.1057984.

Chang, W. R., Etsion, I., & Bogy, D. B. (1987). An Elastic-Plastic Model for the Contact of Rough Surfaces. *Journal of Tribology, 109*(2), 257. doi:10.1115/1.3261348.

Chen, C. Q., Shi, Y., Zhang, Y. S., Zhu, J., & Yan, Y. J. (2006). Size Dependence of Young's Modulus in ZnO Nanowires. *Physical Review Letters, 96*(7). doi:10.1103/physrevlett.96.075505.

Chen, F., Klimchitskaya, G. L., Mostepanenko, V. M., & Mohideen, U. (2006). Demonstration of the Difference in the Casimir Force for Samples with Different Charge-Carrier Densities. *Physical Review Letters, 97*(17). doi:10.1103/physrevlett.97.170402.

Chen, F., Klimchitskaya, G. L., Mostepanenko, V. M., & Mohideen, U. (2007). Control of the Casimir force by the modification of dielectric properties with light. *Physical Review B, 76*(3). doi:10.1103/physrevb.76.035338.

Chen, T., Chiu, M., & Weng, C. (2006). Derivation of the generalized Young-Laplace equation of curved interfaces in nanoscaled solids. *Journal of Applied Physics, 100*(7), 074308. doi:10.1063/1.2356094.

Czaplewski, D. A., Dyck, C. W., Sumali, H., Massad, J. E., Kuppers, J. D., Reines, I., Cowan, W. D., Tigges, C. P. (2006). A Soft-Landing Waveform for Actuation of a Single-Pole Single-Throw Ohmic RF MEMS Switch. *Journal of Microelectromechanical Systems, 15(6),* 1586-1594. doi:10.1109/jmems.2006.883576.

Decuzzi, P., Demelio, G. P., Pascazio, G., & Zaza, V. (2006). Bouncing dynamics of resistive microswitches with an adhesive tip. *Journal of Applied Physics, 100*(2), 024313. doi:10.1063/1.2214348.

Dequesnes, M., Rotkin, S. V., & Aluru, N. R. (2002). Calculation of pull-in voltages for carbon-nanotube-based nanoelectromechanical switches. *Nanotechnology, 13*(1), 120-131. doi:10.1088/0957-4484/13/1/325.

Esquivel-Sirvent, R., Palomino-Ovando, M. A., & Cocoletzi, G. H. (2009). Pull-in control due to Casimir forces using external magnetic fields. *Applied Physics Letters, 95*(5), 051909. doi:10.1063/1.3193666.

Farrokhabadi, A., Mohebshahedin, A., Rach, R., & Duan, J. (2016). An improved model for the cantilever NEMS actuator including the surface energy, fringing field and Casimir effects. *Physica E: Low-dimensional Systems and Nanostructures, 75*, 202-209. doi: 10.1016/j.physe.2015.09.033.

Gallis, M., & Torczynski, J. (2004). An improved Reynolds-Equation Model for Gas Damping of Microbeam Motion. *Journal of Microelectromechanical Systems, 13*(4), 653-659. doi:10.1109/jmems.2004.832194.

Granaldi, A., & Decuzzi, P. (2006). The dynamic response of resistive microswitches: Switching time and bouncing. *Journal of Micromechanics and Microengineering, 16*(7), 1108-1115. doi:10.1088/0960-1317/16/7/002.

Greenwood, J. A., & Williamson, J. B. (1966). Contact of Nominally Flat Surfaces. *Proceedings of the Royal Society A: Mathematical, Physical and Engineering Sciences, 295*(1442), 300-319. doi:10.1098/rspa.1966.0242.

Guo, X., & Alexeenko, A. (2009). Compact model of squeeze-film damping based on rarefied flow simulations. *Journal of Micromechanics and Microengineering, 19*(4), 045026. doi:10.1088/0960-1317/19/4/045026.

Guo, Z. J., McGruer, N. E., & Adams, G. G. (2007). Modeling, simulation and measurement of the dynamic performance of an ohmic contact, electrostatically actuated RF MEMS switch. *Journal of Micromechanics and Microengineering, 17*(9), 1899-1909. doi:10.1088/0960-1317/17/9/019.

Guo, J., & Zhao, Y. (2007). The size-dependent bending elastic properties of nanobeams with surface effects. *Nanotechnology, 18*(29), 295701. doi:10.1088/0957-4484/18/29/295701.

Gurtin, M. E., & Murdoch, A. I. (1975). Addenda to our paper A continuum theory of elastic material surfaces. *Archive for Rational Mechanics and Analysis, 59*(4), 389-390. doi:10.1007/bf00250426.

Hariri, A., Zu, J., & Mrad, R. (2004). Modeling of Surface Forces between Micron-Sized Objects in Dry Condition. *2004 International Conference on MEMS, NANO and Smart Systems (ICMENS04)*. doi:10.1109/icmens.2004.1509026.

He, J., & Lilley, C. M. (2008). Surface Effect on the Elastic Behavior of Static Bending Nanowires. *Nano Letters, 8*(7), 1798-1802. doi:10.1021/nl0733233.

Israelachvili J. N. (1992). *Intermolecular and surface forces* (London: Academic Press), ISBN: 978-0-12-391927-4.

Jang, W. W., Yoon, J., Kim, M., Lee, J., Kim, S., Yoon, E., Park, D. (2008). NEMS switch with 30*nm*-thick beam and 20*nm*-thick air-gap for high density non-volatile memory applications. *Solid-State Electronics, 52(10),* 1578-1583. doi: 10.1016/j.sse.2008.06.026.

Jing, G. Y., Duan, H. L., Sun, X. M., Zhang, Z. S., Xu, J., Li, Y. D., Yu, D. P. (2006). Surface effects on elastic properties of silver nanowires: Contact atomic-force microscopy. *Physical Review B, 73*(23). doi:10.1103/physrevb.73.235409.

Kalos, M. H., & Whitlock, P. A. (2008). *Monte Carlo methods*. Weinheim: Wiley-VCH.

Kim, M., Song, Y., & Yoon, J. (2011). Fast and robust cantilever switch with suppressed bouncing for IC applications. *2011 IEEE 24th International Conference on Micro Electro Mechanical Systems*. doi:10.1109/memsys.2011.5734654.

Klimchitskaya, G. L., Mohideen, U., & Mostepanenko, V. M. (2009). The Casimir force between real materials: Experiment and theory. *Reviews of Modern Physics, 81(4),* 1827-1885. doi:10.1103/revmodphys.81.1827.

Kogut, L., & Komvopoulos, K. (2004). The Role of Surface Topography in MEMS Switches and Relays. *ASME/STLE 2004 International Joint Tribology Conference, Parts A and B*. p 107-110. doi:10.1115/trib2004-64359.

Krylov, S., & Maimon, R. (2004). Pull-in Dynamics of an Elastic Beam Actuated by Continuously Distributed Electrostatic Force. *Journal of Vibration and Acoustics, 126(3),* 332-342. doi:10.1115/1.1760559.

Lamoreaux, S. K. (2004). The Casimir force: Background, experiments, and applications. *Reports on Progress in Physics,68(1),* 201-236. doi:10.1088/0034-4885/68/1/r04.

Leondes, C. T. (2006). *MEMS/NEMS: Handbook techniques and applications*. New York: Springer.

Liao, M., Hishita, S., Watanabe, E., Koizumi, S., & Koide, Y. (2010). Suspended Single-Crystal Diamond Nanowires for High-Performance Nanoelectromechanical Switches. *Advanced Materials, 22(47),* 5393-5397. doi:10.1002/adma.201003074.

Li, P., Hu, R., & Fang, Y. (2007). A new model for squeeze-film damping of electrically actuated microbeams under the effect of a static deflection. *Journal of Micromechanics and Microengineering, 17(7),* 1242-1251. doi:10.1088/0960-1317/17/7/005.

Lin, W., & Zhao, Y. (2005). Casimir effect on the pull-in parameters of nanometer switches. *Microsystem Technologies, 11(2-3),* 80-85. doi:10.1007/s00542-004-0411-6.

Loh, O. Y., & Espinosa, H. D. (2012). Nanoelectromechanical contact switches. *Nature Nanotechnology, 7(5),* 283-295. doi:10.1038/nnano.2012.40.

Liu, C. (2016). Dynamic behavior analysis of cantilever-type nano-mechanical electrostatic actuator. *International Journal of Non-Linear Mechanics, 82,* 124-130. doi: 10.1016/j.ijnonlinmec.2016.03.007.

Liu, C., & Liu, C. (2014). Analysis of nonlinear dynamic behavior of electrically actuated micro-beam with piezoelectric layers and squeeze-film damping effect. *Nonlinear Dynamics, 77(4),* 1349-1361. doi:10.1007/s11071-014-1384-3.

Ma, J. (2011). Nonlinear instabilities in MEM/NEM electrostatic switches, M Sc. Thesis, University of Western Ontario, London, Ontario, Canada.

Ma, J. B., Jiang, L., & Asokanthan, S. F. (2010). Influence of surface effects on the pull-in instability of NEMS electrostatic switches. *Nanotechnology, 21(50),* 505708. doi:10.1088/0957-4484/21/50/505708.

Majumder, S., Mcgruer, N., Adams, G. G., Zavracky, P., Morrison, R. H., & Krim, J. (2001). Study of contacts in an electrostatically actuated microswitch. *Sensors and Actuators A: Physical, 93(1),* 19-26. doi:10.1016/s0924-4247(01)00627-6.

McCarthy, B., Adams, G., Mcgruer, N., & Potter, D. (2002). A dynamic model, including contact bounce, of an electrostatically actuated microswitch. *Journal of Microelectromechanical Systems, 11(3),* 276-283. doi:10.1109/jmems.2002.1007406.

Miller, R. E., & Shenoy, V. B. (2000). Size-dependent elastic properties of nanosized structural elements. *Nanotechnology, 11(3),* 139-147. doi:10.1088/0957-4484/11/3/301.

Mostepanenko, V. M., & Trunov, N. N. (1997). *The Casimir effect and its applications*. Oxford: Clarendon Press, ISBN-10: 0198539983.

Nayfeh, A. H., & Younis, M. I. (2004). A new approach to the modeling and simulation of flexible microstructures under the effect of squeeze-film damping. *Journal of Micromechanics and Microengineering, 14(2),* 170-181. doi:10.1088/0960-1317/14/2/002.

Ostasevicius, V., & Dauksevicius, R. (2010). *Microsystems Dynamics* (Vol. 1). Berlin: Springer Netherland. DOI: ISBN10 0-387-25786-1.

Ostasevicius, V., Gaidys, R., & Dauksevicius, R. (2009). Numerical Analysis of Dynamic Effects of a Nonlinear Vibro-Impact Process for Enhancing the Reliability of Contact-Type MEMS Devices. *Sensors, 9(12),* 10201-10216. DOI:10.3390/s91210201.

Palasantzas, G., Zwol, P. J., & Hosson, J. T. (2008). Transition from Casimir to van der Waals force between macroscopic bodies. *Applied Physics Letters, 93(12),* 121912. doi:10.1063/1.2992030.

Park, H. S. (2009). Quantifying the size-dependent effect of the residual surface stress on the resonant frequencies of silicon nanowires if finite deformation kinematics are considered. *Nanotechnology, 20(11),* 115701. doi:10.1088/0957-4484/20/11/115701.

Park, H. S. (2008). Surface stress effects on the resonant properties of silicon nanowires. *Journal of Applied Physics, 103(12),* 123504. doi:10.1063/1.2939576.

Parkos, D., Raghunathan, N., Venkattraman, A., Sanborn, B., Chen, W., Peroulis, D., & Alexeenko, A. (2013). Near-Contact Gas Damping and Dynamic Response of High-g MEMS Accelerometer Beams. *Journal of Microelectromechanical Systems, 22(5),* 1089-1099. doi:10.1109/jmems.2013.2269692.

Rahim, F. A., & Younis, M. I. (2016). Control of Bouncing in MEMS Switches Using Double Electrodes. *Mathematical Problems in Engineering, 2016, 1-10.* doi:10.1155/2016/3479752.

Ramezani, A., Alasty, A., & Akbari, J. (2007). Closed-form approximation and numerical validation of the influence of van der Waals force on electrostatic cantilevers at nano-scale separations. *Nanotechnology, 19(1),* 015501. doi:10.1088/0957-4484/19/01/015501.

Rotkin, S. V., (2002). Analytical calculations for nanoscale electromechanical systems. *Electromech. Soc. Proc. 6*, pp. 90-97.

Rudd, R., & Lee, B. (2008). Mechanics of silicon nanowires: Size-dependent elasticity from first principles. *Molecular Simulation, 34(1),* 1-8. doi:10.1080/08927020701730435.

Shanmugavalli, M., Uma, G., Vasuki, B., & Umapathy, M. (2006). Design and Simulation of MEMS Devices using Interval Analysis. *Journal of Physics: Conference Series, 34*, 601-605. doi:10.1088/1742-6596/34/1/099.

Snow, M., Bajaj, A. (2010). Uncertainty Quantification Study for a Comprehensive Electrostatic. MEMS Switch Model. *PRISM: NNSA Center of Prediction of Reliability. Integrity and Survivability of Microsystems*, Paper 20.

Soroush, R., Koochi, A., Kazemi, A. S., Noghrehabadi, A., Haddadpour, H., & Abadyan, M. (2010). Investigating the effect of Casimir and van der Waals attractions on the electrostatic pull-in instability of nano-actuators. *Physica Scripta, 82(4),* 045801. doi:10.1088/0031-8949/82/04/045801.

Sumali, H. (2007). Squeeze-film damping in the free molecular regime: Model validation and measurement on a MEMS. *Journal of Micromechanics and Microengineering, 17(11),* 2231-2240. doi:10.1088/0960-1317/17/11/009.

Sumali, H., Massad, J. E., Czaplewski, D. A., & Dyck, C. W. (2007). Waveform design for pulse-and-hold electrostatic actuation in MEMS. *Sensors and Actuators A: Physical, 134(1),* 213-220. doi: 10.1016/j.sna.2006.04.041.

MATLAB (2013) Release 2013b, the MathWorks, Inc., Natick, Massachusetts, United States.

Torricelli, G., Zwol, P. J., Shpak, O., Binns, C., Palasantzas, G., Kooi, B. J., Svetovoy, V. B., Wuttig, M. (2010). Switching Casimir forces with phase-change materials. *Physical Review A, 82(1).* doi:10.1103/physreva.82.010101.

Tung, R. C., Fruehling, A., Peroulis, D., & Raman, A. (2014). Multiple Timescales and Modeling of Dynamic Bounce Phenomena in RF MEMS Switches. *Journal of Microelectromechanical Systems, 23(1),* 137-146. doi:10.1109/jmems.2013.2271252.

Vakili-Tahami, F., Mobki, H., Keyvani-Janbahan, A., Rezazadeh, G (2009). Pull-in Phenomena and Dynamic Response of a Capacitive Nano-beam Switch. *Sensors & Transducers Journal, (11),* 26-37.

Voiculescu, I., & Zaghloul, M. E. (2016). *Nanocantilever beams: Modeling, fabrication and applications*. Singapore: Pan Stanford Publishing, ISBN-13: 978-981-4613-24-8.

Wang, G., & Feng, X. (2007). Effects of surface elasticity and residual surface tension on the natural frequency of microbeams. *Applied Physics Letters, 90(23),* 231904. doi:10.1063/1.2746950.

Wang, T. (2009). *Nonlinear and stochastic dynamics of MEMS-based angular rate sensing and switching systems.* PhD Thesis, University of Western Ontario, London, Ontario, Canada.

Wong, W. S., & Lai, C. (2013). Mitigation of MEMS switch contact bouncing: Effectiveness of dual pulse actuation waveforms and robustness against variations in switch and waveform parameters. *Sensors and Actuators A: Physical, 194*, 188-195. doi: 10.1016/j.sna.2013.02.011.

Xu, L., & Jia, X. (2008). Electromechanical-fluidic coupled dynamics for microbeams. *Proceedings of the Institution of Mechanical Engineers, Part C: Journal of Mechanical Engineering Science, 222(3),* 535-548. doi:10.1243/09544062jmes694.

Yahiaoui, A., Lemoine, E., Pothier, A., & Blondy, P. (2014). Mechanical nanogap switch for low-power on-board electronics. *International Journal of Microwave and Wireless Technologies, 7(05),* 515-520. doi:10.1017/s1759078714000774.

Younis, M., Abdel-Rahman, E., & Nayfeh, A. (2003). A reduced-order model for electrically actuated microbeam-based MEMS. *Journal of Microelectromechanical Systems, 12(5),* 672-680. doi:10.1109/jmems.2003.818069.

Yu, N., & Polycarpou, A. A. (2004). Adhesive contact based on the Lennard–Jones potential: A correction to the value of the equilibrium distance as used in the potential. *Journal of Colloid and Interface Science, 278(2),* 428-435. doi: 10.1016/j.jcis.2004.06.029.

Zavracky, P. M., Mcgruer, N. E., Morrison, R. H., & Potter, D. (1999). Microswitches and micro relays with a view toward microwave applications. *International Journal of RF and Microwave Computer-Aided Engineering, 9(4),* 338-347. doi:10.1002/(sici)1099-047x(199907)9:43.0.co;2-q.

Zhang, W., Meng, G., & Li, H. (2005). Adaptive vibration control of micro-cantilever beam with piezoelectric actuator in MEMS. *The International Journal of Advanced Manufacturing Technology, 28(3-4),* 321-327. doi:10.1007/s00170-004-2363-5.

Zhao, Y., & Chang, L. (2001). A Model of Asperity Interactions in Elastic-Plastic Contact of Rough Surfaces. *Journal of Tribology, 123(4),* 857. doi:10.1115/1.1338482.

Zhao, Y., Maietta, D. M., & Chang, L. (2000). An Asperity Microcontact Model Incorporating the Transition from Elastic Deformation to Fully Plastic Flow. *Journal of Tribology, 122(1),* 86. doi:10.1115/1.555332.

VITA

EDUCATION

Sept. 2013 – Jan. 2019	**Ph.D**, Mechanical and Material Engineering
	The University of Western Ontario, Canada.
Apr. 2003 – Aug. 2006	**MESc.**, Mechanical Engineering
	The University of Duisburg-Essen, Germany
Sept. 1995 – July 1996	Postgraduate subjects in Mechanical design
	University of Benghazi, Benghazi, Libya
Sept. 1989 – July 1993	**B.Sc.**, Mechanical Engineering
	University of Benghazi, Benghazi, Libya

SCHOLARSHIPS

Sept. 2013 – Dec. 2018	Libyan-North American Scholarship program by
	Libyan Ministry of Higher Education, Libya
Apr. 2002 – July 2006	Libyan-North American Scholarship program by
	Libyan Ministry of Higher Education, Libya

WORK EXPERIENCE

Jan. 2014 – April. 2018	**Research/Teaching Assistant**
	Mechanical and Materials Engineering
	The University of Western Ontario, Canada
Nov. 2006 – Dec. 2012	**Lecturer**
	Mechanical Engineering
	University of Benghazi, Benghazi, Libya
Jan. 1999– Aug. 2002	**Teaching Assistant**
	Mechanical Engineering
	University of Benghazi, Benghazi, Libya
Jan. 1996– Aug. 1999	**Technical affairs department**
	Ghot Sultan Project, Al-abiar, Libya
Jan. 1995- Aug. 1999	**Teaching Assistant**
	Mechanical Engineering
	University of Benghazi, Benghazi, Libya

PUBLICATIONS

Articles published in refereed journals

1. Asokanthan, S. F., Arghavan, S., Bognash, M., (2017). Stability of Ring-Type MEMS Gyroscopes Subjected to Stochastic Angular Speed Fluctuation. *ASME Journal of Vibration and Acoustics*, 139(4), 040904. doi:10.1115/1.4036452.

2. Bognash, M., & Asokanthan, S. F., (2018). Uncertainty Considerations for Nonlinear Dynamics of a Class of MEMS Switches undergoing Tip Contact Bouncing. *Journal of Computational and Nonlinear Dynamics*. doi:10.1115/1.4041773

3. Bognash, M., Asokanthan, S. F., (2018). Stochastic Stability of a Class of MEMS-Based Vibratory Gyroscopes under Input Rate Fluctuations. *Vibration*,1(1), 69-80. doi:10.3390/vibration1010006.

Papers published in refereed conference proceedings

4. Bognash, M., Wang, T., and Asokanthan, S. F., (2015). Bouncing Dynamics Considerations for Micro Switch Design, *Proc. Canadian Congress of Applied Mechanics(CANCAM)*, London, ON, June 2015

5. Arghavan, S., Bognash, M., and Asokanthan, S. F., (2015). Stochastic Dynamics and Stability of a Class of MEMS Gyroscopes, *Proc. Canadian Congress of Applied Mechanics(CANCAM)*, London, ON, June 2015.

6. Arghavan, S., Bognash, M., Cho, J., and Asokanthan, S. F., (2016). Mass Anomaly and Random Rate Fluctuation Effects on Vibratory Gyroscope Dynamics. *Proc. International Congress of Theoretical and Applied Mechanics (ICTAM))*, Montreal, QC, August 2016.

7. Bognash M. & Asokanthan S. F., (2016). Uncertainty Quantification for cantilever based MEMS Switches Considering Bouncing Dynamics, *Proc. ASME International*

Mechanical Engineering Congress and Exposition (IMECE), Phoenix, Arizona, Nov 2016, paper # 2016-67083.

8. Bognash M. & Asokanthan S. F., (2018). Dynamic Behavior of a Class of Casimir Actuated NEM Switches, Proc. *ASME 2018 International Design Engineering Technical Conferences IDETC 2018*, Quebec City, Quebec, Canada.